8411-6002-RU000

STUDY OF LUNAR LANDING SENSOR PERFORMANCE INTERIM REPORT No. 3

Contract No. NAS8-5205

31 JULY 1964

Prepared for
GEORGE C. MARSHALL SPACE FLIGHT CENTER
Huntsville, Alabama

TRW SPACE TECHNOLOGY LABORATORIES

8411-6002-RU000

STUDY OF LUNAR LANDING SENSOR PERFORMANCE INTERIM REPORT NO. 3

31 July 1964

Contract No. NAS8-5205
(Modification No. 5)

Prepared for

George C. Marshall Space Flight Center
Huntsville, Alabama

Prepared: S. D. Kindorf
S. D. Kindorf
Project Engineer

Approved: J. E. Holland
J. E. Holland, Manager
Guidance Sensors Department

J. Heilfron, Director
Guidance Laboratory

TRW SPACE TECHNOLOGY LABORATORIES
THOMPSON RAMO WOOLDRIDGE INC.

CONTENTS

ILLUSTRATIONS

TABLES

Section 1. REVIEW OF PROJECT TASKS AND RESULTS

A. INTRODUCTORY REMARKS

The investigations depicted in this report were conducted in fulfillment of Contract NAS8-5205, Modification No. 5, dated 31 January 1964. The scope of the work performed under this contract modification was 1) to evaluate lunar navigation accuracies achievable when an altimeter is used as the only external sensor and 2) to evaluate varactor bias modulation as a means of achieving transmit-receiver isolation in high duty factor radar systems.

Previous work performed under the basic contract (NAS8-5205) involved the preliminary analysis, design, and computer simulation of an all solid-state "extended range" altimeter (Reference 1). The overall performance and accuracies of the altimeter itself were evaluated at that time. In that work, the question of the full applicability of such an altimeter to lunar navigation (i.e., the determination of three-dimensional trajectional parameters) arose. The analysis of achievable navigation accuracies presented herein was performed specifically to answer that inquiry. Of particular concern was the net effect of lunar terrain irregularities and uncertainties on altimeter performance and navigation accuracies.

The type of application under prime consideration requires that the altimeter be designed to operate up to altitudes on the order of 220 kilometers. The round-trip signal attenuation associated with such altitudes introduces the requirements of high transmit-receive isolation levels (i.e., the rejection of the strong "leakage" signal in favor of the weak return signal). The method proposed in the previous work for achieving the required isolation levels requires asynchronous gating of the transmitter and first local oscillator outputs in a high duty factor mode. A candidate method for achieving the gating function involves square wave modulation of the bias levels of the varactor diodes which are contained in the output stages of both the transmitter and local oscillator solid state power sources. The experimental program presented herein was conducted specifically for the purpose of investigating the isolation levels actually achievable by using the varactor bias gating method.

B. SUMMARY OF LUNAR NAVIGATION ANALYSES

The evaluation of lunar navigation accuracies attainable by use of altimeter data was conducted by an error analysis computer program developed during the study. The analysis was based on the use of Kalman filtering techniques* to process the altitude data. Essential inputs to the program were nominal flight trajectories, a statistical model of the moon's surface irregularities, a statistical model of altimeter thermal noise errors, and a mathematical model of the altimeter tracker dynamics.

The trajectories considered were circular orbits and Hohmann ellipse descents. The statistical lunar model was derived by sampling surface altitude, as indicated by available lunar contour maps, relative to a reference ellipse at discrete points along the surface. The sampled data were then combined by means of a computer program to give an autocorrelation function** for the terrain features. This function was found to have the form of a damped cosine with the first zero crossing at about 14 deg central angle. The form suggests that the departure of the lunar shape from a true ellipse and the more gross terrain features such as large plateaus are dominant factors in overall navigation accuracy, while the local terrain irregularities become dominant in the strict determination of altitude. The basic altimeter error and tracker models were taken directly from the results of the altimeter design study. The tracker model was transformed mathematically into a form suitable for error analysis computations. This transformation, which preserves the tracker dynamics, is described in Appendix C.

The results of the error analysis program indicate that the exclusive use of altitude data can provide a good estimate of vertical position, vertical velocity, and downrange velocity. In particular, it was shown that in the duration of about one orbit, the uncertainty associated with vertical

---

* See Appendix A for a derivation of the Kalman filtering equations
** See Appendix B

position (i.e., distance to the center of the moon) can be reduced to approximately the uncertainty of the moon's radius. The latter was found to be the primary limiting factor in most of the analyses. Numerically, this uncertainty was taken to be about 1-1/2 km, 1σ. This may be a pessimistic estimate, however. It was also shown that in about one-half orbit, the error in the two velocity parameters were both reduced to less than 1 meter/sec, 1σ. Similar results were obtained for the Hohmann descent cases. It was also found that the use of altimeter measurements does not provide good downrange position, crossrange position, or crossrange velocity information. It was shown, however, that the altitude measurements can limit either the growth or the rate of growth of the downrange position uncertainties. It was also found that a Kalman filter can be used to reduce the errors in determination of altitude (i.e., distance to the lunar surface) to less than 1/2 km, 1σ, in about one-half orbit.

The final step in the analysis was the removal of the statistical model of the lunar terrain from the error analysis program. Evaluations of the navigation errors under this condition indicated the primary effect of the terrain irregularities is to reduce the rate at which the errors approach values dictated primarily by the lunar radius uncertainty. A reduction in downrange position uncertainty was also found to occur in the absence of terrain effects.

C. SUMMARY OF VARACTOR BIAS GATING EXPERIMENTS

The investigation of varactor bias modulation as a means of achieving transmit-receive isolation was conducted primarily by means of laboratory experimentation. Two power sources (which contain the varactor diodes) were built and tested statically to determine the ON-OFF ratios achievable when the varactor bias voltage was appropriately varied. It was found that control of the input varactors gave the best results (over 100 db) for both sources. These measurements were limited to the 100-db level by the relative insensitivity of the particular instrumentation used.

The primary transmitter-receiver elements of the envisioned altimeter were assembled in the laboratory so that further static tests (using the greater sensitivity of the narrow-band receiver) and the required dynamic tests could be conducted. The subsequent static tests indicated ON-OFF ratios of approximately 133 db for one of the sources and greater than 139 db for the other (the two sources are not identical, as depicted in B of Section 4.

The dynamic tests (i.e., system operating in gated mode) were conducted by using available gate generators which allowed manual variation of system pulse repetition frequency (PRF), duty factor and relative pulse position. The range of PRF's considered was from about 300 cps to 40 K cps. Consistently better isolation was obtained as initial system deficiencies were systematically eliminated. At the termination of the investigations, relative power measurements indicating isolation levels ranging from 114 to 125 db, depending upon PRF, where actually being obtained and recorded in the laboratory.

From the measured data it is believed that the primary limitation at this point is more closely related to system measurement capabilities than isolation achievability as such. In particular, the measurements appear to be limited both by receiver thermal noise and by local oscillator (LO) and leakage self-intermodulation components entering the receiver bandpass. It is believed that such phenomena, the latter may be considered as being associated with the gating action itself, could be significantly reduced by suitable receiver modifications and by bandwidth limitation measures*. The work was not continued in that direction because of economic and schedule considerations.

The primary method used for evaluating the measured results was by direct comparison with isolation requirements derived for an altimeter

* The value of this approach was in fact demonstrated by including RF filters in the transmitter and local oscillator lines.

application wherein altitude was to be determined up to about 220 km. These requirements range from about 141 db at maximum altitude to about 120 db at a minimum altitude of 1.85 km. These requirements were derived on the basis of the assumption that frequency discrimination is not applicable (i.e., zero altitude rate). A second assumption was that an increasing signal-to-leakage ratio (and thus, increasing system performance) is required with decreasing altitude.*

In conclusion, it is our belief that the feasibility of varactor bias modulation as a means of achieving transmit-receive isolation has been demonstrated. Admittedly, the hypothetical ultimate goal of achieving a sufficient level of isolation to permit the stated altimetry function by means of varactor bias gating along up to altitudes of 220 km has not been demonstrated. However, the variance may be attributed to instrumentation limitations, and is not necessarily assignable to the techniques evaluated. Moreover, other methods of gating, not necessarily related to varactor bias modulation, appear feasible in terms of contributing to the total required system isolation. In any case, it may be necessary to provide further precautionary measures against component-to-component leakage coupling than was attempted in the investigations reported here in order to realize the full isolation potential.

REFERENCE

1. "Study of Lunar Landing Sensor Performance," Interim Report Nos. 1 and 2, Contract NAS8-5205, 21 June and 30 October, 1963.

* Such assumptions are of course dependent on detailed mission and accuracy requirements and are therefore subject to conjecture.

Section 2. BACKGROUND

A. APPLICATION OF ON-BOARD ALTIMETRY TO LUNAR NAVIGATION

The general type of mission of concern in this portion of the Lunar Landing Sensor Performance investigations is shown in Figure 2-1. The concept involves lunar approach and circular orbit, elliptical free-fall descent (e.g., Hohmann transfer ellipse), and powered landing. Ascent, orbit, and lunar escape involve a similar procedure, but in reverse order. It is, of course, necessary to monitor trajectory parameters throughout the entire sequence for navigation and guidance purposes. When the lunar vehicle approaches and remains in the vicinity of the moon, the long range from Earth-based stations (e.g., the DSIF) and the limited times of observation (i.e., tracking is interrupted when the vehicle passes behind the moon) makes the applicability of Earth-based tracking questionable as a primary navigational tool. This suggests the use of on-board sensors to gather data relative to the nearby lunar surface such that moon-referenced navigation may become plausible. The obvious applicable sensors are horizon scanners, altimeters, beacon-trackers, map-matching devices, or some combination thereof.

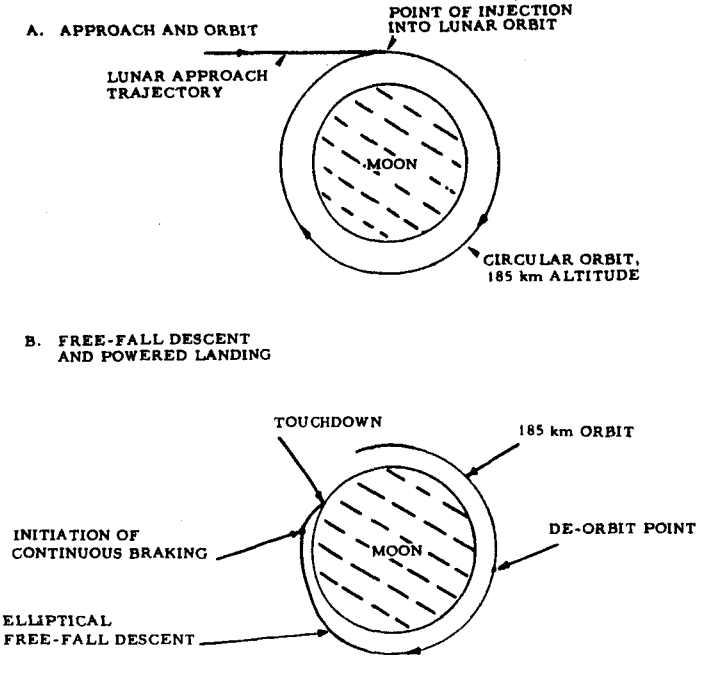

Figure 2-1. Lunar Landing Concept (Not to Scale)

The investigation reported here specifically considers the exclusive application of an on-board radar altimeter for navigational purposes during non-thrust (free-fall) portions of flight. In regard to the general mission described above, the portions of immediate concern occur during the circular orbit and elliptical descent. In this concept, the altimeter provides altitude data up to orbital altitudes on the order of 185 km. Data processing techniques (sometimes referred to as filtering or smoothing) are then applied directly to the altitude data to derive the desired trajectory parameters. The predicted accuracy of the latter as a function of processing time forms a major portion of the study reported here. The use of altimeter data during the initial lunar approach and during the powered landing phase (i.e., below about 18.5-km altitude) for navigation purposes is <u>not</u> considered here.

B. ALTIMETER REQUIREMENTS AND TECHNIQUES

To perform the sensor function described in the foregoing section, the lunar landing altimeter must be capable of determining vehicle altitude up to altitudes of about 220 km (i.e., 185-km orbit altitude plus 20 percent design margin) with an accuracy of about 1 percent (1σ). A basic design for such an altimeter has been derived and is specified in Interim Report No. 1 of the "Study of Lunar Landing Sensor Performance" series. The basic configuration for this "extended range" altimeter is shown in Figure 2-2.

The altimeter design is based upon a high duty factor modulation scheme wherein altitude is determined by matching the PRF to twice the round-trip propagation time. The high duty factor concept allows the use of low peak output powers which in turn allows the use of all solid-state transmitter elements. The latter inherently results in potentially high reliability and RF coherency. The system uses an on-board reference to direct its single beam approximately along the local lunar vertical. The frequency tracking loop tracks the center of the doppler shifted return spectrum.

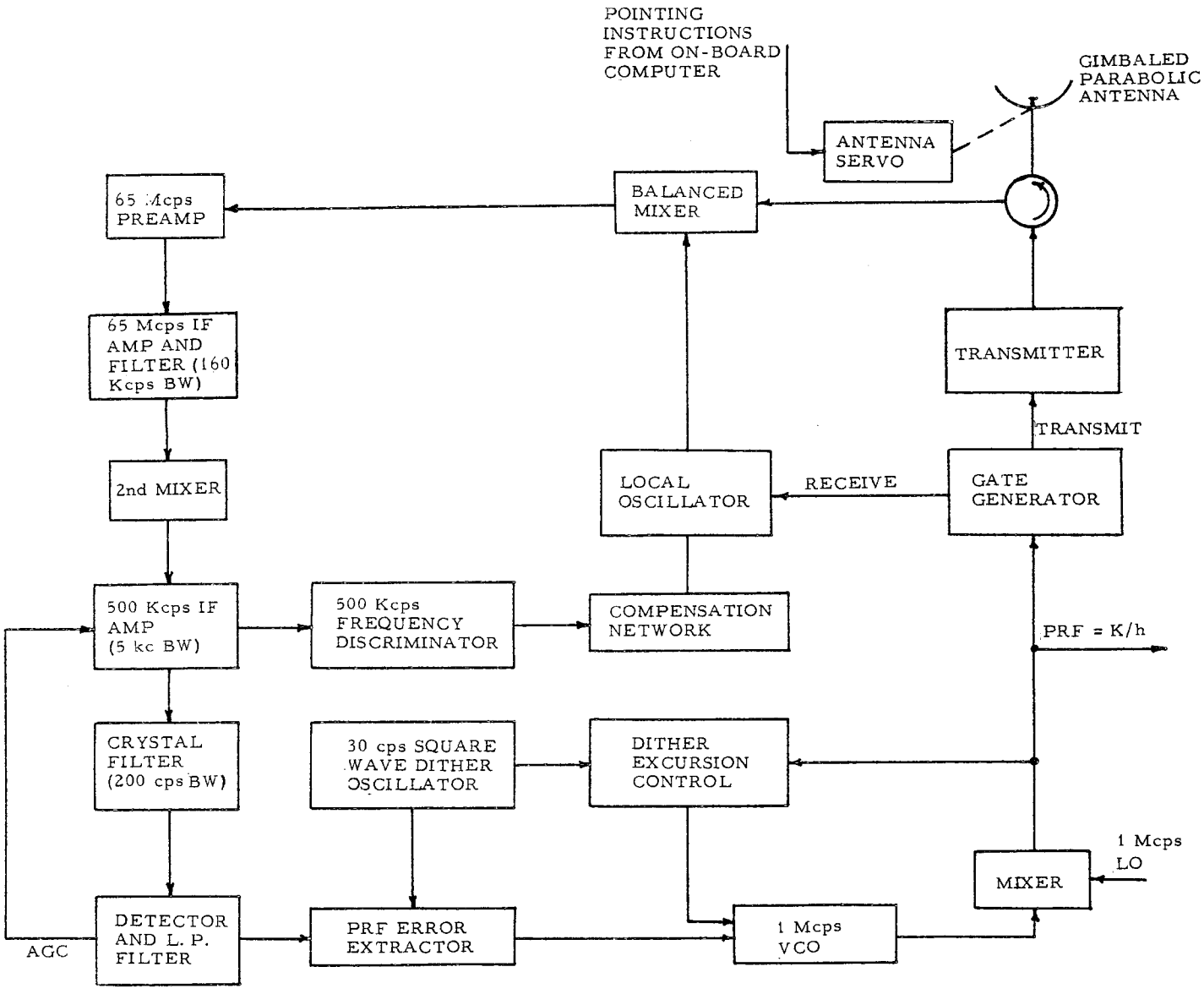

Figure 2-2. Extended Range Altimeter — Basic Configuration

It has been shown (see Appendix D) that transmitter-receiver isolation levels ranging from 165 db at the maximum design altitude of 220 km down to about 144 db at the minimum design altitude of 1.85 km are required in order to ensure proper system operation. About 24 db may be achieved by the use of the circular shown in Figure 2-2. Frequency discrimination cannot, of course, be assumed under near-zero doppler conditions such as encountered while in circular orbit. Thus in the worst case, the remaining 141 db must be derived entirely by means of time discrimination (i.e., asynchronous gating of the transmitter and receiver).

The output stages of the transmitter and local oscillator sources shown in Figure 2-2 are X16 (i.e., times 16) frequency multipliers which operate at X-band output frequencies. It has been noted in previous laboratory investigations that these multipliers may be deactivated by appropriate reverse-biasing of the internal varactor diodes (these diodes normally contribute a multiplication function). These findings suggest the use of squarewave modulation of the varactor bias in order to achieve the gating function. The feasibility of this approach and the determination of transmit-receive isolation levels achievable thereby forms a major portion of the investigation reported here. Although it is meaningful to obtain and evaluate experimental results for and on the basis of the particular altimeter system described above, it is not intended that the investigation be totally restricted to that system.

Section 3.0 LUNAR NAVIGATION ANALYSES

A. STATEMENT OF PROBLEM AND APPROACH

The task to be fulfilled in this portion of the study was the evaluation of achievable lunar navigation accuracies when the data output of an altimeter is processed exclusively the Kalman filtering techniques. Of particular concern is the effect of lunar terrain irregularities and uncertainties on the result. Since the moon is not close at hand to allow the performance of actual trial measurements, the investigator must either establish a means of simulating the phenomena, establish a statistical-analytical representation of the phenomena, or establish some combination of both. The approach used here was the second, since it provides the greatest flexibility as compared to relatively brute force methods associated with simulation.

The first step is to establish a statistical model of the lunar terrain features with respect to a reference ellipse which approximates the shape of the moon. This model can then be used to represent (with the inclusion of appropriate trajectory dynamics) the input to an altimeter tracker model. The statistics of the altimeter output may then, in turn, be used as the input to the appropriate Kalman filter. The output of the latter, in terms of the statistical character of certain navigational parameters, is the desired result.

In the actual analyses described in this section and in Appendicies A, B, and C, the statistics of the lunar surface were derived by appropriately combining the sampled altitude data obtained from available lunar contour maps. The altimeter tracker model used included the tracker dynamics and thermal noise characteristics specified in Interim Report No. 1. Neither the effects of the finite illumination beamwidth, namely 1) pulse distortion because of terrain irregularities and 2) frequency spreading of the return signal, nor the effect of nonconstant terrain reflectivity were considered in the analysis.* The entire data processing function and error analysis were

*The adequate consideration of these effects on altimeter performance would require a rather extensive study in itself and was therefore considered beyond the scope of the present work. In view of the relative smoothness of the local terrain and the relative insignificance of altimeter errors, as found in performing the work, it is not believed that the inclusion of these factors would significantly effect the outcome of the study.

incorporated into a single computer program. The flexibility of this program allowed the analysis of several trajectorial and statistical cases of interest.

Greater navigational accuracy than that quoted in this report could be obtained from the altimeter if a countour map of the moon is stored in the space-borne computer and map-matching techniques are used. Consideration of this type of scheme was, however, beyond the scope of this study.

B. GENERAL DESCRIPTION OF ANALYSIS

The method used to perform the analysis is schematically depicted in Figure 3-1.

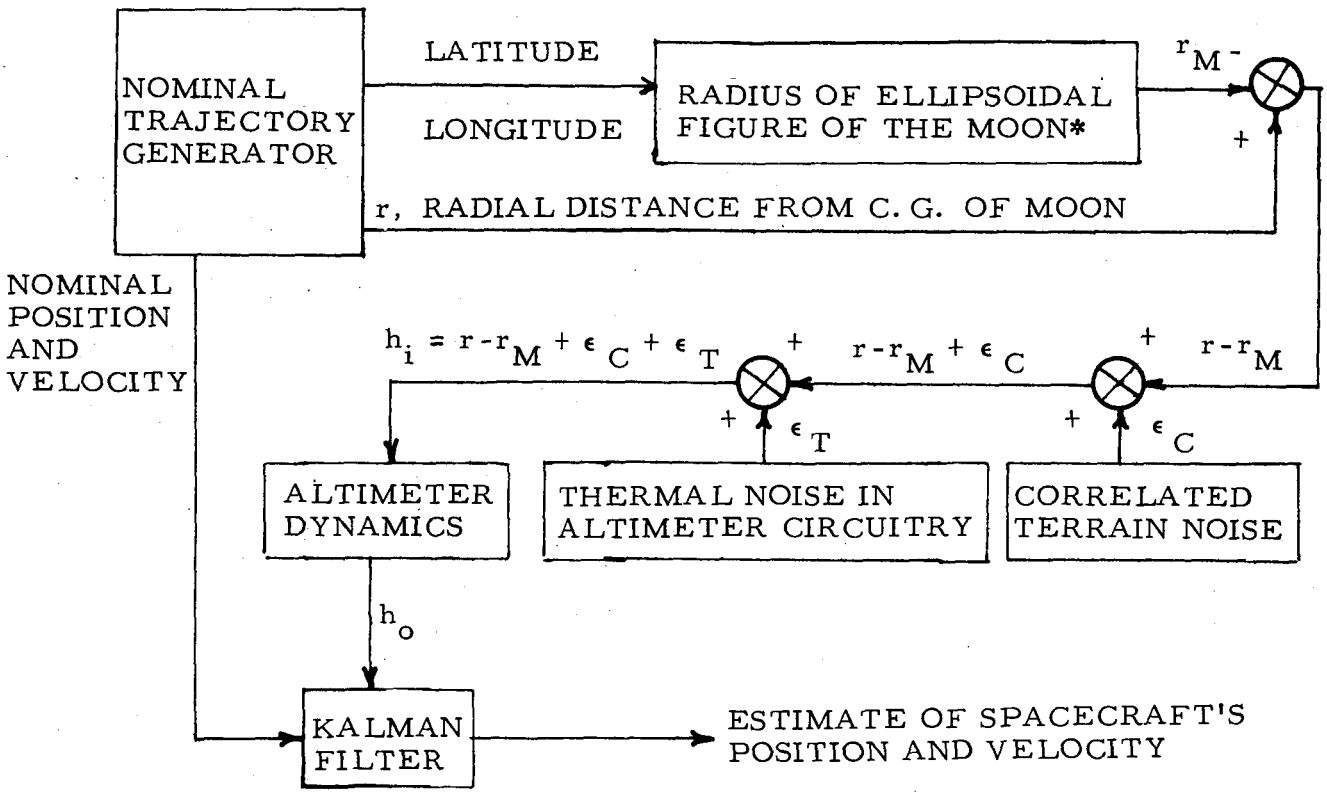

*r_M includes an unknown bias due to the uncertainty of the radius of the moon.

Figure 3-1. Altimeter Error Analysis Flow Diagram

Actual estimates of position and velocity were not obtained from the Kalman filter since only the error covariance matrix of these estimates was needed for this study and not the estimates themselves.* The Kalman filter was used only to generate the error covariance matrix. The nominal trajectory generator generated a nominal trajectory which included the effects of the moon's nonspherical gravitational potential (J_2 harmonic). The coordinate system used is shown in Figure 3-2.

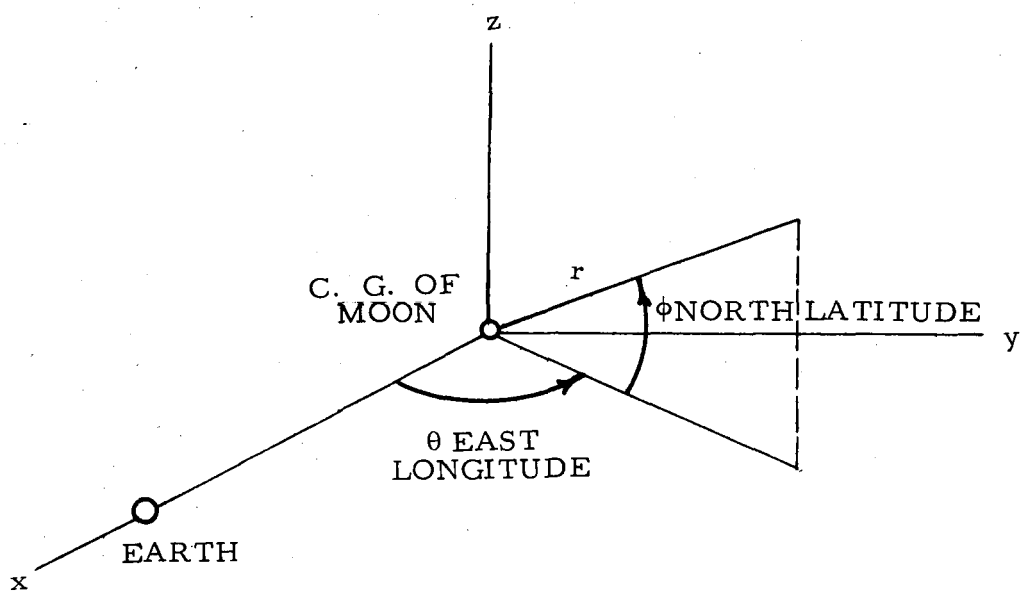

Figure 3-2. Coordinate System for Navigation Analysis

The figure of the moon was taken to be an ellipsoid represented by the equation

$$r_m = \frac{r_b}{\sqrt{1 - 2e \cos^2 \theta \cos^2 \Phi}} \qquad (3.1)$$

where

r_b = 1735 km ± 1.483 km (standard deviation)

e = ellipticity = $0.3186 \cdot 10^{-2}$ (Earth = $0.335 \cdot 10^{-2}$)

r_m = radius of moon at θ, Φ deg

*A discussion of the Kalman filter equations appears in Appendix A.

Equation (3.1) is only approximate off the equator. A discussion of its derivation will be found in Appendix B.

The correlated terrain noise, ε_c, is primarily the result of the fact that the actual shape of the moon deviates from the assumed figure of the moon. That is, long plateaus and valleys rise above and below the assumed figure of the moon, just as Colorado, Utah, and Nevada rise above the spheroid of the Earth. These plateaus and valleys give rise to long term correlated "noise" on the altimeter measurements of the altitude above the ellipsoidal figure of the moon. The autocorrelation function of this noise was taken to be

$$\phi_{(\theta_c)} = \Phi_o \, e^{-a\theta_c} \cos b\theta_c \tag{3.2}$$

where

$\phi_o = 2.59 \text{ km}^2$

$a = 1.73 \text{ radians}^{-1} = 0.0302 \text{ deg}^{-1}$

$b = 6.57$

θ_c = orbit plane central angle

Note that the first zero crossing of this autocorrelation function occurs at 13.7 deg. A derivation of the above autocorrelation function is given in Appendix B.

The thermal noise in the altimeter is assumed to be white noise with an autocorrelation function of

$$\phi_{(\tau)} = \phi_o \, \delta_{(\tau)} \tag{3.3}$$

where

$$\phi_o = 0.295 \cdot 10^{-8} \, (r - r_m)^4 \text{ km}^2 \text{ sec.} \tag{3.4}$$

The actual autocorrelation function used for the digital study was as shown in Figure 3-3.

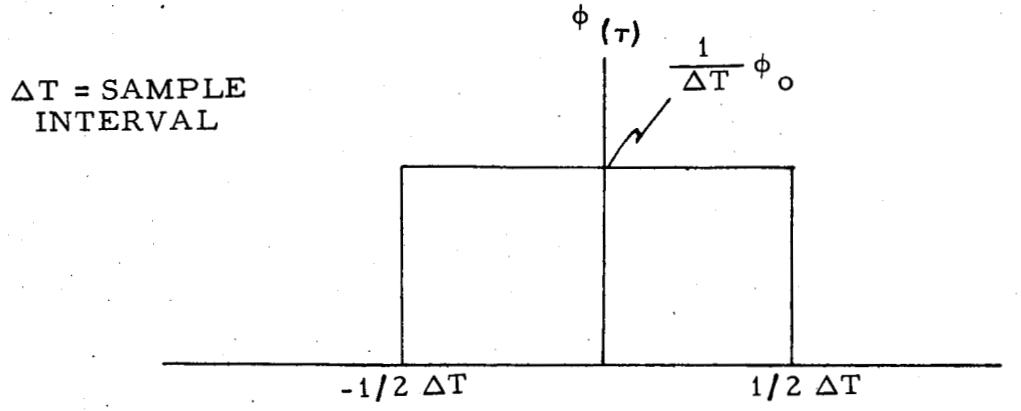

Figure 3-3. Analytical Model of Thermal Noise Autocorrelation Function

Thus, white noise was replaced by uncorrelated noise whose variance was $\frac{1}{\Delta T}\Phi_o$. The digitalized white noise might look like that shown in Figure 3-4.

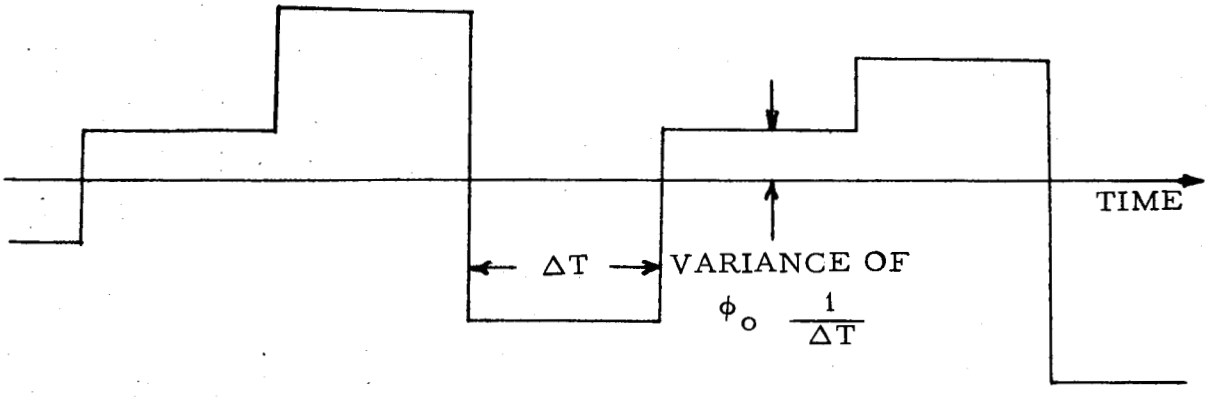

Figure 3-4. Digitalized White Noise

As the sample interval $\Delta T \rightarrow 0$, the autocorrelation function of the digitalized white noise approaches that for true white noise. As long as ΔT is small as compared to the time constants in the system, white noise and digitalized white noise will be indistinguishable from each other. The sample intervals used in this study were carefully checked to insure that the above assumption was not violated.

The mathematical model for the altimeter is given by the nonlinear integral equation:

$$\left[1 - \frac{h_i(t)}{h_o(t)}\right] * g_{(t)} + K = \frac{c}{2h_o(t)}$$

where K is a constant, c is the speed of light, and the symbol * represents the convolution integral in the time domain. $g_{(t)}$ is the inverse Laplace transform of a two pole, one zero system. The time to peak, T_p, for the altimeter is about 2 sec. A more thorough discussion of the altimeter dynamics is given in Appendix C.

C. DISCUSSION OF RESULTS

A simple example will show that an altimeter is useful not only for obtaining radial distance to the center of the moon, r, and perhaps $\dot{r}$ but is also useful for determining downrange velocity. For example, consider a nominal circular orbit. In this case $\dot{r} = 0$ and r, when divided into the moon's gravitational constant, gives the downrange velocity squared (assuming a spherical gravitational field).

If the moon had a spherical gravitational field and were round, it is obvious that there would be no way of determining latitude and longitude from an altimeter. However, the moon is not round and does not have a spherical gravitational field. Thus, for example, the acceleration because of the J_2 harmonic in the moon's gravitational field would supply latitude information and the moon's elliptically shaped equator would supply longitude information. The $J_2^{(2)}$ harmonic in the moon's gravitational field (not included in this study) would also supply longitude information. Thus the possibility exists for determining the complete position and velocity vectors from altimeter measurements; albeit downrange position, crossrange position, and crossrange velocity estimates will depend on second-order effects.

Two types of nominal orbits were considered in this study. The first was a circular, 185 km altitude orbit, and the second was a Hohmann transfer orbit. The Hohmann transfer orbit was an elliptical orbit with an aposelenum altitude of 185 km and a periselenum altitude of 18.5 km. Navigation was assumed to commence at aposelenum and stop at periselenum. Two orbit inclinations were considered. One at 0 deg inclination (equatorial orbit), the other was inclined at 10 deg to the equator. Virtually identical numerical results were obtained for both inclinations so only the 0 deg inclination results are shown in this report.

Also error analysis runs were made with and without the altimeter dynamics (as shown in Figure 3-1). That is, in one case the measurement to the Kalman filter was the output of the altimeter and in the other case the measurement to the Kalman filter was the input to the altimeter. The error analysis results were identical in both cases, confirming the theoretical expectations. Since the Kalman filter must relate whatever it measures to the differential equations of motion governing the spacecraft, the filter in effect removes the altimeter dynamics when it relates altimeter output to the equations of motion. The advantage of being able to leave out the altimeter dynamics when making error analysis runs was that the computing (or integration) time interval was no longer restricted to be less than the time constants in the altimeter dynamics and thus error analysis runs could be made using less 7094 computing time.

Just how well the altimeter can be used to estimate position and velocity can be seen from Tables 3-I through 3-III. The nomenclature used in these tables is as follows: the subscripts r, d and C stand for radial position, downrange position and crossrange position; $\dot{r}$, $\dot{d}$, and $\dot{C}$ indicate velocities in these directions, and the quantity σ_{rb} appearing in these tables is the standard deviation of the uncertainty in the moon's radius. That is, σ_{rb} is the uncertainty associated with the quantity r_b in Equation (3.1), which is the equation for the figure of the moon. The effect of not knowing r_b exactly is equivalent to having a bias on the altitude measurements. This bias or uncertainty is probably the most important (damaging) source of error in this study. σ_{rb} more or less sets a lower limit for σ_r and $\sigma_{\dot{d}}$.

The effect of choosing various a priori values of σ_{rb} upon navigational accuracy can be seen from Tables 3-IV through 3-VI. The a priori value of $\sigma_{rb} = 1.48$ km was indicated by footnotes on the lunar countour maps used for this study. The footnotes also indicated that this uncertainty was tentative and would soon be improved. Therefore, an alternate value of $\sigma_{rb} = (1/3)\,1.48 = 0.49$ km was used.

As can be seen from the tables, the altimeter does reasonably well in obtaining estimates of radial distance r, radial rate $\dot{r}$, and downrange velocity $\dot{d}$. Note that for circular orbits, downrange velocity, $\dot{d}$, and total velocity, V, are equivalent. So for these orbits $\sigma_{\dot{d}} = \sigma_V$. This relationship is also true of the Homann transfer orbit at periselenum and aposelenum.

Table 3-I. Navigation Errors With/Without Altimeter Measurements for a 185 km, Circular, Lunar, Equatorial Orbit (A Priori σ_{rb} = 1.48 km*)

Central Angle (deg)	σ_r (km)	σ_d (km)	$\dot{\sigma}_r$ (m/sec)	$\dot{\sigma}_d$ (m/sec)	σ_{rb} (km)
0	10.0/10.0	9.8/9.8	10.0/10.0	13.0/13.0	1.48/1.48
30	2.10/15.6	11.1/11.6	5.82/18.1	7.82/10.1	1.46/1.48
60	2.03/29.5	11.5/19.3	4.76/27.9	3.82/9.6	1.44/1.48
90	1.90/47.9	10.9/43.7	2.95/31.7	1.36/21.7	1.44/1.48
120	1.78/66.2	11.0/89.0	1.78/28.0	0.78/36.1	1.44/1.48
150	1.71/79.6	11.5/152	1.14/18.1	0.73/46.9	1.44/1.48
180	1.65/84.5	12.1/224	0.77/10.0	0.72/50.9	1.44/1.48
210	1.60/79.7	12.8/297	0.54/18.0	0.72/47.0	1.44/1.48
240	1.56/66.5	13.4/359	0.38/27.8	0.72/36.3	1.44/1.48
270	1.53/48.2	14.1/405	0.29/31.7	0.72/21.9	1.44/1.48
300	1.50/29.8	14.8/431	0.24/28.0	0.72/9.7	1.44/1.48
330	1.45/15.7	15.6/440	0.25/18.2	0.70/10.0	1.44/1.48
360	1.43/10.0	16.4/438	0.29/10.0	0.63/12.8	1.43/1.48

*A listing of σ_C and $\dot{\sigma}_C$ is omitted since they are the same with or without altimeter measurements. See Table 3-II for listing of σ_C and $\dot{\sigma}_C$.

Table 3-II. Navigation Errors for 185 km Circular, Lunar, Equatorial Oribt
(A Priori σ_{rb} = 0.49 km)

Number Orbits	σ_r(km)	σ_d(km)	σ_C(km)	$\dot{\sigma}_r$(m/sec)	$\dot{\sigma}_d$(m/sec)	$\dot{\sigma}_C$(m/sec)	σ_{rb}(km)
0	10.00	9.81	9.81	10.00	13.00	9.81	0.49
0.125	1.46	11.43	10.85	5.04	5.75	9.01	0.49
0.250	1.31	10.43	11.80	2.95	1.23	8.14	0.49
0.375	1.06	10.08	10.86	1.39	0.47	9.01	0.49
0.500	0.90	10.18	9.81	0.74	0.47	9.80	0.49
0.625	0.78	10.33	10.85	0.42	0.44	9.02	0.49
0.750	0.69	10.47	11.80	0.26	0.39	8.14	0.49
0.875	0.62	10.67	10.85	0.21	0.34	9.01	0.49
1.000	0.58	10.92	9.81	0.21	0.30	9.81	0.49
2.000	0.54	13.56	9.81	0.15	0.26	9.81	0.49
3.000	0.52	16.93	9.81	0.12	0.24	9.80	0.49
4.000	0.51	20.51	9.81	0.11	0.23	9.80	0.48
5.000	0.49	23.99	9.81	0.10	0.22	9.80	0.47
6.000	0.48	27.18	9.81	0.09	0.21	9.80	0.46
7.000	0.46	29.96	9.81	0.08	0.20	9.80	0.44
8.000	0.44	32.25	9.81	0.08	0.19	9.80	0.42
9.000	0.41	34.05	9.81	0.07	0.18	9.80	0.40
10.000	0.39	35.37	9.81	0.07	0.17	9.80	0.38

Table 3-III. Navigation Errors With/Without Altimeter Measurements for 185 to 18.5 km Hohmann Transfer Around Lunar Equator*

Central Angle (deg)	σ_r(km)	A Priori σ_{rb} = 1.48 km			σ_{rb}(km)
		σ_d(km)	$\sigma_{\dot{r}}$(m/sec)	$\sigma_{\dot{d}}$(m/sec)	
0	10.0/10.0	9.8/9.8	10.0/10.0	12.9/12.9	1.48/1.48
30	2.10/15.1	11.1/11.4	5.88/17.5	8.31/10.3	1.46/1.48
60	2.03/28.0	11.4/17.9	5.07/27.5	4.31/9.4	1.45/1.48
90	1.88/45.5	10.5/39.8	3.16/32.1	1.61/21.9	1.44/1.48
120	1.75/63.0	10.4/83.3	1.92/27.8	0.92/38.7	1.44/1.48
150	1.66/74.2	10.7/145	1.23/15.2	0.85/50.9	1.44/1.48
180	1.58/74.2	11.3/218	0.82/16.1	0.82/51.4	1.44/1.48
		A Priori σ_{rb} = 0.49 km			
0	10.0/10.0	9.8/9.8	10.0/10.0	12.9/12.9	0.49/0.49
30	1.51/15.1	11.1/11.4	5.83/17.5	8.29/10.3	0.49/0.49
60	1.45/28.0	11.3/17.9	5.07/27.5	4.28/9.4	0.49/0.49
90	1.29/45.5	10.1/39.8	3.16/32.1	1.47/21.9	0.49/0.49
120	1.11/63.0	9.5/83.3	1.92/27.8	0.62/38.7	0.49/0.49
150	0.97/74.2	9.4/145	1.22/15.2	0.52/50.9	0.49/0.49
180	0.87/74.2	9.4/218	0.81/16.1	0.51/51.4	0.49/0.49

*A listing of σ_C and $\sigma_{\dot{C}}$ is omitted. Maximum and minimum values of σ_C are 11.6 and 9.1 km. Maximum and minimum values of $\sigma_{\dot{C}}$ are 10.6 and 8.3 m/sec. A priori values are 9.8 km and 9.8 m/sec.

Table 3-IV. Effect of σ_{rb} on Navigation Errors at the End of One Circular Orbit

	σ_r(km)	σ_d(km)	$\dot{\sigma}_r$(m/sec)	$\dot{\sigma}_d$(m/sec)
σ_{rb} = 1.48 km	1.36	16.4	0.29	0.63
σ_{rb} = 0.49 km	0.58	10.9	0.21	0.30
σ_{rb} = 0	0.31	9.9	0.21	0.22

Table 3-V. Effect of σ_{rb} on Navigation Errors at the End of Ten Circular Orbits

	σ_r(km)	σ_d(km)	$\dot{\sigma}_r$(m/sec)	$\dot{\sigma}_d$(m/sec)
σ_{rb} = 0.49 km	0.39	35.4	0.07	0.17
σ_{rb} = 0	0.10	10.6	0.07	0.07

Table 3-VI. Effect of σ_{rb} on Navigation Errors at the End of 180 Deg on a Hohmann Transfer Orbit

	σ_r(km)	σ_d(km)	$\dot{\sigma}_r$(m/sec)	$\dot{\sigma}_d$(m/sec)
σ_{rb} = 1.48 km	1.58	11.3	0.82	0.82
σ_{rb} = 0.49 km	0.87	9.4	0.81	0.51
σ_{rb} = 0	0.72	9.1	0.81	0.46

The a priori values of σ_r, $\sigma_{\dot{r}}$, and $\sigma_{\dot{d}}$ were taken to be 10 km, 10 m/sec and 13 m/sec, respectively. These represent rather poor preliminary estimates, so that the final navigational accuracies obtained for r, $\dot{r}$, and $\dot{d}$ are relatively independent of the a priori standard deviations used. That is, larger a priori sigmas should not significantly change the final navigational accuracies obtained for r, $\dot{r}$, $\dot{d}$. Therefore, the navigational estimates are almost entirely derived from altimeter data.

The altimeter does a reasonably good job of keeping the downrange position uncertainty, σ_d, from growing. Observe from Table 3-I that with no altimeter measurements the downrange position uncertainty grows from 10 km to 450 km in one orbit. But with altimeter measurements σ_d grows very slowly, depending on the a priori value of σ_{rb}.

Since the Kalman filter does not receover (solve for) downrange position well, the final uncertainty on downrange position will be dependent on the initial uncertainty on downrange position. (In this study σ_d, a priori, was 9.8 km.) It may also depend to some extent on the a priori standard deviations of the uncertainties on r, $\dot{r}$, and $\dot{d}$. A parametric study of this was not performed. However, one would be reasonably safe in assuming that altimeter measurements could be used to keep downrange position uncertainty from growing rapidly.

Altimeter measurements seem to be of little or no use in obtaining crossrange velocity or position information when the orbit inclination is small. In all of the cases studied no improvement in crossrange position and velocity uncertainties was obtained as compared with orbits in which no measurements at all were taken. Indeed, upon looking at the error covariance matrix of 0 deg inclination orbits, it was observed that crossrange position and velocity were not correlated with any other state variable. Hence the filter was in effect not solving for crossrange position and velocity. That is, C and $\dot{C}$ were nonobservables. On 10 deg inclination orbits C and $\dot{C}$ were observables, but the Kalman filter was not able to appreciably reduce their uncertainties under those that would exist if no measurements were taken.

The analytic expressions for crossrange position and velocity uncertainties are, for circular orbits and no measurements, and for spherical gravitational fields

$$\sigma_C^2 = \bar{\sigma}_C \cos^2 \theta_C + \bar{\sigma}_{\dot{C}}^2 \frac{1}{\dot{\theta}_C^2} \sin^2 \theta_C$$

$$\sigma_{\dot{C}}^2 = \bar{\sigma}_C^2 \theta_C^2 \sin^2 \theta_C + \bar{\sigma}_{\dot{C}}^2 \cos^2 \theta_C$$

where the bar over the sigmas indicates a priori values and θ_C represents central orbit angle. Note that the equations for σ_C^2 and $\sigma_{\dot{C}}^2$ contain no secular terms that grow beyond all bounds. That is, the bounds of σ_C are $\bar{\sigma}_C$ and $\frac{1}{\dot{\theta}_C} \bar{\sigma}_{\dot{C}}$ · $\sigma_{\dot{C}}$ is bounded by $\bar{\sigma}_C \dot{\theta}_C$ and $\bar{\sigma}_{\dot{C}}$. For this study the a priori values of σ_C and $\sigma_{\dot{C}}$ were chosen to be

$$\bar{\sigma}_C = 9.8 \text{ km} \quad , \quad \bar{\sigma}_{\dot{C}} = 9.8 \text{ m/sec}$$

For a circular 185 km altitude orbit,

$$\dot{\theta}_C = 0.830 \cdot 10^{-3} \text{ rad/sec}$$

Thus, σ_C was bounded by

$$9.81 \leq \sigma_C \leq 11.8 \text{ km}$$

and $\sigma_{\dot{C}}$ was bounded by

$$8.14 \leq \sigma_{\dot{C}} \leq 9.81 \text{ m/sec}$$

Table 3-VII shows the effect of correlated terrain noise on navigational accuracy. The only random noise in the system, when the terrain noise is removed, is the thermal noise introduced by the altimeter circuitry. Perhaps the most interesting result in Table 3-VII is that the downrange position

uncertainty is actually improved after one orbit. Removing the terrain noise corresponds to orbiting a smooth, elliptical moon and thus is not a physically real situation. However, it does give an indication of the accuracies achievable with map matching techniques, although map matching undoubtedly would be more accurate than indicated by Table 3-VII. Map matching merely means that a much more sophisticated figure of the moon, than is given by Equation (3.1) (an ellipsoid), would be used.

Table 3-VII. Navigation Errors With/Without Correlated Terrain Noise for Circular Orbit (A Priori σ_{rb} = 0.49 km*)

Central Angle (deg)	σ_r(km)	σ_d(km)	$\sigma_{\dot{r}}$ (m/sec)	$\sigma_{\dot{d}}$ (m/sec)
0	10.0/10.0	9.81/9.81	10.0/10.0	13.00/13.00
45	1.46/0.52	11.43/9.82	5.04/0.87	5.75/1.01
90	1.31/0.51	10.43/9.77	2.95/0.29	1.23/0.24
135	1.06/0.51	10.08/9.82	1.39/0.15	0.47/0.21
180	0.90/0.50	10.18/9.53	0.74/0.08	0.47/0.21
225	0.78/0.49	10.33/9.26	0.42/0.06	0.44/0.21
270	0.69/0.49	10.47/9.14	0.26/0.04	0.39/0.20
315	0.62/0.49	10.67/8.09	0.21/0.03	0.34/0.21
360	0.58/0.49	10.92/7.99	0.21/0.02	0.30/0.21

*See Table 3-II for a listing of σ_C and $\sigma_{\dot{C}}$.

D. CONCLUSIONS

The major assumptions made in performing this study were as follows. The first zonal harmonic, $J_2^{(2)}$, of the moon's gravitational field was assumed to be known perfectly and that its value was zero. Assuming a non-zero value of $J_2^{(2)}$ should help in determining downrange position around the equator since $J_2^{(2)}$ causes predictable altitude variations which are longitude dependent. Assuming a non-zero variance for $J_2^{(2)}$ would tend to degrade the navigational accuracies since altitude variations would not be exactly predictable. For single orbit cases it is doubtful that any significant

change in the results of the error analysis would occur if $J_2^{(2)}$ and its uncertainty had been included in the error analysis.

The autocorrelation function used for the correlated ground terrain noise was taken as [see Equation (3.2) .]

$$\phi_{(\theta_C)} = \phi_o \, e^{-a\theta_C} \cos b\theta_C$$

As the spacecraft orbits the moon in an equatorial orbit it will see the same ground terrain noise on every pass. Therefore the autocorrelation function of the terrain noise is periodic and should be given by the Fourier expansion

$$\phi_{(\theta_C)} = \frac{1}{2} a_o + \sum_{n=1}^{\infty} a_n \cos n\,\theta_C \qquad (3.5)$$

where

$$a_n = \frac{2}{\pi} \phi_o \int_o^{\pi} e^{-a\theta_C} \cos b\theta_C \cos n\theta_C \, d\theta_C \qquad (3.6)$$

The computational difficulties associated with including such an autocorrelation function in a Kalman filter appeared to be so formidable that it was considered to be beyond the scope of this study to consider such an autocorrelation function. The effect of including such a sophisticated autocorrelation function to the study would be to enhance the navigational accuracies, since on multiple orbits the Kalman filter would recognize that it was seeing the same noise over and over again. For single orbits it is doubtful that much improvement would be noticed.

One final assumption is worth noting about the navigational accuracies listed in this report. Position and velocity information supplied by an altimeter must be referenced to a coordinate system which is supplied by an inertial platform. An uncertainty as to how the platform is aligned would

degrade the accuracy of the information supplied by the altimeter-Kalman filter when this information was transformed into platform coordinates. This problem is not unique to an altimeter. Most navigational devices encounter this problem.

The degree of sophistication used for the mathematical models in this study would insure that the numerical results of the study are reliabile. For example, a spherical model of the moon would have given the result that no downrange position information could be obtained from altimeter measurements. Using correlated noise insured that an uncorrelated noise assumption would not be violated (which it would have been at the sample rates used for this study). Runs were made to see if the Earth's gravitational field had any effect on the error analysis; it did not. Any further improvements of the mathematical models will probably show only minor adjustments of the numerical results presented here.

Altitude above the actual surface of the moon is $h = r - r_M + \varepsilon_C$, where r_M is given by Equation (3.1). The raw output of the altimeter gives h to an accuracy* of about 1 percent, 1σ, at 185 km. The Kalman filter may also be used to give an estimate of h, using the raw altimeter data as an input. A spot check of the results showed that for a circular, 185-km altitude orbit, the Kalman filter would give h to ± 0.33 km, 1σ, after one-half orbit and to ± 0.25 km after one orbit. Thus, for applications such as high altitude contour mapping, optimally filtered altimeter data is superior to the raw altimeter output. When the terrain noise was removed, then h was obtained to ± 0.086 km after one-half orbit, thus illustrating that the correlated variations in terrain are a major error source in the determination of actual altitude.

In summary, the study shows that an altimeter is capable of determining downrange and vertical velocity to accuracies better than 1 m/sec in one-half orbit, and hence the velocity magnitude to better than 1 m/sec.

---

*Due to thermal noise. The overall effect of finite beamwidth and nonconstant terrain reflectivity may not truly be negligible when considering the accuracy of altitude-only determinations such as done here. The same trend in results as indicated here would be expected, however.

The radial position uncertainty can be reduced to approximately the uncertainty in the astronomic knowledge of the moon's radius, and for multiple orbits the uncertainty of the moon's radius itself will be reduced. An altimeter can be used to keep downrange position uncertainty from growing rapidly. For small orbit inclinations the altimeter offers little or no crossrange (latitude) position or velocity information. However, crossrange position and velocity errors contain no secular terms so if a priori estimates of these quantities are good then crossrange position and velocity errors will remain small.

4. VARACTOR BIAS GATING EXPERIMENTS

A. STATEMENT OF PROBLEM AND APPROACH

The problem of determining and evaluating the effective isolation levels achievable by means of varactor bias modulation will be discussed in this section. Theoretically, perfect isolation can be obtained simply by asynchronously gating the transmitter and local oscillator of a high duty-factor system such that there is no overlap of the gating functions. In a typical operation, the gating is accomplished at such a rate that the energy returning from the target (e.g., the lunar surface) arrives precisely during the interval that the receiver is ON. In practice, one does not of course expect perfect isolation because of imperfect turn-off, finite rise and decay characteristics, spurious spectral components generated by the periodic gating function itself, and mutual coupling between system components. These factors obviously cannot be predicted analytically with any degree of accuracy. The investigator must therefore employ an entirely experimental approach to determine achievable isolation levels. Evaluation of the results can, however, be approached analytically.

The approach used in the actual investigation reported here involved three basic steps. The first was the static testing of the power sources used as the output stages of the transmitter and local oscillator chains. The purpose of these tests was to determine the ON-OFF ratios achievable when the bias of the contained varactors was appropriately varied. The second step involved setting up the primary transmitter-receiver elements of the extended range altimeter* in the laboratory. Some of these elements were available in the laboratory while others were fabricated specifically for this investigation. The leakage levels at the output of the first mixer (see Figures 2-2 and 4-1) could then be monitored to the extent limited by narrow-band receiver sensitivity. A gate generation scheme which would allow manual variation of the system PRF duty factor and pulse position was required so that system performance could

*Following the essence of the design specified in Interim Report No. 1.

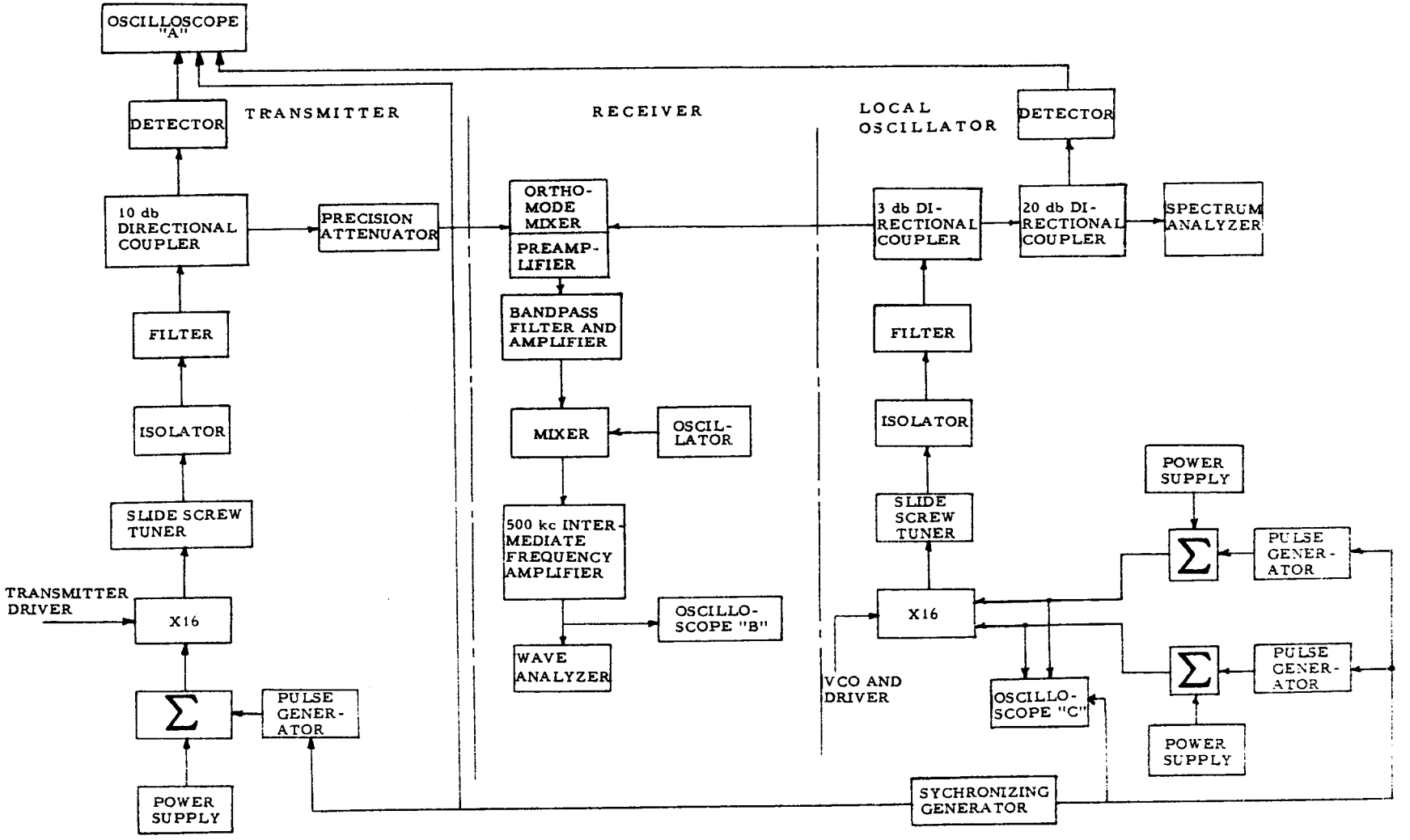

Figure 4-1. Laboratory Set Up for Isolation Measurement — Block Diagram

be monitored as a function of these parameters. System isolation could then be determined by observing relative power levels at the output of the first mixer when the transmitter and receiver were gated synchronously and asychronously, corresponding to maximum ON and OFF conditions, respectively.

The last step in the general procedure was that of evaluating the experimental results. The primary criterion for evaluation was derived on the basis of isolation requirements as envisioned for the extended range altimeter. A complete derivation of these requirements, including the assumed definition of isolation can be found in Appendix D. Thus, comparison of the experimental results with the requirements can serve as a tangible means of evaluation.

B. LABORATORY PROCEDURES AND FINDINGS

1. STATIC MULTIPLIER TESTS

Two separate UHF to X-band varactor power sources were constructed. The first contained two varactors with each varactor providing a times-four multiplication function. Initially, provision was made for gating the second of the two varactors, i.e., the higher frequency varactor. Static variation of the bias voltage of the high frequency varactor indicated an achievable ON-OFF power ratio of about 67 db for the multiplier chain. It was also found that forward biasing the varactor provides a better means of switching the multiplier OFF than detuning by reverse bias. A plot of multiplier power output versus bias voltage for the static test condition is given in Figure 4-2. Since the ON-OFF ratio achieved by this technique obviously cannot provide the high altitude altimeter with a sufficient level of transmit-receive isolation, the lower frequency times four multiplier was modified to provide accessibility of its varactor. A static bench check of the lower frequency varactor indicated an ON-OFF power ratio for the multiplier chain better than 100 db (these preliminary tests employed an Empire Devices Field Intensity Meter Model NF-112 which is incapable of determining isolation values greater than 100 db for the power levels involved here). The second X16 (times 16) power source built contained four varactors with each varactor acting as a doubler. This unit provides a greater power handling capability and is referred

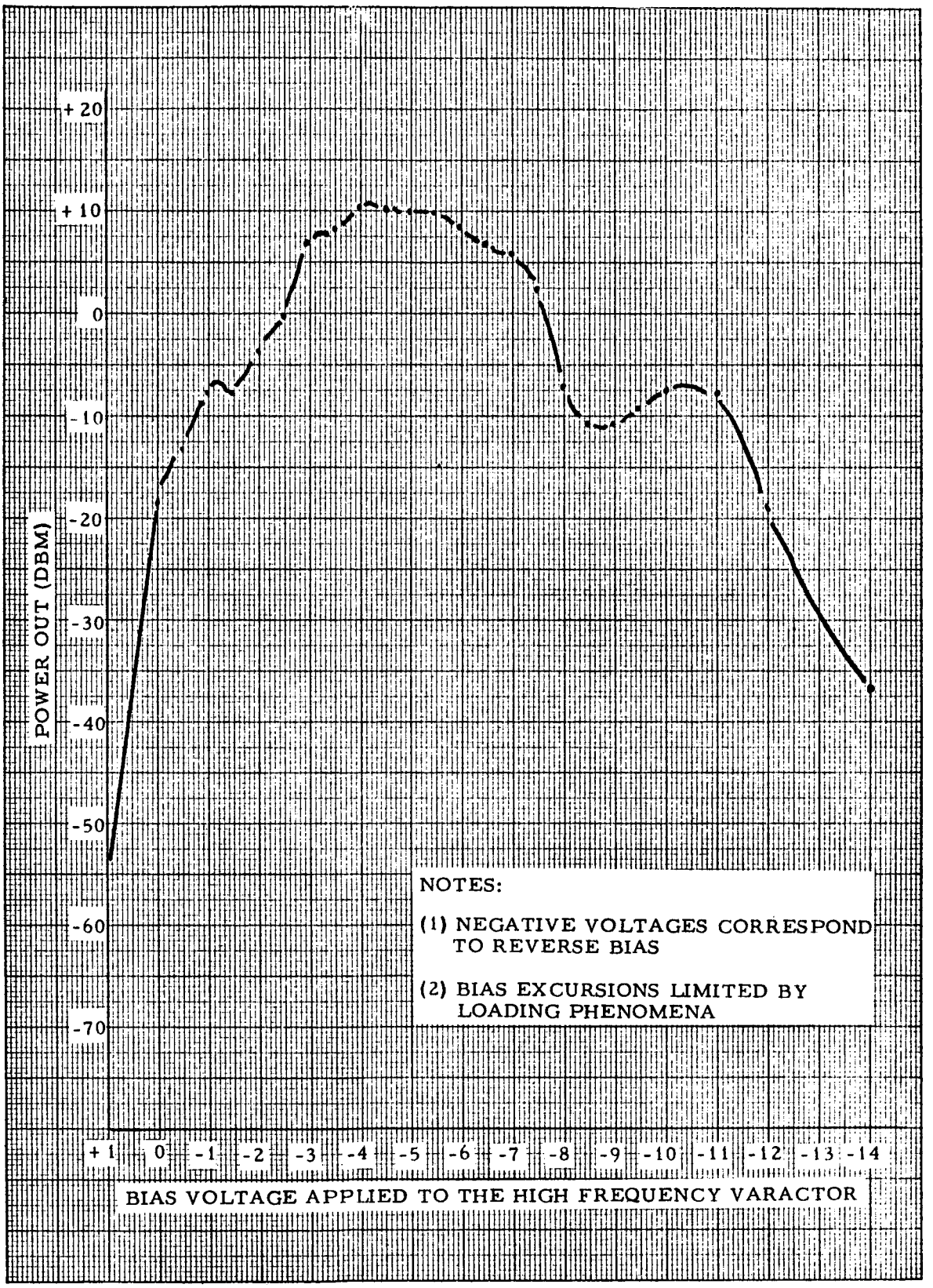

Figure 4-2. Low Power Multiplier Output Characteristics

to as the high power source while the first is referred to as the low power source. Bench testing of the high power source with the Empire Devices Field Intensity Meter indicated isolation capabilities in excess of 100 db.

2. LABORATORY SETUP FOR ISOLATION MEASUREMENTS

In order to determine the static and dynamic transmit-receive isolation of the extended-range altimeter through varactor bias gating to a value in excess of 100 db, the primary transmitter receiver elements of the altimeter were assembled in the laboratory. Leakage levels out of the first mixture were monitored to an extent limited by narrow-band receiver sensitivity. A gate generation system was used which allowed manual variation of system PRF, duty factor, and relative pulse position. Figure 4-1 is a block diagram of the test set up. The test setup may be described as follows:

(1) The output of the LO (local oscillator) X16 varactor source is fed through a slide screw tuner for matching to the waveguide. The signal then passes through an isolator, X-band filter and a 3-db coupler. One branch of the 3-db coupler is fed to the input part of the Orthomode balanced mixer. The other branch of the 3-db coupler is fed to a crystal detector for presentation of the LO RF envelope by oscilloscope "A". A portion of this signal is also fed to an X-band spectrum analyzer, Polarad Model TSA.

(2) The RF output of the transmitter X16 varactor source is fed through a slide screw tuner, an isolator, X-band filter, and a 10-db directional coupler. The low power level signal at the output of the coupler is fed to a crystal detector for presentation of the transmitter RF envelop by the dual trace oscilloscope "A". The high power level signal from the 10-db directional coupler is passed through a precision X-band variable attenuator, PRD type X101, and then into the receiver part of the Orthomode mixer.

(3) The transmitter and LO frequencies are such that the frequency of the IF output of the Orthomode mixer is 65 Mcps. A 65 Mcps preamplifer has been built directly onto the Orthomode mixer to help minimize the receiver noise figure and provide more optimum matching. After filtering

and additional amplification the receiver signal is again mixed, this time with a 65.5 Mcps sec LO signal. After amplification through two stages of IF at 500 Kcps with approximately 60-Kcps bandwidth, the signal is amplitude monitored by the Hewlett Packard 310A wave analyzer. The wave analyzer provides an overall noise bandwidth of about 200 cps. The center frequency of the wave analyzer filter can be AFC'd to the received signal frequency. Oscilloscope "B" presents the total wave form of the signal present at the output of the 500 Kcps IF.

(4) The two varactors of the LO are bias-controlled by dc power supplies with ac modulation from the Rutherford Electronics Company Pulse Generators Model B7B, superimposed on the dc level in the adder networks. The first (low frequency) varactor in the X16 power source of the transmitter is bias-controlled in the same manner as that of the LO varactors.

Photographs of the laboratory set-up, including call-outs of the essential components, are shown in Figure 4-3 and 4-4.

3. SYSTEM STATIC TESTS

The ON-OFF power ratio of the transmitter when dc gating the low frequency varactor was determined with the aid of the aforementioned test set up. Dc voltage only was applied to the varactors of the LO and transmitter sources. The levels were adjusted to provide maximum stable RF output signals. The variable attenuator in the transmitter leg was adjusted to develop a relatively large output of 130 mv from the 500 Kcps IF amplifier. However, this signal amplitude is well within the linear dynamic range of the system. The transmitter low frequency varactor was gated OFF by forward biasing it with a current of 7 ma. Under this condition, the wave analyzer measured 25 μv. Reducing the RF attenuator from 65 to 0 db showed no change in the wave analyzer's indicated signal strength of 25 μv. Hence, the ON-OFF power ratio in db is greater than

$$20 \log \frac{130 \times 10^{-3}}{25 \times 10^{-6}} + 65 \text{ db} = 74 + 65 = 139 \text{ db.}$$

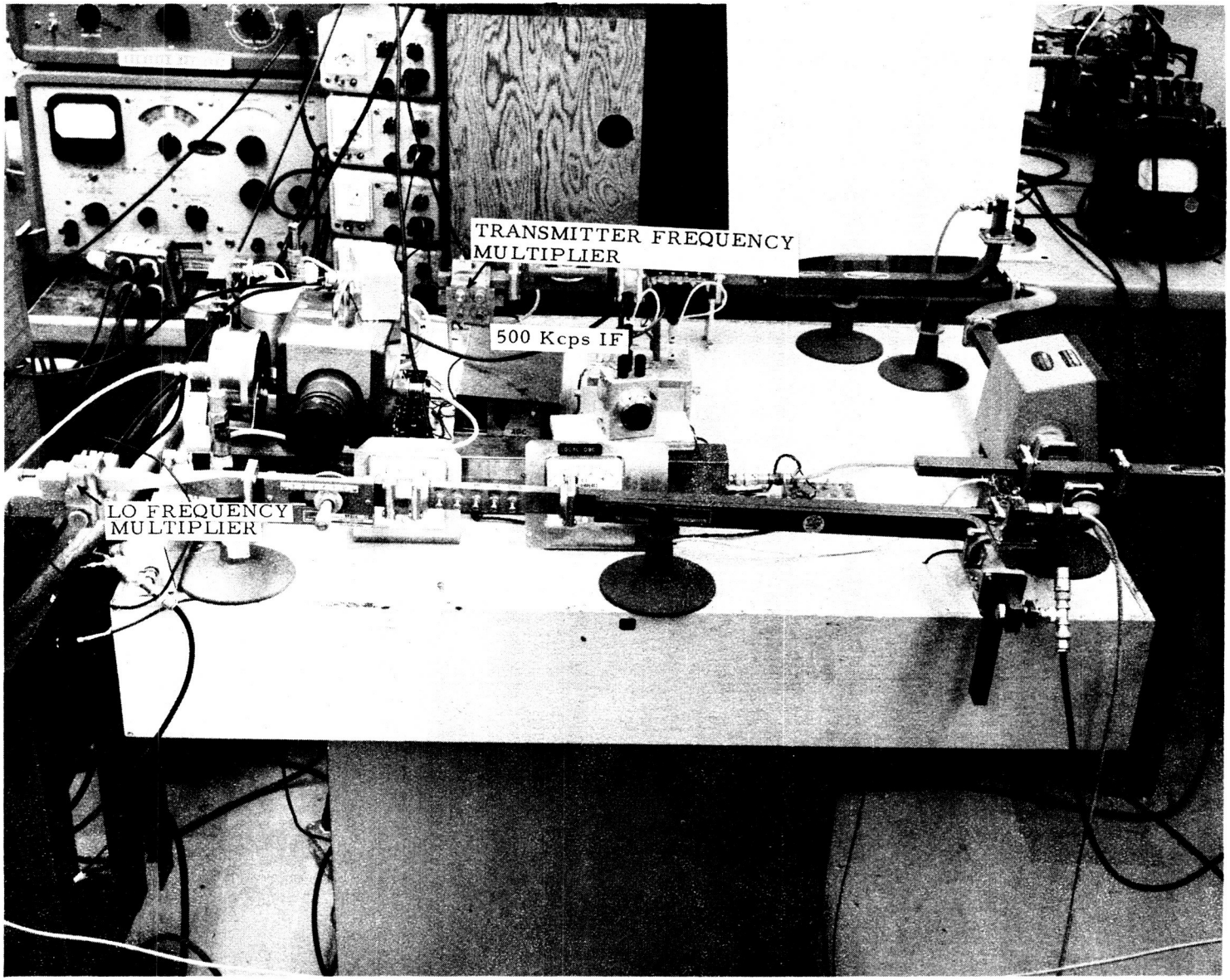

Figure 4-3. Primary Transmitter and Receiver Components

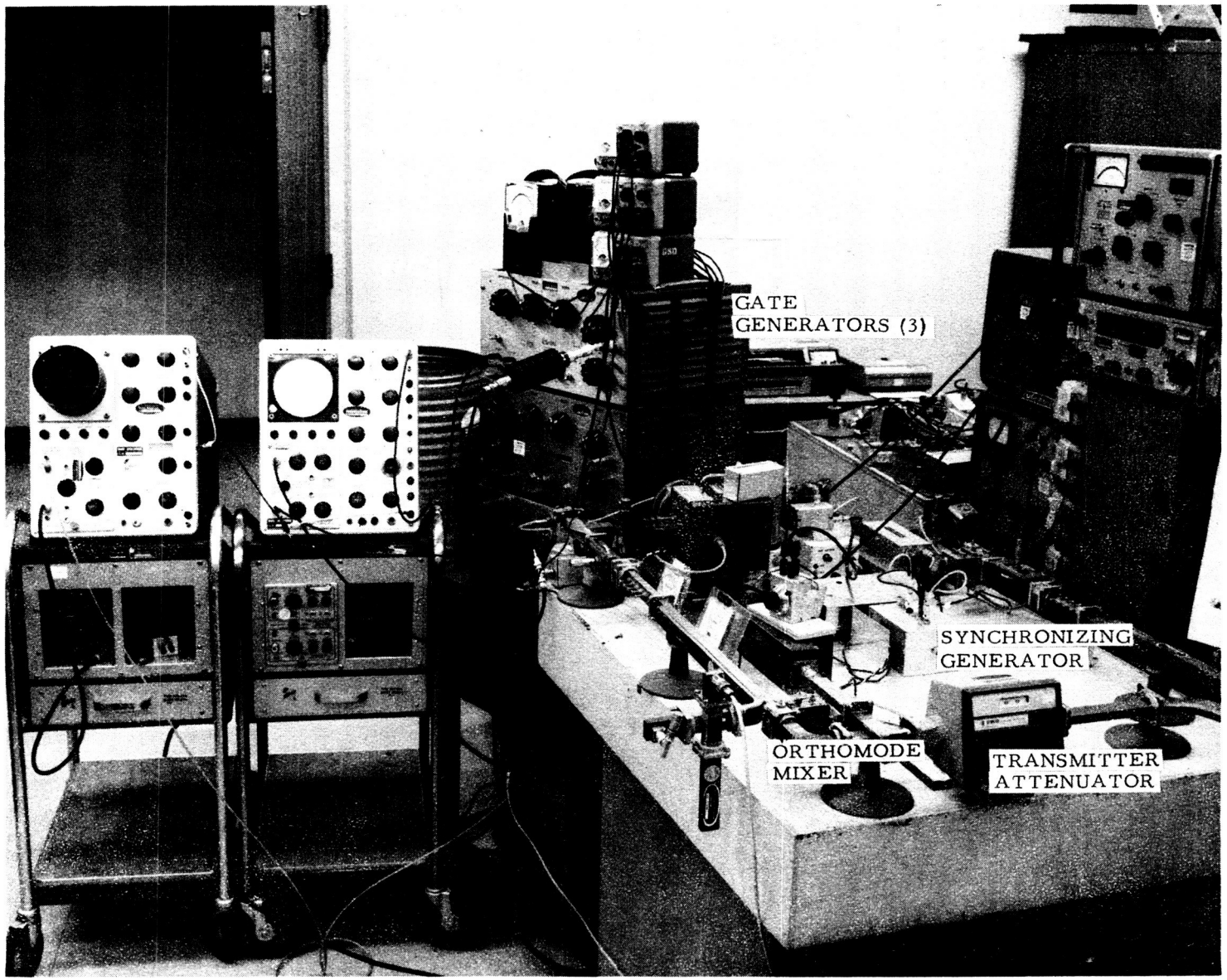

Figure 4-4. Laboratory Set Up and Peripheral Equipment

In a similar manner, but by placing the variable RF attenuator in the LO line, the ON-OFF power ratio of the LO output for gating the low frequency varactor was found to be 118 db. The forward bias current was set at 4 ma. Additional forward bias did not improve the ON-OFF power ratio. By dc gating (i.e., stepwise varying the dc bias between maximum ON and maximum OFF values) both varactors of the LO, it was found that the ON-OFF power ratio improved to a value of 133 db. The signal level in the wave analyzer was 32 μvolts with both varactors biased OFF. The LO was then completely shut off by disconnecting its excitation. The receiver thermal noise under this condition was measured as 25 μvolts. In order to reduce further the gated OFF LO signal while still employing the technique of varactor bias gating, the LO should be constructed like the transmitter power source and consist of four x2 varactor multipliers in cascade. It would be expected from the previous results with the transmitter that only the first low frequency varactor would require gating.

The noise figure (N. F.) for the entire receiver can be calculated from the data obtained for determining the transmitter ON-OFF power ratio with the knowledge that the transmitter X-band output is 5.6 mw.

$$P_{on} = K\ T\ B\ G\ N.F.$$

where

P_{on} = the output noise power from the 500 Kcps IF.

KT = Boltzman's constant times the absolute temperature (4×10^{-21}) watts/cps

G = The power gain of the entire receiver

B = The noise bandwidth of the measuring system, 200 cps

$$N.F. = \frac{P_{on}}{KTBG} = \frac{(V_{on})^2 (P_{is})}{R_o KTB \frac{(V_{os})^2}{R_o}} = \frac{P_{is}\ V_{on}^{\ 2}}{KTB\ V_{os}^{\ 2}}$$

where

V_{os} = the output voltage level measured by the wave analyzer for an input power level at the first mixer of P_{is}. The latter power level differs from the transmitter output by the amount of attenuation (65 db) inserted.

V_{on} = the output noise level measured by the wave analyzer with no signal input from the transmitter

since

P_{is} = -57.5 dbm

KTB = -151 dbm

$\frac{V_{on}^2}{V_{os}}$ = -74 db

hence

N. F. = -57.5 + 151 - 74 = 19.5 db

This value for the receiver noise figure is high, relative to values measured previously. It is suspected that a mixer crystal has deteriorated or the first IF stage has become excessively noisy. The noise figure may be improved by about 10 db, making it possible to measure the static transmitter ON-OFF ratio with an additional sensitivity factor of 10 db.

4. DYNAMIC TESTS

The first set of formal measurements were taken with gating the first varactor in the transmitter power source and the first varactor in the LO source. The two pulse generators employed, one for driving the transmitter varactor and the other for driving the LO varactor, were adjusted to have a pulse repetition frequency of 570 cps with approximately 50 percent duty cycle. The two generators were synchronized by the external synchronizing generator. Initially the varactors of both the transmitter and the LO were turned ON and OFF coincidentally (i. e., gated in synchronism). With the variable RF attenuator in the transmitter line set at 65 db, (a level sufficient to keep the incident power below receiver saturation levels) the receiver signal measured by the wave analyzer was 56 mV. By adjusting the delay controls of the pulse generators, the ON-OFF occurrences of the transmitter and LO were brought into anticoincidence. Sufficient dead times between transmitter and LO pulses were provided so that there was no pulse overlap. This action was monitored by the dual trace scope connected to the transmitter and LO envelope detectors. The oscilloscope was externally synchronized by the synchronizing generator. The receiver noise with the transmitter completely

disconnected, as measured by the wave analyzer, was 32 μvolts. During anticoincidence gating, the receiver had an output level as a function of transmitter RF attenuation as given in the following tabulation:

Attenuation Setting (db)	Wave Analyzer (μvolts)
65	32
40	32
25	32
20	56
15	100
10	140

The sudden increase in the receiver output when the attenuator setting was decreased below the 25-db level can be attributed to the radical change in conversion efficiency of the mixer with the incremental increase in applied transmitter signal. During the transmitter ON time, the low level LO leakage signal is ineffectual in mixing with the transmitter signal for transmitter power levels below 0.05 milliwatts. At the higher transmitter power levels, attenuator settings of 20 db or less, linear mixer action begins to take place and the mixer conversion efficiency increases markedly. A verification of the fact that it is the LO OFF leakage signal that was the primary factor causing the output to increase was obtained by physically disconnecting the drive to the LO source and noting that the receiver output drops to 22 μvolts. This premise is further supported by the better results obtained when double-gating the LO, as described in the following paragraphs. The isolation measurement for this case at a 10 db attenuator setting* may be derived in accordance with the measurement techniques described in Appendix D as follows:

$$55 \text{ db} + 20 \log \frac{56 \times 10^{-3}}{140 \times 10^{-6}} = 107 \text{ db}$$

* An attenuator setting of 10 db provides a transmitter leakage level at the input to the mixer which corresponds approximately to the level anticipated to occur in the case of the extended range altimeter, which is of prime, but not exclusive, interest here.

5. DOUBLE VARACTOR GATING OF THE LOCAL OSCILLATOR

Additional dynamic tests were performed while simultaneously gating both varactors of the LO source. Data was taken at PRF's of 300 cps and 1, 10, and 40 Kcps. A compilation of this data is given in Table 4-I. In the strict sense of the definition given in Appendix A, the tabulated isolation values* represent the actual achieved isolation levels. Analysis of the measurements recorded under various conditions of disconnect (i. e., the numbered tabulations) show that the power levels being measured in the anticoincidence mode were generated primarily by self-intermodulation of the gated transmitter and LO waveforms rather than by direct feedthrough of the transmitter signal. These components may equally validly be associated with either the varactor modulation technique itself or with the effective receiver noise level. If the former association is accepted, then the calculated isolation values are indeed the values of interest. Since the extent of the intermodulation is necessarily dependent upon operational bandwidths as discussed in the next paragraph, then isolation must also be considered bandwidth dependent. If, on the other hand, the receiver noise association is accepted, then the actual isolation levels (i. e., those levels limited only by incomplete transmitter and LO turnoff) must be considered as greater than those calculated. In particular, in the latter case, it may be said that at no time was it possible to make a measurement of the actual isolation value, as the effective background noise in the receiver was the limiting factor.

The data in Table 4-I shows that the effective receiver background noise (including self-intermodulation components) increases with increasing pulse repetition rates. This is understandable since the order of harmonic sideband required of the LO or transmitter to produce a 65 Mcps intermodulation tone in the mixer drops with increasing repetition frequency. After the data of Table 4-I had been taken, a relatively narrowband RF filter was inserted between the output of the LO and mixer, and another

* The isolation values are indicated at attenuator settings of 0 db since this is about the level at which the output readings increase significantly with decreasing attenuation. Similar values could be derived at the attenuation settings of 10 db (see previous footnote). Since the output power levels at this point are clearly below the effective receiver noise level, however, the result would be a pessimistic estimate of the true isolation achieved.

Table 4-I. Isolation Measurements

	Transmitter RF Attenuation Setting (db)	Receiver Output Voltage for Transmitter and LO Coincidence (mv)	Receiver Output Voltage for Anticoincidence (μvolts)	Measured* Value of Isolation (db)
PRF = 300 cps	60	54		
	60		18	
	14		18	
	10		18	
	5		18	
	0		30	125.1
1. Disconnect LO Drive	0		26	
2. Reconnect LO Drive and Disconnect Transmitter Drive	0		18	
3. Disconnect LO Drive and Transmitter Drive	0		18	
PRF = 1 kcps	60	64		
	60		22	
	14		22	
	10		22	
	5		24	
	0		50	122.1
1. Disconnect LO Drive	0		42	
2. Reconnect LO Drive and Disconnect Transmitter Drive	0		35	
3. Disconnect LO Drive and Transmitter Drive	0		18	
PRF = 10 kc	60	52		
	60		44	
	17.5		44	
	14		44	
	10		44	
	5		60	
	0		100	114.3
1. Disconnect LO Drive	0		70	
2. Reconnect LO Drive and Disconnect Transmitter Drive	0		100*	
3. Disconnect LO Drive and Transmitter Drive	0		18	
PRF = 40 kcps	50	72		
	50		200	
	17.5		160	
	14		170	
	12.6		170	
	10		160	
	5		160	
	0		300	97.6**
1. Disconnect LO Drive	0		100	
2. Reconnect LO Drive and Disconnect Transmitter Drive	0		240*	
3. Disconnect LO Drive and Transmitter Drive	0		17	
4. Disconnect Transmitter Drive and Connect LO Drive	60		100*	

* As the transmitter attenuation is increased (transmitter disconnected) the LO noise drops back to nominal value. There appears to be reflection in the transmitter line when attenuation is minimum which unbalances the mixer.

** The isolation measurement at this point was improved by about 22 db by including RF filters in the transmitter and LO lines.

narrowband filter was placed between the transmitter output and mixer. By reducing the sidebands associated with the modulation of the RF signals, the effective receiver sensitivity was considerably increased at the higher pulse repetition frequencies. A measurement of the isolation ratio was repeated at a PRF of 40 Kcps. The measured value improved from the previously measured 97 to 119 db.

For the transmitter RF attenuation setting of 0 db, the background noise limiting the sensitivity of the receiver is wholly attributed to the intermodulation of the transmitter sidebands. By inserting a filter with a sharper cutoff than the one used, the noise level can be reduced further.

It is possible to further improve the measuring capability of the test setup by using a better 65 Mcps preamplifier whose noise figure in combination with the Orthomode mixer could provide a minimum 10 db N. F. rather than the approximately 20 db of the present system. The noise bandwidth of the measuring system can be decreased from the 200 cps furnished by the Hewlett-Packard 310A wave analyzer to the 3-1/2 cps bandwidth of the Hewlett-Packard 302A by further mixing the output of the present receiver with a third LO down to the 50 Kcps IF acceptable for measurement by the 302A wave analyzer. The signal from the receiver at 500 Kcps can still be fed directly into the 310A wave analyzer and the signal to be mixed down for driving the 302A can come from the narrowband amplifier output of the 310A. However, there may be a problem of maintaining the IF signal within the 3-1/2 cps bandwidth even with the AFC controls turned to the ON position in both wave analyzers. Figures 4-5 and 4-6 contain a series of photographs that were taken of the more important waveforms appearing at the various points in the test setup. Photographs a through d are for the 1 Kcps modulation rate. Photograph a) shows the IF wave from the receiver output, b) shows the two signals of the squarewave generators driving the LO varactors, c) shows the dual trace presentation of the outputs from the two RF crystal detectors with the transmitter envelope appearing on top and the LO envelope at the bottom of the photograph, and d) is an expanded view of c). Photographs e through h are the same as the aforementioned pictures but were taken with the modulation frequency at 40 Kcps.

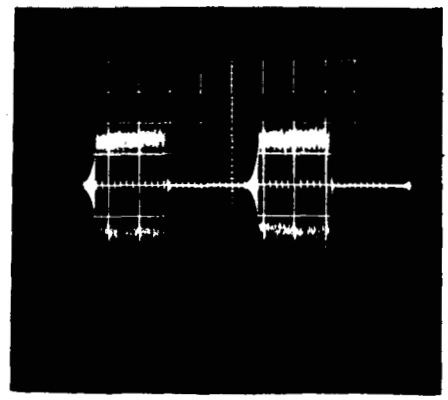

(a) IF Wave Form at the Receiver Output, PRF = 1 Kcps, Vertical = 0.1 volt/cm, Horizontal = 200 μs/cm

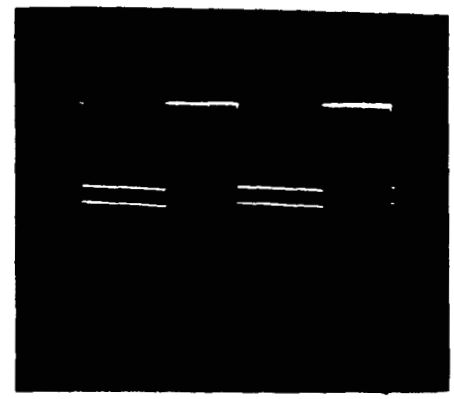

(b) The Two Square Wave Generator Signals Driving the LO Varactors, PRF = 1 Kcps, Vertical = 5 v/cm, Horizontal = 200 μs/cm

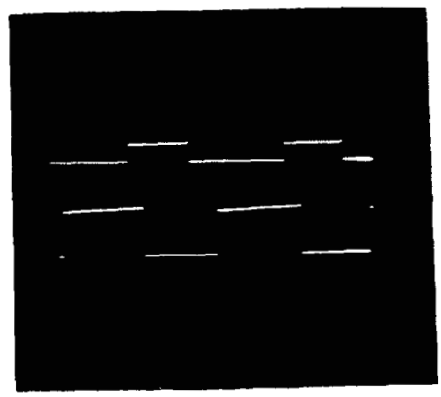

(c) Dual Trace Presentation of the Outputs from RF Crystal Detectors With the Transmitter Envelope at the Bottom of the Photograph, PRF = 1 Kcps, Vertical = 50 mv/cm, Horizontal = 200 μs/cm

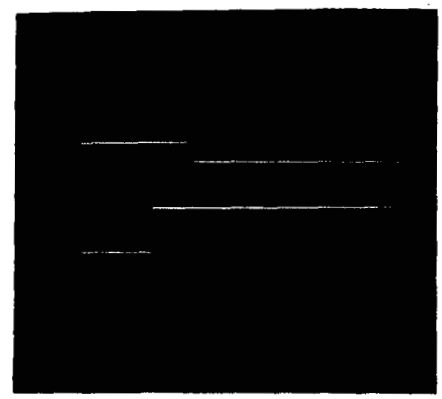

(d) Expanded View of (c) for Investigating Overlap Conditions, PRF = 1 Kcps, Vertical = 50 mv/cm, Horizontal = 2 μs/cm

Figure 4-5. Pertinent Waveforms — 1 Kcps Modulation Rate

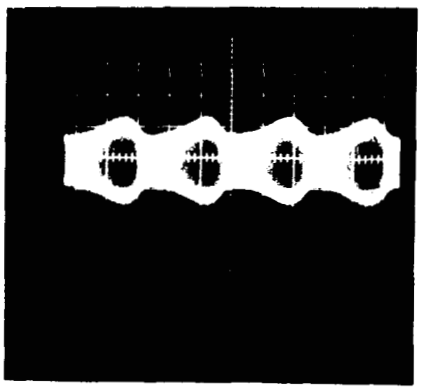

(e) IF Wave Form at the Receiver Output, PRF = 40 Kcps, Vertical = 50 mv/cm, Horizontal = 10 μs/cm

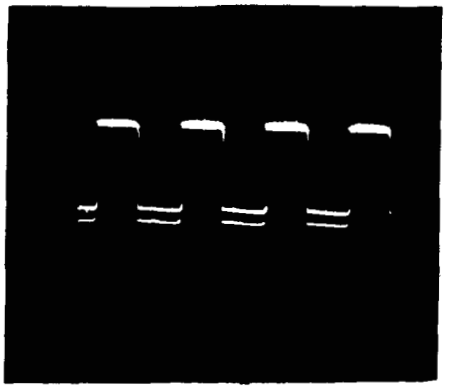

(f) The Two Square Wave Generator Signals Driving the LO Varactors, PRF = 40 Kcps, Vertical = 5 volts/cm, Horizontal = 10 μs/cm

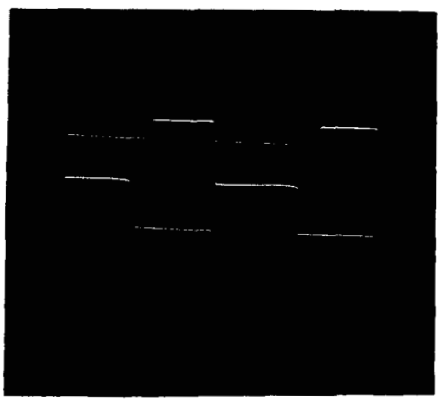

(g) Dual Trace Presentation of the Outputs from RF Crystal Detectors With the Transmitter Envelope Appearing on Top and LO Envelope at the Bottom of the Photograph, PRF = = 40 kc, Vertical = 50 mv/cm, Horizontal = 5 μs/cm

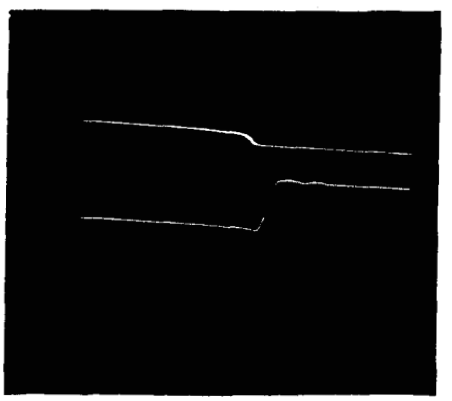

(h) Expanded View of (g) for Investigating Overlap, PRF = 40 Kcps, Vertical = 50 mv/cm, Horizontal = 0.2 μs/cm

Figure 4-6. Pertinent Waveforms — 40 Kcps Modulation Rate

6. DEAD ZONE AND ISOLATION

It was of interest to determine if any isolation requirements existed on the dead zones of time between the LO and the transmitter pulses. It was found, to the best that one can measure, that the only fundamental limitation is that no detectable overlapping of the two pulses can be allowed to occur.

The outputs of the two crystal detectors in the transmitter and LO RF lines were presented on the dual trace oscilloscope. By shifting the delay control on the transmitter pulse generator, observing the waveforms on the oscilloscope, and monitoring the effect on the wave analyzer, it was noted that at the instant of time at which overlap occurs between switching OFF one signal and switching ON the other that the signal strength in the receiver jumps up rapidly. At the 40 Kcps rate it was possible to ascertain the instant of overlap to within 0.04 μ sec.

C. CONCLUSIONS

It is significant to note the trend of the laboratory investigations. As is typical with most any experimental program involving hardware components and peripheral instrumentation, much of which has not previously been interfaced, the initial laboratory configuration contains many inherent deficiencies. The most outstanding and obvious of these are removed early in the work. The remaining deficiencies are located and removed in a serial fashion according to their relative effect on system performance. At each step, increasingly better results are obtained. Thus, the tabulated data should not be considered as representing the ultimate potential of the technique. Rather, it is the latest data actually obtained in the laboratory. In fact, certain deficiencies are known to still exist in the present set up and are correctable. Some of these have been pointed out in B of Section 4. The prospects of obtaining and/or measuring greater isolation levels may be considered as bolstered, or hindered, by certain factors which may be summarized as follows:

(1) The receiver-noise figure is about 10 db higher than reasonable and can be improved.

(2) Large amounts of additive noise are being generated by LO and leakage self-intermodulation. This factor can be reduced appreciably (as discussed in B. 5) to an extent limited by practicality and minimum bandwidth constraints by inclusion of narrow RF filters. An increase in the frequency of the first IF would reduce the effect of the self-intermodulation phenomena.

(3) The four-diode source has been found to exhibit turn-off capabilities superior to the two-diode version. A second four-diode source could be fabricated to replace the existing two-diode unit.

(4) As isolation levels in excess of about 130 db are attempted, component-to-component leakage coupling (leak-around) starts becoming an important factor in a laboratory configuration not specially configured with extensive precautionary measures.

(5) Gating of more than one varactor diode in the four-diode source should increase isolation levels (recall the improvement noted for the two-diode multiplier). Increases in this type of regulation, however, increase system complexity.

(6) Multiplier operation in the gated mode was found to be sensitive to PRF and gating levels. The data in Table 3-I was obtained by optimizing operation (e. g., retuning the sources) at each data point*.

The results achieved to date were shown in Table 4-1. The most tangible method of evaluating these results is by comparison to the isolation requirements derived in Appendix D for altimeter operation up to 220 km. The data of Table 4-I and Figure D-3 is shown in Figure 4-7 to an appropriate scale for direct comparison. Note the improvement in results at a PRF of 40 Kcps when RF filters were placed in the transmitter and LO lines. Similar results would be expected at the other data points if the experiment were rerun. The results would be expected to be less pronounced, however, since the intermodulation phenomena decreases with decreasing PRF.

In conclusion, it is felt that the feasibility of varactor bias modulation as a means of achieving transmit-receive isolation has in fact been demonstrated. The hypothetical ultimate goal of achieving a sufficient level of isolation by gating to permit solid-state altimetry up to altitudes

* See special note at end of Section 4.

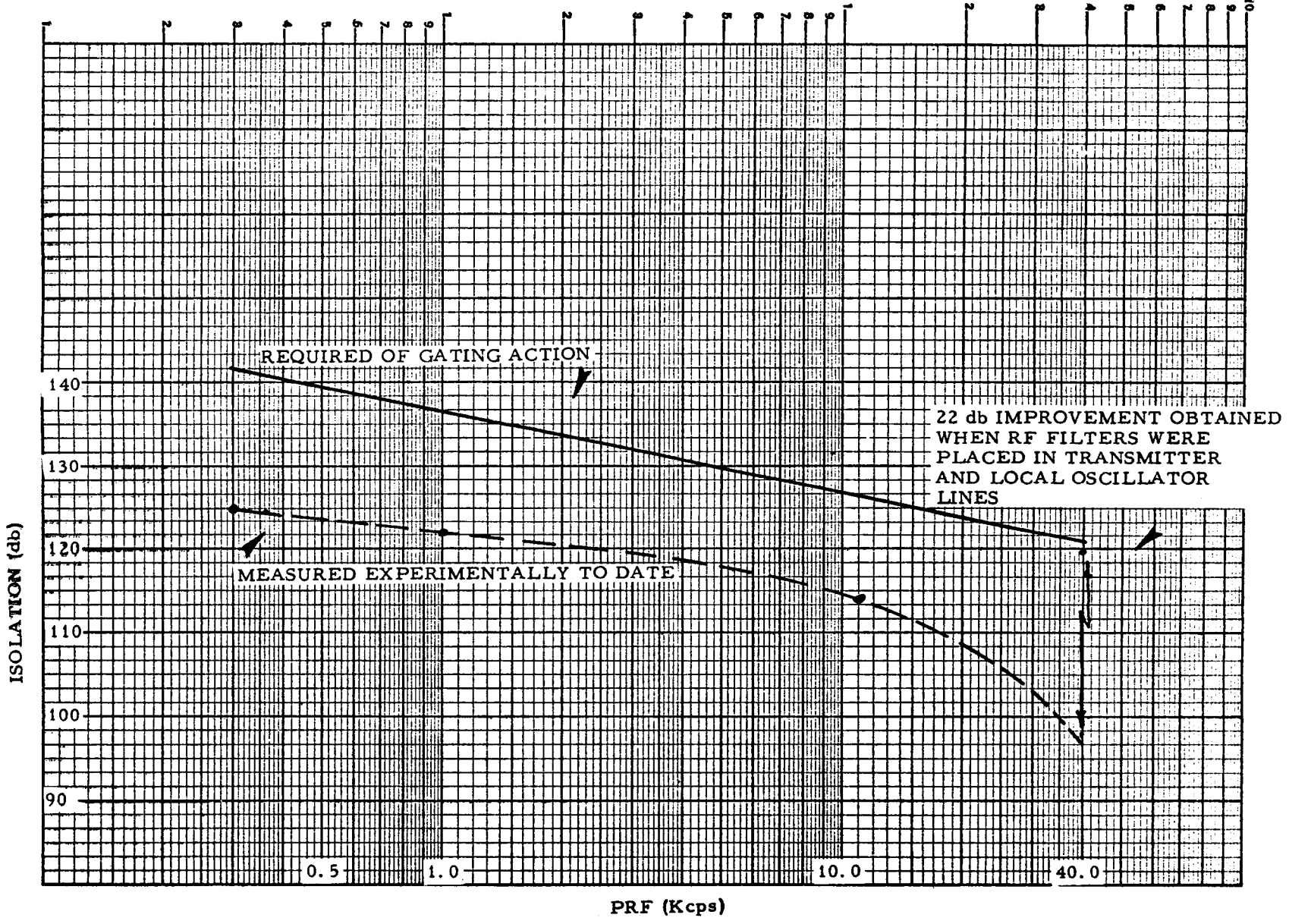

Figure 4-7. Comparison of Isolation Requirements and Measurements

of 220 km has not been experimentally demonstrated in the work performed to date. However, it is not believed that the results obtained to date represent the full capabilities of the approach. The investigation was terminated for economic and schedule considerations and not for technical reasons. Also, several possibilities which are not necessarily related to varactor bias modulation exist for enhancing total system isolation (recall that the criteria used here imply that varactor bias modulation must provide all the isolation and may therefore be overly severe and nonoptimum). These possible methods include: gating by means of RF switches at the transmitter output, LO output, and at the mixer input; bias-gating the diodes contained in the balanced mixer, and gating the IF amplifier circuits and/or the second LO.

SPECIAL NOTE:

While this report was in preparation, work was continuing in the laboratory on the gate generation scheme. In particular, the synchronizing generator shown in Figures 4-1 and 4-4 of the test was modified to provide the transmitter and receiver gating waveforms without the need for the laboratory gate generators used previously. Using the new set-up, which provides greater control of voltage and impedance parameters, the feasibility of varying the system repetition rate over the dynamic range of interest without the need to retune the transmitter and local oscillator power sources has been demonstrated. Specifically, the repetition rate was varied from about 100 cps to 52 Kcps withough any noticable RF waveform degradation. No attempt has yet been made to provide variation of either interpulse dead times or output (square-wave) voltage levels. Both of these factors can effect system performance (particularly system isolation) significantly. Thus, further development of the system is evidently required. However, the primary question of feasibility of repetition rate variation has been satisfied.

APPENDIX A

THE KALMAN FILTER EQUATIONS

A. THE MINIMUM VARIANCE ESTIMATE

The problem of deriving the Kalman filter equations is one of obtaining a minimum variance estimate given an a priori estimate. The derivation of the equations will be formal. All equations shown in this appendix will be matrix equations.

Let the quantity to be estimated be x, an m by one vector. Let the measured quantity without random noise be y, an n by one vector. Let the relation between y and x be given by

$$y = Mx \tag{A.1}$$

where M is the n x m measurement matrix. Note that this equation restricts each measurement element, y_i, of the vector y to be a linear combination of the elements x_j, of the unknown vector x. When this is not the case, the equations are linearized (as shown later) to get them into this form.

Let ϵ be the n by one vector of random noise on the actual measured quantity y^*. Then the noisy measurements are

$$y^* = Mx + w \tag{A.2}$$

It is assumed that w has a zero mean. That is,

$$E[w] = 0 \tag{A.3}$$

The covariance matrix of w is assumed to be given as

$$W = E\left[ww^T\right] \tag{A.4}$$

where the superscript T stands for transpose. Note that W is n x n, symmetric, and is positive semidefinite (as all covariance matrices must be†).

† Consider an arbitrary, nonzero, n by one vector a. The associated quadratic form for W is

$$a^T W a = a^T E\left[ww^T\right]a = E\left[a^T w\,(a^T w)^T\right]$$

Let x_a be an unbiased a priori estimate of x, where unbiased means $E\left[x-x_a\right] = 0$. Let the m x m error covariance matrix of x_a be given as

$$A = E\left[(x-x_a)(x-x_a)^T\right] \tag{A.5}$$

It will further be assumed that the measurement error w and the estimation error of x_a, $(x-x_a)$, are uncorrelated. That is

$$E\left[w(x-x_a)\right] = 0 \tag{A.6}$$

Note that A is m x m, symmetric, and positive semidefinite.

The problem is to find a new and better estimate of x from the measurement y* and the a priori estimate x_a. Let the new estimate of x be $\hat{x}$, and let $\hat{x}$ be a linear combination of y* and x_a. Thus

$$\hat{x} = By^* + Cx_a \tag{A.7}$$

In order that $\hat{x}$ be an unbiased estimate, $E[\hat{x}]$ must equal $E[x]$. Thus

$$E[\hat{x}] = E\left[By^* + Cx_a\right] = E[x]$$

but

$$y^* = Mx + w$$

so

$$E[x] = E\left[BMx + Bw + Cx_a\right] = (BM + C)\,E[x]$$

But $a^T w$ is a scalar. Thus

$$a^T W a = E\left[(a^T w)^2\right] \geq 0$$

and W is positive semidefinite.

Hence

$$BM + C = I \tag{A.8}$$

for an unbiased estimate. I is an m x m identity matrix.

Define the error covariance matrix of the estimate $\hat{x}$ by

$$J = E\left[(x-\hat{x})(x-\hat{x})^T\right] \tag{A.9}$$

Using previous definitions and equations, it is easily shown that

$$J = (I-BM)\, A\, (I-BM)^T + BWB^T \tag{A.10}$$

Before proceeding to obtain an optimum value of the B matrix, consider the quantities x' and $\hat{x}'$ defined by

$$x' = Lx \qquad \text{and} \qquad \hat{x}' = L\hat{x} \tag{A.11}$$

Equation (A. 11) represents a change of coordinates from the unprimed to the primed coordinate system. Note that when L = M, then $x' = y$. Now consider the error covariance matrix in the primed coordinates. By definition

$$J' = E\left[(Lx-L\hat{x})(Lx-L\hat{x})^T\right]$$

or

$$J' = LJL^T \tag{A.12}$$

The main diagonal of J' consists of the elements $E\left[(x_i' - \hat{x}_i')^2\right]$ which is equal to the variance of the error on the estimate of the ith element of x'. The matrix B in Equation (A. 10) will be obtained such that the variance of each estimation error $x_i' - \hat{x}_i'$ is minimized for any and all L matrices. In particular when L is taken to be the measurement matrix, M, then the variance of each estimation error $y_i - \hat{y}_i$ is minimized. This is the significant difference between a minimum variance estimation and a least squares estimation. In a least squares estimation, the sum of the residuals of the estimates compared with the measured quantities

$$\sum_i (y_i^* - \hat{y}_i)^2$$

is minimized, whereas in a minimum variance estimate each

$$E\left[(y_i - \hat{y}_i)^2\right]$$

is minimized. Thus, it might be said that the least squares approach makes a fit to the noisy measurements whereas the minimum variance technique attempts to make a fit to the true value of the measurement.

Define z' to be any nonzero vector. Then the associated quadratic form for J' is

$$s = (z')^T J' z' = (z')^T L\, J\, L^T z' \qquad \text{(A. 13)}$$

By letting

$$z' = \begin{bmatrix} 1 \\ 0 \\ 0 \\ . \\ . \\ . \end{bmatrix}, \quad \begin{bmatrix} 0 \\ 1 \\ 0 \\ . \\ . \\ . \end{bmatrix}, \text{ etc.}$$

we can pick out the diagonal elements of J'. And it is these elements which we choose to minimize for all L matrices by picking a proper B matrix. By letting

$$z = L^T z'$$

Equation (A. 13) may be rewritten as

$$s = z^T J z \qquad \text{(A. 14)}$$

where, since L was arbitrary, z will be any m by one vector. Taking the variation of s gives

$$\delta s = z^T \delta J\, z$$

but from Equation (A. 10)

$$\delta s = z^T \left[-\delta BMA(I-BM)^T - (I-BM)AM^T \delta B^T + \delta BWB^T + BW\delta B^T\right] z$$

or, collecting terms,

$$\delta s = z^T \left[- (I-BM)\, AM^T + BW \right] \delta B^T z + \left\{ z^T \left[- (I-BM)\, AM^T + BW \right] \delta B^T z \right\}^T \quad \text{(A. 15)}$$

But both terms on the right hand side of Equation (A. 15) are scalars, so

$$\delta s = 2z^T \left[- (I-BM) AM^T + BW \right] \delta B^T z \quad \text{(A. 16)}$$

Thus s will be minimized by setting

$$(I-BM)\, AM^T = BW$$

solving for B gives

$$B = AM^T (MAM^T + W)^{-1} \quad \text{(A. 17)}$$

which in turn will give the minimum variance estimate $\hat{x}$ of x.

In review, the minimum variance estimate $\hat{x}$ of x is given by

$$\hat{x} = By^* + Cx_a \quad \text{(A. 18)}$$

where

$$B = AM^T (MAM^T + W)^{-1} \quad \text{(A. 19)}$$

$$C = I - BM \quad \text{(A. 20)}$$

The error covariance matrix of the estimate $\hat{x}$ was [from Equation (A. 10)]

$$J = CAC^T + BWB^T \quad \text{(A. 21)}$$

which, incidentally, is true for any C and B. Substituting the optimum values of B and C into the equation for J will give the optimum value of J as

$$J = CA \quad \text{(A. 22)}$$

Another, seldom seen, form for J is obtained from Equations (A. 20), (A. 21), and (A. 22).

$$J = A - BMAM^T B^T - BWB^T \tag{A. 23}$$

An interesting alternate form in which the B and C matrices are given in terms of information matrices can be obtained by using Ho's lemma*. An information matrix is defined as the inverse of an error covariance matrix. Applying Ho's lemma to Equations (A. 19) and (A. 20) gives

$$B = (A^{-1} + M^T W^{-1} M)^{-1} M^T W^{-1} \tag{A. 19'}$$

and

$$C = (A^{-1} + M^T W^{-1} M)^{-1} A^{-1} \tag{A. 20'}$$

and J^{-1} becomes

$$J^{-1} = A^{-1} + M^T W^{-1} M \tag{A. 22'}$$

Now that the minimum variance equations, given an a priori estimate, have been derived it is an easy matter to introduce the Kalman filter concept. Suppose that a minimum variance estimate of the state vector, x, at time t_{n-1} is obtained. Let the state of the system at time t_n be given by

$$x_n = Ux_{n-1} + r_n \tag{A. 24}$$

---

* Ho's lemma is

$$(A_1^{-1} + A_2^T A_3^{-1} A_2)^{-1} = A_1 - A_1 A_2^T (A_2 A_1 A_2^T + A_3)^{-1} A_2 A_1$$

which is easily proved by multiplying the right side by the inverse of the left side, and then factoring out $A_1 A_2^T (A_2 A_1 A_2^T + A_3)^{-1}$. This lemma was first shown by Y. C. Ho in a RAND Corporation Memorandum, RM-3329-PR, "The Method of Least Squares and Optimal Filtering Theory," dated October 1962.

where r_n is an m by one vector which represents a random disturbance acting on the system. For example, a random wind force. The m x m matrix U is called the updating or transition matrix. It is assumed that

$$E\left[x_{n-1}r_n\right] = 0 \text{ and } E\left[r_n\right] = 0 \tag{A.25}$$

Since $E[r] = 0$, the best estimate of x at time t_n is $U\hat{x}_{n-1}$. Thus the a priori estimate of x at t_n is

$$\hat{x}_{n/n-1} = U\hat{x}_{n-1/n-1} \tag{A.26}$$

where the subscript n/n-1 means estimate at time t_n based on n-1 measurements. n-1/n-1 means estimate at time t_{n-1} based on n-1 measurements. The a priori error covariance matrix is

$$\underline{\underline{A}} \triangleq J_{n/n-1} \triangleq E\left[(x_n - \hat{x}_{n/n-1})(x_n - \hat{x}_{n/n-1})^T\right] \tag{A.27}$$

Substituting Equations (A.24), (A.25), and (A.26) into Equation (A.27) gives

$$J_{n/n-1} = UJ_{n-1/n-1}U^T + R_n \tag{A.28}$$

where

$$R_n = E\left[r_n r_n^T\right] \tag{A.29}$$

Thus the minimum variance estimate of x at time t_n is, as given by Equations (A.18) through (A.20),

$$\hat{x}_{n/n} = By_n^* + Cx_{n/n-1} \tag{A.30}$$

where

$$B = J_{n/n-1}M_n^T\left(M_nJ_{n/n-1}M_n^T + W_n\right)^{-1} \tag{A.31}$$

$$C = I - BM_n \tag{A.32}$$

and where now y_n^* is only the measurement made at time t_n. The relationship between the measurement and the state of the system at t_n being given by

$$y_n^* = M_n x_n + w_n \tag{A.33}$$

and where by definition

$$W_n \triangleq E\left[w_n w_n^T\right] \tag{A.34}$$

The error covariance matrix of the estimate $\hat{x}_{n/n}$ is given by Equation (A.22) as

$$J_{n/n} = C\, J_{n/n-1} \tag{A.35}$$

or its alternate forms as shown in Equations (A.21), (A.23), or (A.22').

This ends the derivation of the Kalman filter equations. As in many problems, the equations are deceptively simple looking and indeed they are very simple to apply when filtering polynomial signals such as

$$y_n = x_o + x_1 t_n + x_2 t_n^2 + x_3 t_n^3 \tag{A.36}$$

In this case the measurement matrix is

$$M_n = \begin{bmatrix} 1 & t_n & t_n^2 & t_n^3 \end{bmatrix} \tag{A.37}$$

and the updating matrix is

$$U = \begin{bmatrix} 1 & 0 & 0 & 0 \\ 0 & 1 & 0 & 0 \\ 0 & 0 & 1 & 0 \\ 0 & 0 & 0 & 1 \end{bmatrix} \tag{A.38}$$

However, nature is seldom so kind as to provide signals that may be adequately represented by polynomials. In general

$$y_n = y_n(x_1, x_2, \ldots, x_m; t_n)$$

and similarly for x_n in terms of $x_{i,n-1}$. Thus in general, before the equations derived in this section can be used, it will be necessary to linearize the equations describing the system to get them into the proper form.

B. LINEARIZING THE EQUATIONS

The equations describing the system will be linearized so that the Kalman filter equations [Equations (A.26) through (A.35)] may be used. The linearization process used here is not unique to Kalman filters. The same procedure is used for least squares and conventional minimum variance estimators.

The relationship between the true value (no noise) of the measurement and the state of the system was given by Equation (A.33) as

$$y_n = M_n x_n$$

Note that if more than one measurement is made at time t_n then y_n will be a vector. This equation says that each component $y_{n,i}$ of y_n is a linear combination of the elements of the state vector, x_n. However, it is not generally true that each measurement component is a linear combination of the elements of the state vector. In general

$$y_n = y_n(x_n) \tag{A.39}$$

Let the nominal value of x_n be x'_n, where nominal value means <u>any</u> value close to the true value x_n. Then the m by one state vector can be written as

$$x_n = x'_n + \Delta x_n \tag{A.40}$$

where Δx_n is a small unknown correction factor. Substituting Equation (A.40) into (A.39) and expanding (assuming Δx_n is small) gives

$$y_n = y_{n(x'_n)} + \left(\frac{\partial y_n}{\partial x_n}\right)' \Delta x_n \tag{A.41}$$

where the prime on the partial means that it is evaluated with the nominal value of x_n existing at time t_n. Defining the nominal value of y_n as

$$y'_n = y_{n(x'_n)} \tag{A.42}$$

then

$$y_n - y'_n \triangleq \Delta y_n = \left(\frac{\partial y_n}{\partial x_n}\right)' \Delta x_n \tag{A.43}$$

where Δy_n could now be thought of as the observed quantity, and Δx_n the state or unknown vector. Thus the measurement matrix, M, is given by

$$M = \begin{bmatrix} \left(\frac{\partial y_1}{\partial x_1}\right)' & \left(\frac{\partial y_1}{\partial x_2}\right)' & \cdots & \left(\frac{\partial y_1}{\partial x_m}\right)' \\ \left(\frac{\partial y_2}{\partial x_1}\right)' & \left(\frac{\partial y_2}{\partial x_2}\right)' & \cdots & \left(\frac{\partial y_2}{\partial x_m}\right)' \\ \text{etc.} & & & \end{bmatrix} \tag{A.44}$$

where, for clarity, the subscript n has been dropped.

The measurement matrix for the Kalman filter is merely an expression concerning the geometry of the system and does not include the dynamics or equations of motion in its derivation. For example, suppose that the state vector of a system is the position and velocity of the system. Thus the position and velocity at time t_n is

$$x_n = \begin{bmatrix} \xi_n \\ \eta_n \\ \dot{\xi}_n \\ \dot{\eta}_n \end{bmatrix}$$

Now suppose that measurements are made of

$$r = \sqrt{\xi^2 + \eta^2}$$

then the measurement matrix would be

$$M_n = \begin{bmatrix} \frac{\xi'_n}{r_n} & \frac{\eta'_n}{r'_n} & 0 & 0 \end{bmatrix}$$

where the primes indicate nominal values.

The updating of the state from t_{n-1} to t_n was given by Equation (A.24) as

$$x_n = Ux_{n-1} + r_n$$

Here again the equations of the system will be linearized to get them in the form of

$$\Delta x_n = U\Delta x_{n-1} + r_n \qquad \text{(A.45)}$$

where

$$\Delta x_n = x_n - x'_n \qquad \Delta x_{n-1} = x_{n-1} - x'_{n-1}$$

and*

$$\Delta r_n = r_n - r'_n = r_n$$

since r'_n will be taken as $r'_n \equiv E[r_n] = 0$. The U matrix in Equation (A.45) may be derived by finding an expression

$$x_n = f(x_{n-1}) \qquad \text{(A.46)}$$

Then the U matrix will be given by

$$U = \left(\frac{\partial f}{\partial x_{n-1}}\right)' \qquad \text{(A.47)}$$

* Note also that $\Delta w_n = w_n - w'_n = w_n$.

where the prime means that the partial is evaluated at the nominal value of x_{n-1}. Writing out Equation (A.47) yields

$$U = \begin{bmatrix} \left(\frac{\partial x_{1,n}}{\partial x_{1,n-1}}\right)' & \left(\frac{\partial x_{1,n}}{\partial x_{2,n-1}}\right)' & \cdots & \left(\frac{\partial x_{1,n}}{\partial x_{m,n-1}}\right)' \\ \left(\frac{\partial x_{2,n}}{\partial x_{1,n-1}}\right)' & \left(\frac{\partial x_{2,n}}{\partial x_{2,n-1}}\right)' & \cdots & \left(\frac{\partial x_{2,n}}{\partial x_{m,n-1}}\right)' \\ \text{etc.} & & & \end{bmatrix} \qquad \text{(A.48)}$$

The quantity $x_n = f(x_{n-1})$ as given by Equation (A.46) may be found by use of a Taylor series expansion. For example, consider the equations of motion

$$\ddot{\xi} = -\frac{g}{L}\xi \qquad \ddot{\eta} = -\frac{g}{L}\eta \qquad \text{(A.49)}$$

which represent the horizontal projection of the motion of a long pendulum whose length is L. g is the acceleration because of gravity. Suppose that g is not known exactly and thus a solution for g is necessary to determine the state of the system. Let the state vector be

$$x = \left[\xi \quad \eta \quad \dot{\xi} \quad \dot{\eta} \quad g\right]^T \qquad \text{(A.50)}$$

The truncated Taylor series expansion for ξ_n is

$$\xi_n = \xi_{n-1} + \dot{\xi}_{n-1}\Delta T + \frac{1}{2}\ddot{\xi}_{n-1}\Delta T^2 + \frac{1}{6}\dddot{\xi}_{n-1}\Delta T^3 + \frac{1}{24}\ddddot{\xi}_{n-1}\Delta T^4 \qquad \text{(A.51)}$$

where

$$\ddot{\xi}_{n-1} = -\frac{g}{L}\xi_{n-1}$$

$$\dddot{\xi}_{n-1} = -\frac{g}{L}\dot{\xi}_{n-1}$$

$$\ddddot{\xi}_{n-1} = -\frac{g}{L}\ddot{\xi}_{n-1} = \frac{g^2}{L^2}\xi_{n-1}$$

Thus

$$\xi_n = \left(1 - \frac{1}{2}\frac{g}{L}\Delta T^2 + \frac{1}{24}\frac{g^2}{L^2}\Delta T^4\right)\xi_{n-1} + \left(\Delta T - \frac{1}{6}\frac{g}{L}\Delta T^3\right)\dot{\xi}_{n-1} \qquad (A.52)$$

Likewise

$$\eta_n = \left(1 - \frac{1}{2}\frac{g}{L}\Delta T^2 + \frac{1}{24}\frac{g^2}{L^2}\Delta T^4\right)\eta_{n-1} + \left(\Delta T - \frac{1}{6}\frac{g}{L}\Delta T^3\right)\dot{\eta}_{n-1} \qquad (A.53)$$

and

$$\dot{\xi}_n = \left(-\frac{g}{L}\Delta T + \frac{1}{6}\frac{g^2}{L^2}\Delta T^3\right)\xi_{n-1} + \left(1 - \frac{1}{2}\frac{g}{L}\Delta T^2\right)\dot{\xi}_{n-1} \qquad (A.54)$$

and

$$\dot{\eta}_n = \left(-\frac{g}{L}\Delta T + \frac{1}{6}\frac{g^2}{L^2}\Delta T^3\right)\eta_{n-1} + \left(1 - \frac{1}{2}\frac{g}{L}\Delta T^2\right)\dot{\eta}_{n-1} \qquad (A.55)$$

The updating for the constant g is merely

$$g_n = g_{n-1} \qquad (A.56)$$

Hence the elements of the updating matrix, U, are

$$u_{11} = \frac{\partial \xi_n}{\partial \xi_{n-1}} = 1 - \frac{1}{2}\frac{g}{L}\Delta T^2 + \frac{1}{24}\frac{g^2}{L^2}\Delta T^4 \quad , \quad u_{12} = \frac{\partial \xi_n}{\partial \dot{\xi}_{n-1}} = 0$$

$$u_{13} = \frac{\partial \xi_n}{\partial \dot{\xi}_{n-1}} = \Delta T - \frac{1}{6}\frac{g}{L}\Delta T^3, \qquad u_{14} = \frac{\partial \xi_n}{\partial \dot{\eta}_{n-1}} = 0$$

$$u_{15} = \frac{\partial \xi_n}{\partial g_{n-1}} = \frac{\partial \xi_n}{\partial g} = \left(-\frac{1}{2}\frac{1}{L}\Delta T^2 + \frac{1}{12}\frac{g}{L^2}\Delta T^4\right)\xi_{n-1} - \frac{1}{6}\frac{1}{L}\Delta T^3\dot{\xi}_{n-1}$$

and so on for the rest of the rows in the u matrix. All the elements u_{ij} are evaluated with the nominal values of the state. Note that the last row of the u matrix is particularly simple.

$$u_{51} = u_{52} = \cdots = u_{54} = 0 \qquad u_{55} = \frac{\partial g_n}{\partial g_{n-1}} = 1$$

Another way of obtaining the u matrix is to integrate the variational equations. To obtain the variational equations for our example, note that the state vector was

$$x = \begin{vmatrix} \xi \\ \eta \\ \dot{\xi} \\ \dot{\eta} \\ g \end{vmatrix} \quad . \quad \text{Thus} \quad \dot{x} = \begin{vmatrix} \dot{\xi} \\ \dot{\eta} \\ \ddot{\xi} \\ \ddot{\eta} \\ \dot{y} \end{vmatrix}$$

Taking the variation of these equations yields

$$\Delta x = \begin{bmatrix} \delta\xi \\ \delta\eta \\ \delta\dot{\xi} \\ \delta\dot{\eta} \\ \delta g \end{bmatrix} \qquad \text{and} \qquad \Delta\dot{x} = \begin{bmatrix} \delta\dot{\xi} \\ \delta\dot{\eta} \\ \delta\ddot{\xi} \\ \delta\ddot{\eta} \\ \delta\dot{g} \end{bmatrix}$$

Now note, for example, that

$$\delta\ddot{\xi} = \frac{\partial\ddot{\xi}}{\partial\xi}\delta\xi + \frac{\partial\ddot{\xi}}{\partial\eta}\xi\eta + \frac{\partial\ddot{\xi}}{\partial\dot{\xi}}\delta\dot{\xi} + \frac{\partial\ddot{\xi}}{\partial\dot{\eta}}\delta\dot{\eta} + \frac{\partial\ddot{\xi}}{\partial g}\delta g \qquad \text{(A.57)}$$

Thus, from Equation (A.49)

$$\delta\ddot{\xi} = -\frac{g}{L}\delta\xi - \frac{1}{L}\xi\delta g \qquad \text{(A.58)}$$

Likewise

$$\delta\ddot{\eta} = -\frac{g}{L}\delta\eta - \frac{1}{L}\eta\delta g \qquad \text{(A.59)}$$

and

$$\dot{\delta\xi} = \delta\dot{\xi} \qquad \dot{\delta\eta} = \delta\dot{\eta} \qquad \dot{\delta g} = 0 \tag{A.60}$$

Thus

$$\Delta\dot{x} = \begin{bmatrix} 0 & 0 & 1 & 0 & 0 \\ 0 & 0 & 0 & 1 & 0 \\ -g/L & 0 & 0 & 0 & -\xi/L \\ 0 & -g/L & 0 & 0 & -\eta/L \\ 0 & 0 & 0 & 0 & 0 \end{bmatrix} \Delta x \tag{A.61}$$

or

$$\Delta\dot{x} = G\Delta x \tag{A.62}$$

Again employing a truncated Taylor series expansion

$$\Delta x_n = \Delta x_{n-1} + \Delta\dot{x}_{n-1}\Delta T + \frac{1}{2}\Delta\ddot{x}_{n-1}\Delta T^2 + \frac{1}{6}\Delta\dddot{x}_{n-1}\Delta T^3 \tag{A.63}$$

where

$$\Delta\dot{x}_{n-1} = G_{n-1}\Delta x_{n-1}$$

$$\Delta\ddot{x}_{n-1} = \dot{G}_{n-1}\Delta x_{n-1} + G_{n-1}\Delta\dot{x}_{n-1} = \left(\dot{G}_{n-1} + G_{n-1}^2\right)\Delta x_{n-1}$$

$$\Delta\dddot{x}_{n-1} = \left(\ddot{G}_{n-1} + G_{n-1}\dot{G}_{n-1} + 2\dot{G}_{n-1}G_{n-1} + G_{n-1}^3\right)\Delta x_{n-1}$$

Thus

$$\Delta x_n = \left[I + G_{n-1}\Delta T + \frac{1}{2}\left(\dot{G}_{n-1} + G_{n-1}^2\right)\Delta T^2 + \frac{1}{6}\left(\ddot{G}_{n-1} + G_{n-1}\dot{G}_{n-1} + 2\dot{G}_{n-1}G_{n-1} + G_{n-1}^3\right)\Delta T^3 \right] \Delta x_{n-1} \tag{A.64}$$

and by definition the U matrix is the quantity in the brackets. Note that the G, $\dot{G}$, and $\ddot{G}$ matrices are liberally sprinkled with zeros. If the U matrix is directly calculated from Equation (A.64) by means of matrix

multiplications, it is quite often very time consuming in terms of digital computer time. In general, Equation (A.64) would only be used to update position and velocity. Updating of such things as biases are best done separately.

Before proceeding to the next section, a word about the nominal values of the state vector. As mentioned previously, the nominal values of the state vector are used in evaluating the partial derivatives appearing in the measurement and updating matrices. The nominal values are obtained by integrating the equations of motion. In the case of error analysis studies, an initial position and velocity determines the nominal values. In the case of real time navigation or filtering, the nominal trajectory will be redetermined after each measurement is processed. Thus the nominal value at the next time will be based on the best estimate of the state at this time. This redetermination of nominal trajectory after each measurement is one advantage of the Kalman filter over conventional least squares and minimum variance programs. These programs must restrict their nominal trajectory to be the one determined by the initial estimate of the state of the system and, in most instances, this nominal trajectory will deviate noticeably from the actual trajectory. Thus these programs must make several fits of the data in which each fit uses the results of the previous run to obtain an improved estimate of the initial state.

Another advantage of a Kalman filter is its ability to easily handle certain types of correlated noise. The next section will explain this.

C. TIME CORRELATED NOISE

How the Kalman filter handles time correlated noise is perhaps best illustrated by an example. Consider the case when the noise on the measurement is given by

$$w_n = \epsilon_{u,n} + \epsilon_{c,n} \tag{A.65}$$

where ϵ_u is uncorrelated noise and ϵ_c is time correlated noise. Suppose that the autocorrelation function of ϵ_c is given by

$$\phi_{(\tau)} = \phi_o e^{-a\tau} \cos b\tau \tag{A.66}$$

A model for this noise is obtained from the difference equation

$$\varepsilon_{c,n} = b_1\varepsilon_{c,n-1} - b_2\varepsilon_{c,n-2} + a_1\varepsilon_{w,n-1} + a_2\varepsilon_{w,n-2} \qquad \text{(A.67)}$$

where

$$E\left[\varepsilon_{w,n}\right] = 0$$

$$E\left[\varepsilon_{w,n}\varepsilon_{w,n-i}\right] = 0 \qquad i \neq 0$$

$$= 1 \qquad i = 0$$

$$b_1 = 2e^{-a\Delta T}\cos b\Delta T$$

$$b_2 = e^{-2a\Delta T}$$

$$a_1 = \frac{1}{2}\sqrt{(1-b_2)\phi_o}\left[\sqrt{1+b_2-b_1} - \sqrt{1+b_2+b_1}\right]$$

$$a_2 = \frac{1}{2}\sqrt{(1-b_2)\phi_o}\left[\sqrt{1+b_2-b_1} + \sqrt{1+b_2+b_1}\right]$$

ΔT = the computing or integration interval

By taking $E\left[\varepsilon_{c,n}\varepsilon_{c,n-i}\right]$ it can be shown that

$$E\left[\varepsilon_{c,n}\varepsilon_{c,n-i}\right] = \phi_o e^{-ai\Delta T}\cos bi\Delta T$$

Define $\varepsilon_{d,n}$ by

$$\varepsilon_{d,n} = \varepsilon_{c,n-1} - \frac{a_2}{b_2}\varepsilon_{w,n-1} \qquad \text{(A.68)}$$

Equation (A.51) may now be rewritten as

$$\varepsilon_{c,n} = b_1\varepsilon_{c,n-1} - b_2\varepsilon_{d,n-1} + a_1\varepsilon_{w,n-1} \qquad \text{(A.69)}$$

Note that both $\varepsilon_{c,n}$ and $\varepsilon_{d,n}$ are written in terms of values existing at t_{n-1}.

Referring back to Equation (A.6), it is seen that one of the assumptions made in deriving the Kalman filter equations was that w_n and $x_n - \hat{x}_{n/n-1}$ were uncorrelated. However, with time correlated noise this assumption would be violated. This difficulty can easily be avoided by making ε_d and ε_c part of the state vector of the system and setting $w_n = \varepsilon_u$ only. That part of the updating matrix concerned with updating ε_d and ε_c is given by

$$U_\varepsilon = \begin{bmatrix} 0 & 1 \\ b_1 & -b_2 \end{bmatrix} \tag{A.70}$$

That part of the random disturbance vector associated with ε_d and ε_c is

$$r_\varepsilon = \begin{bmatrix} -\frac{a_2}{b_2}\,\varepsilon_{w,n-1} \\ a_1\,\varepsilon_{w,n-1} \end{bmatrix} \tag{A.71}$$

and that part of the random disturbance, error covariance matrix is

$$R_\varepsilon = E\left[r_\varepsilon r_\varepsilon^T\right] = \begin{bmatrix} \left(\frac{a_2}{b_2}\right)^2 & -\frac{a_1 a_2}{b_2} \\ \frac{-a_1 a_2}{b_2} & a_1^2 \end{bmatrix} \tag{A.72}$$

An interesting situation now arises if ε_c is the only noise on the measurements. That is

$$w_n = 0$$

In this case $W_n = \left[E\ w_n w_n^T\right] = 0$. Equation (A.35) gave the error covariance matrix of the estimate $\hat{x}_{n/n}$ as

$$J_{n/n} = C\, J_{n/n-1}$$

Equation (A.21) gives as an alternate expression

$$J_{n/n} = CJ_{n/n-1}C^T + BW_nB^T$$

But $W_n = 0$, so

$$J_{n/n} = CJ_{n/n-1}C^T$$

Thus, since $J_{n/n}$ is symmetric

$$J_{n/n} = J_{n/n}C^T = CJ_{n/n} = C^2J_{n/n-1}$$

so

$$C^2J_{n/n-1} = CJ_{n/n-1}$$

It can also be shown that

$$C(J_{n/n} - J_{n/n-1}) = 0$$

The matrix C is known as an idempotent matrix. Because of this peculiar nature of C when correlated noise is the only noise on the measurements, one might expect some difficulty with the Kalman filter equations. Several simulations have been run, however, which show that no difficulty is encountered when C is idempotent.

APPENDIX B

FIGURE OF THE MOON AND TERRAIN NOISE IRREGULARITIES

A. FIGURE OF THE MOON

Detailed contour maps of the lunar surface were used to obtain an altitude profile of the lunar surface with respect to a reference sphere with a radius of 1735.4 kilometers.* Altitude data were recorded at 300 meter intervals. Altitude versus longitude along the equator was plotted as shown in Figures B-2 through B-15. Figure B-2 shows the same information as Figures B-3 through B-15, only to a greatly reduced horizontal scale. A table of altitude versus longitude in 0.1 deg (central angle) increments was then compiled from the figures. The table contained 1,204 data points.

The shape of the moon's equator (Figure B-1) was assumed to be an ellipse.

$$\frac{x^2}{r_a^2} + \frac{y^2}{r_b^2} = 1 \qquad \text{(B.1)}$$

Let $x = r_m \cos\theta$, $y = r_m \sin\theta$.

Then,

$$r_m^2 \left[\frac{\cos^2\theta}{r_a^2} + \frac{1-\cos^2\theta}{r_b^2} \right] = 1$$

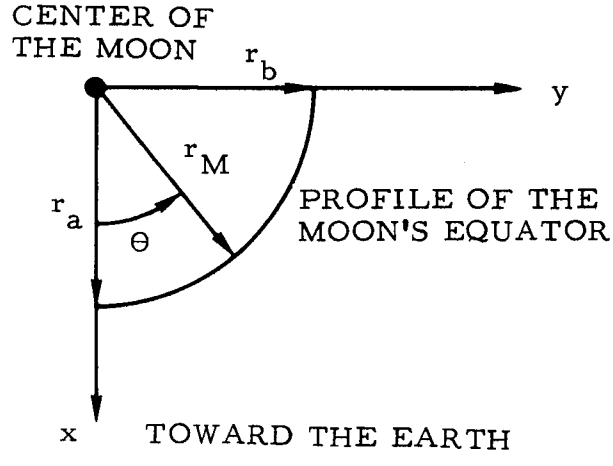

Figure B-1. Profile of the Moon's Equator

* See "U.S.A.F. Lunar Charts and Mosaics," published for the United States Air Force and National Aeronautics and Space Administration by Aeronautical Chart and Information Center, United States Air Force, St. Louis, Missouri, 63118. Charts are available from Superintendent of Documents, Government Printing Office, Washington, D.C., 20402.

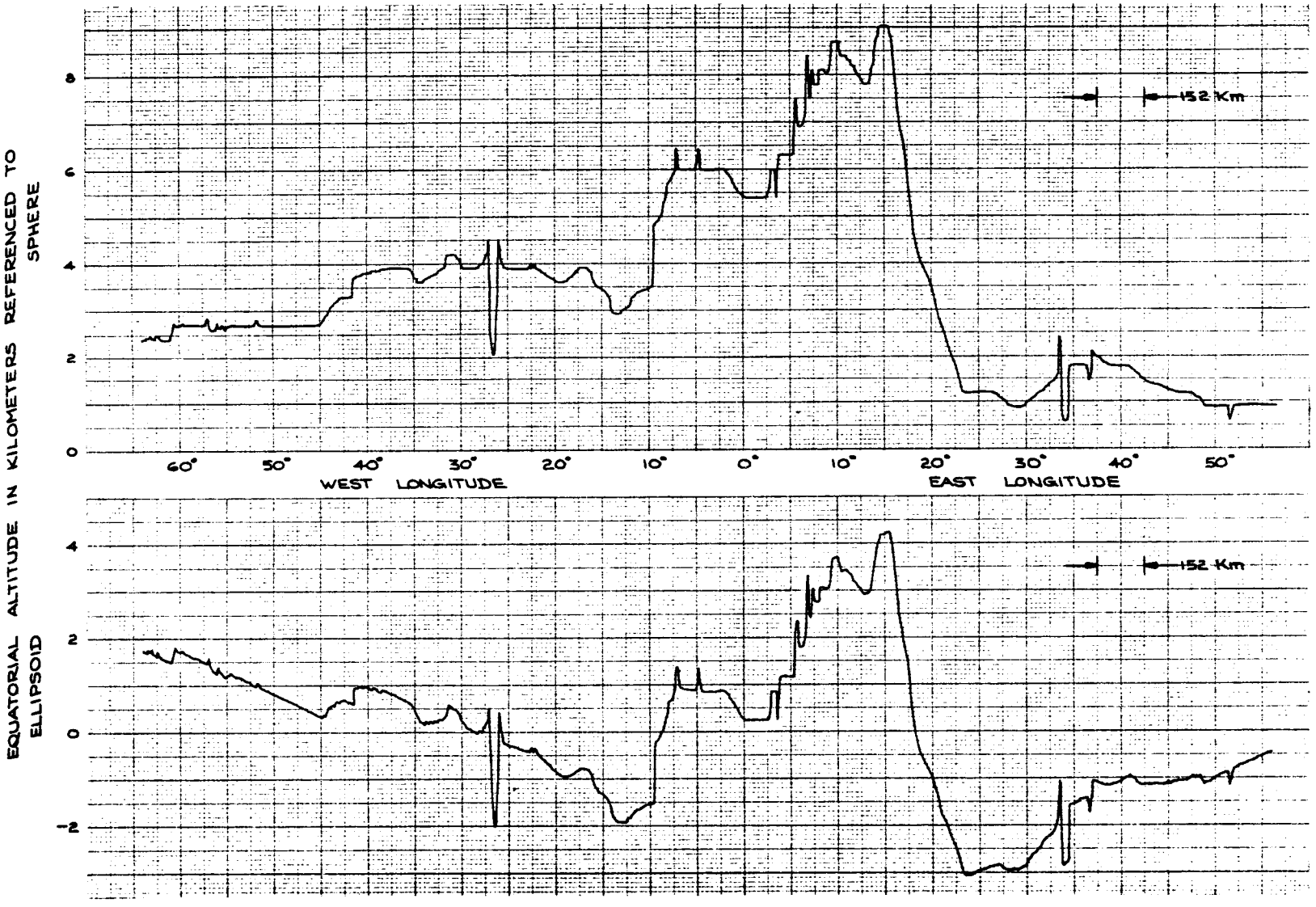

Figure B-2. Equatorial Altitude Versus Longitude

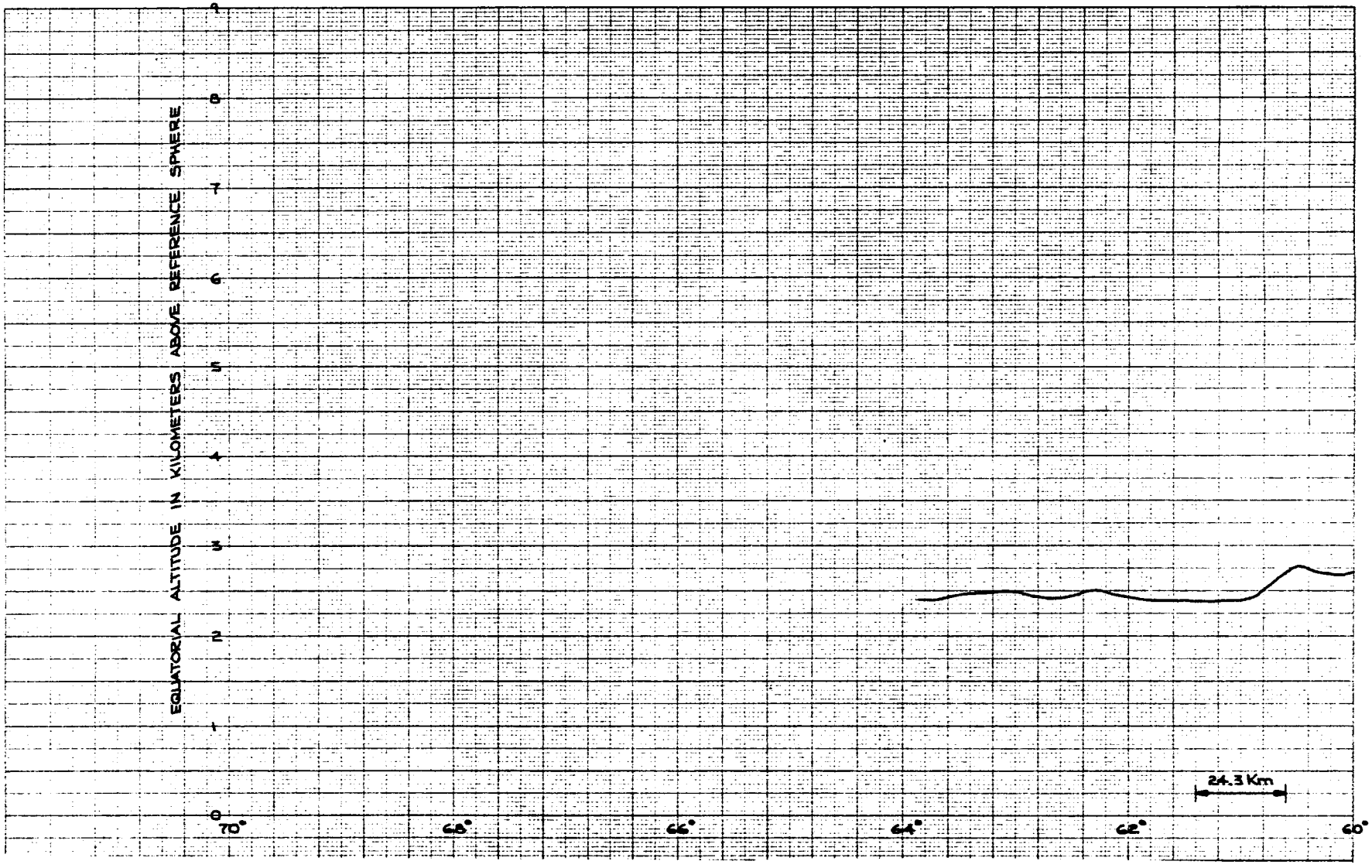

Figure B-3. Lunar Equatorial Altitude Versus West Longitude (View 1)

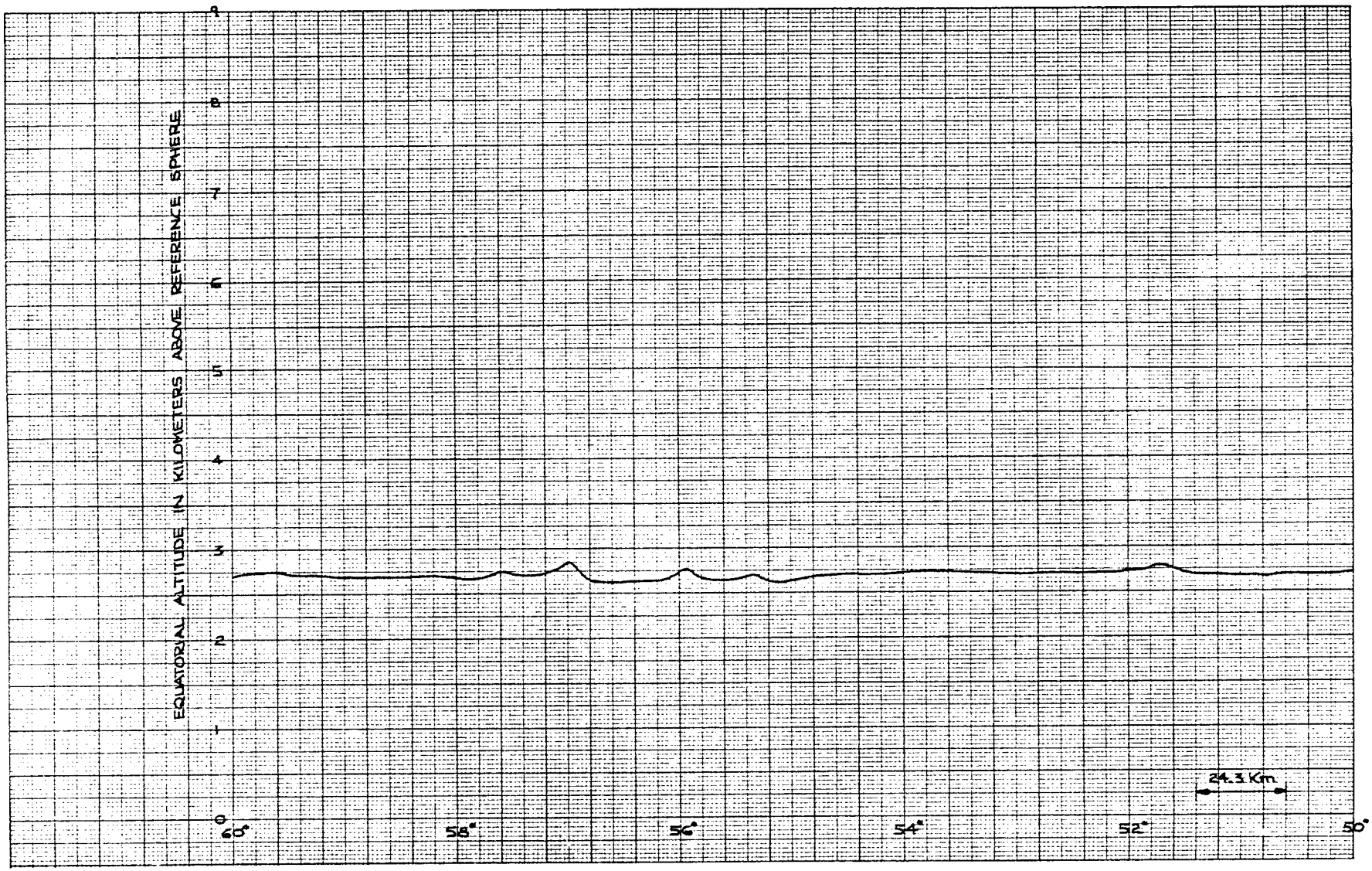

Figure B-4. Lunar Equatorial Altitude Versus West Longitude (View 2)

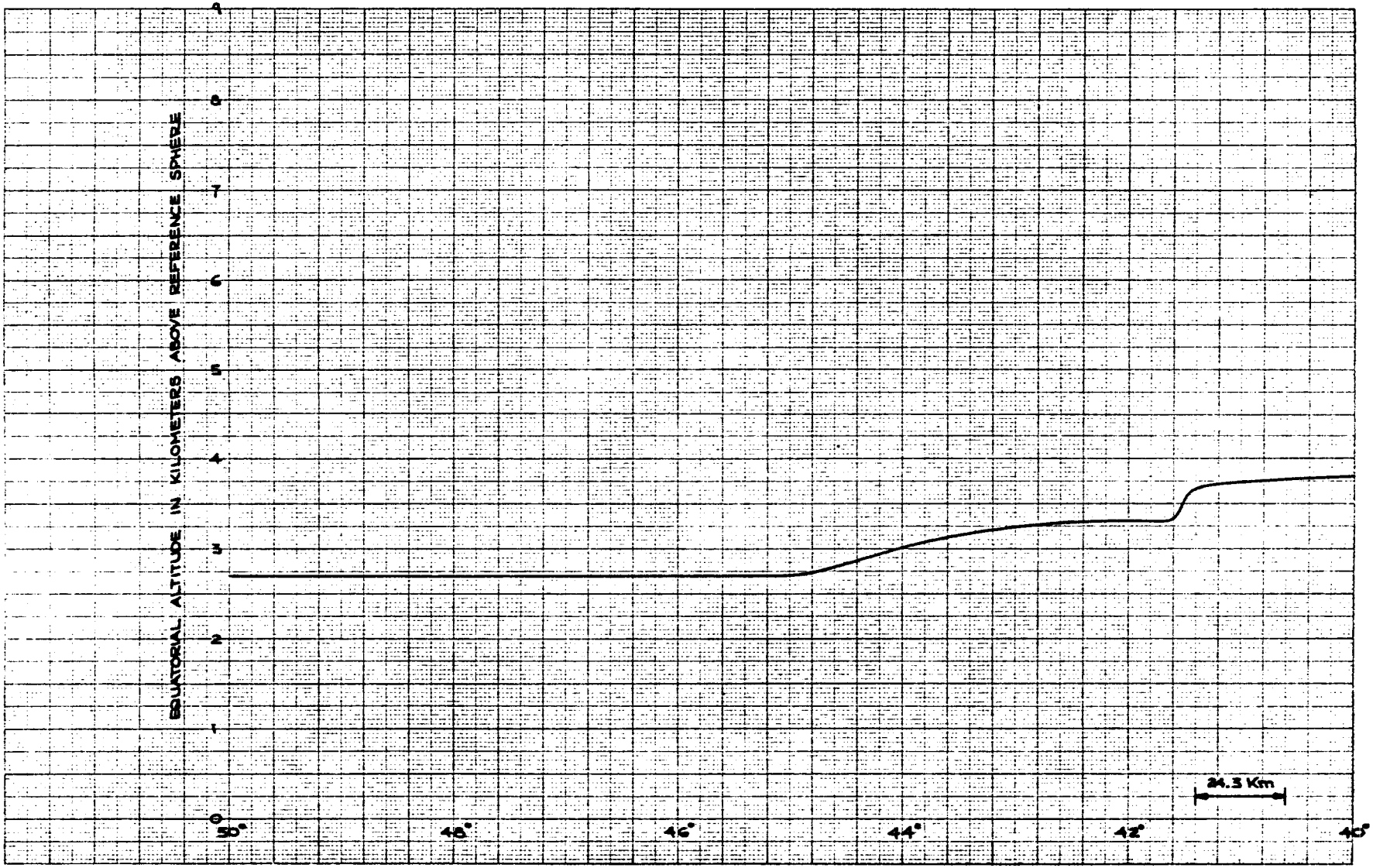

Figure B-5. Lunar Equatorial Altitude Versus West Longitude (View 3)

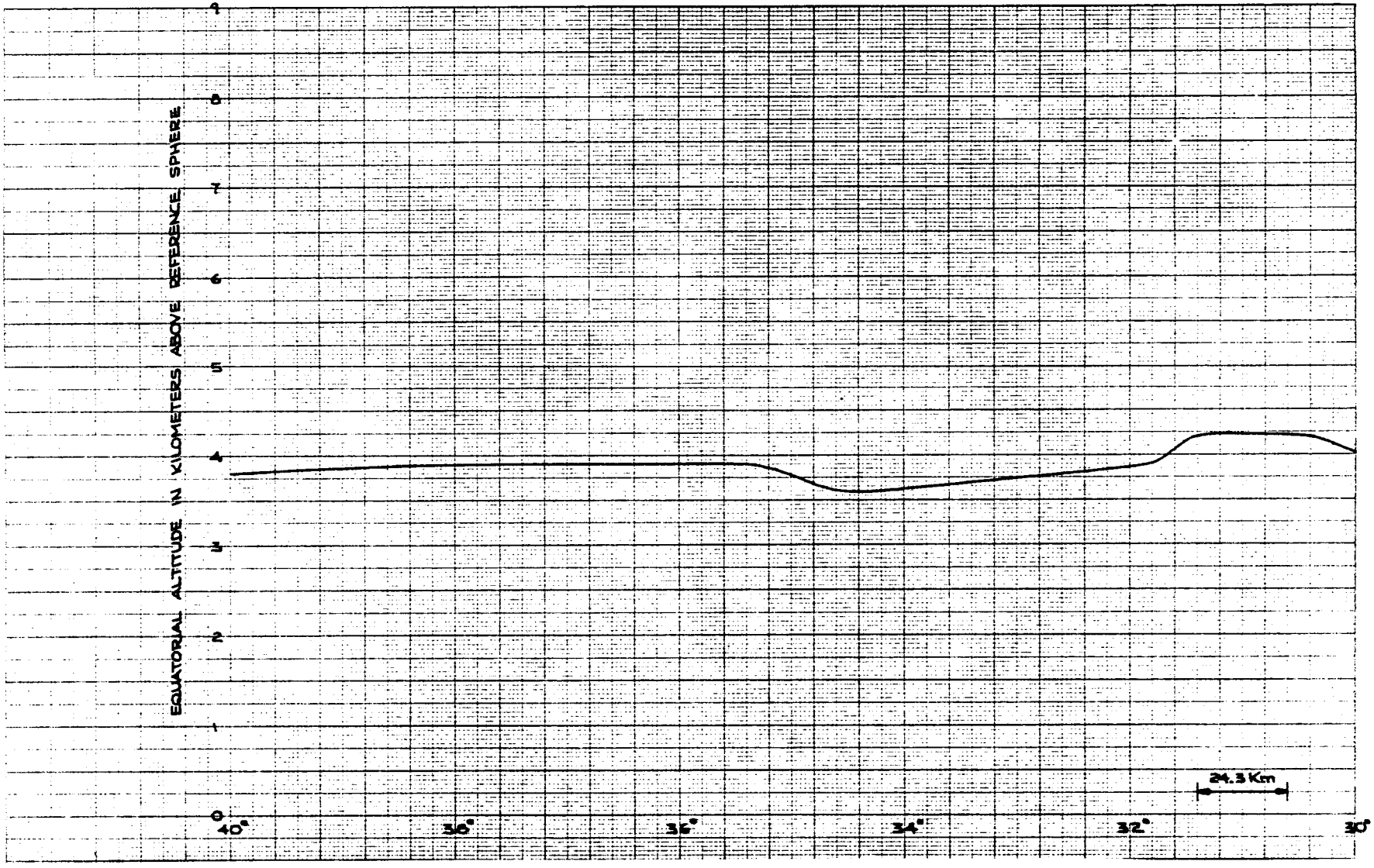

Figure B-6. Lunar Equatorial Altitude Versus West Longitude (View 4)

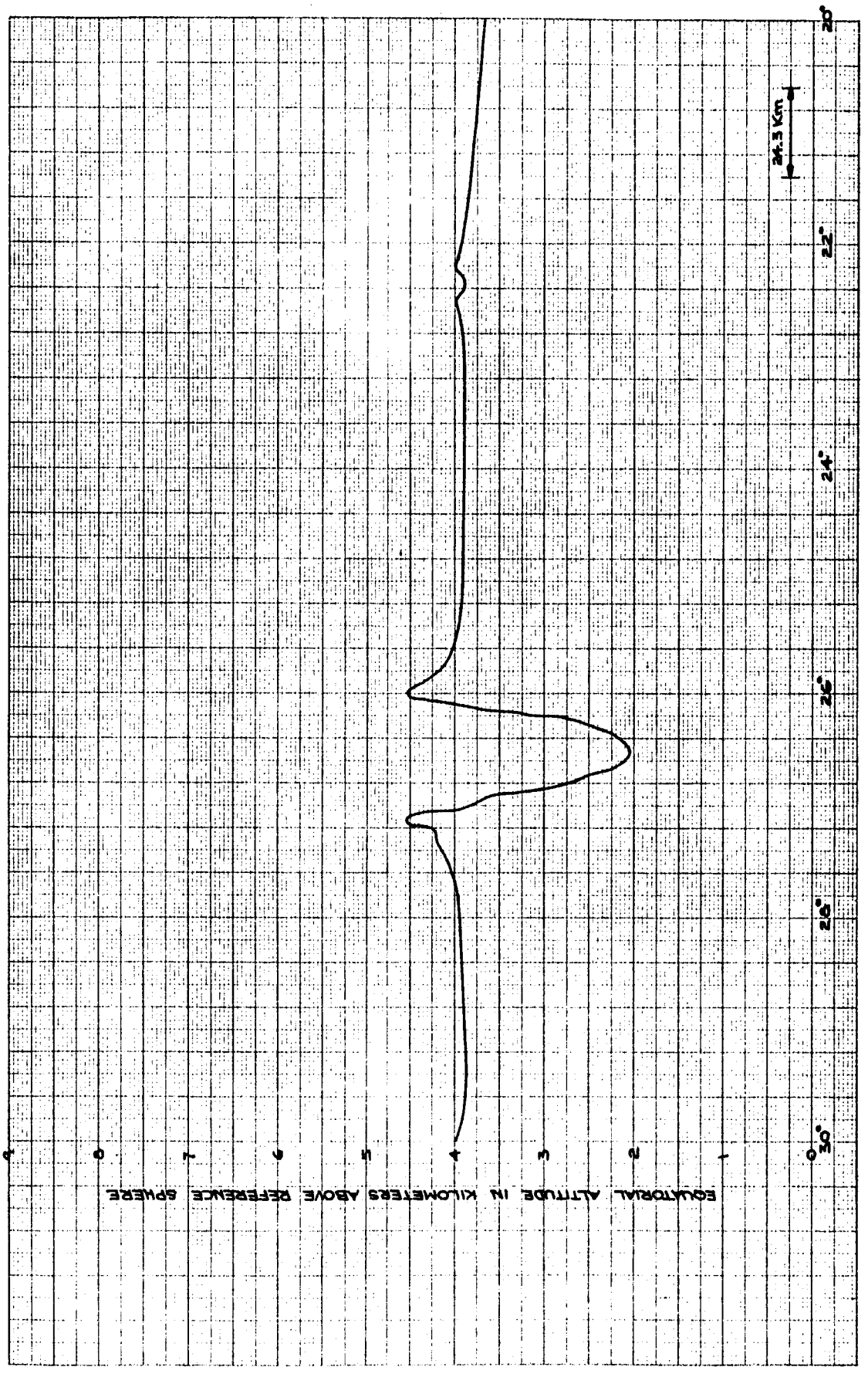

Figure B-7. Lunar Equatorial Altitude Versus West Longitude (View 5)

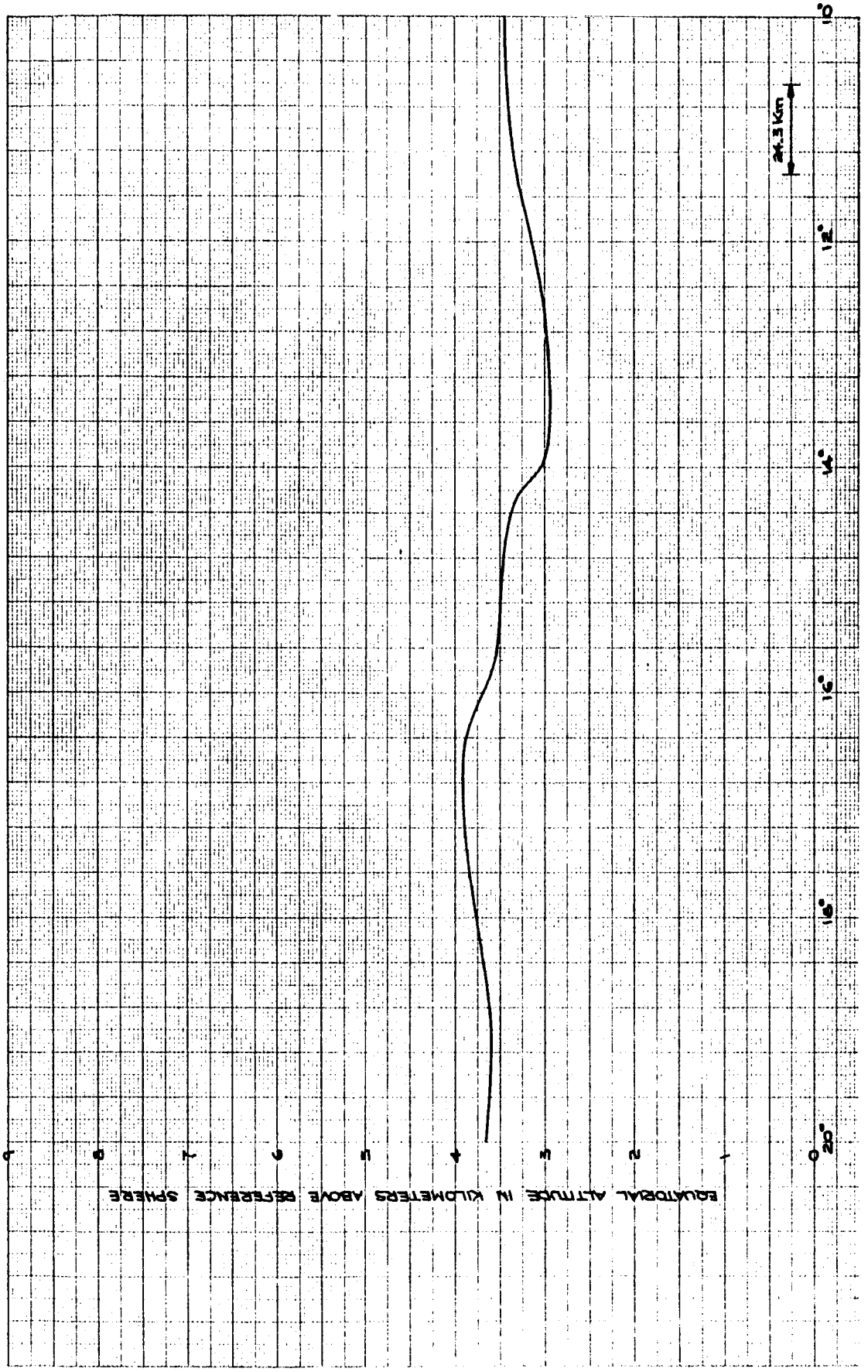

Figure B-8. Lunar Equatorial Altitude Versus West Longitude (View 6)

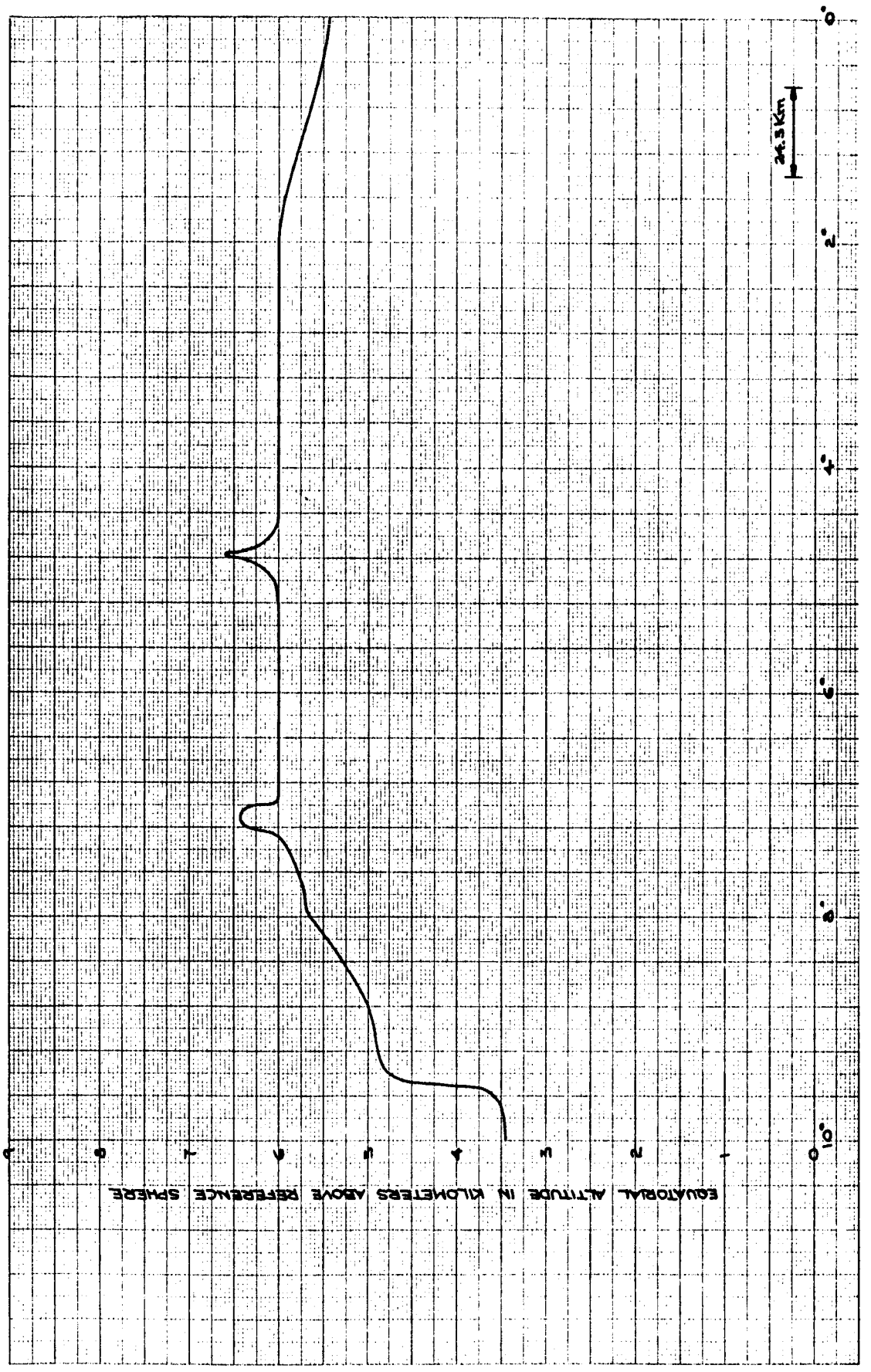

Figure B-9. Lunar Equatorial Altitude Versus West Longitude (View 7)

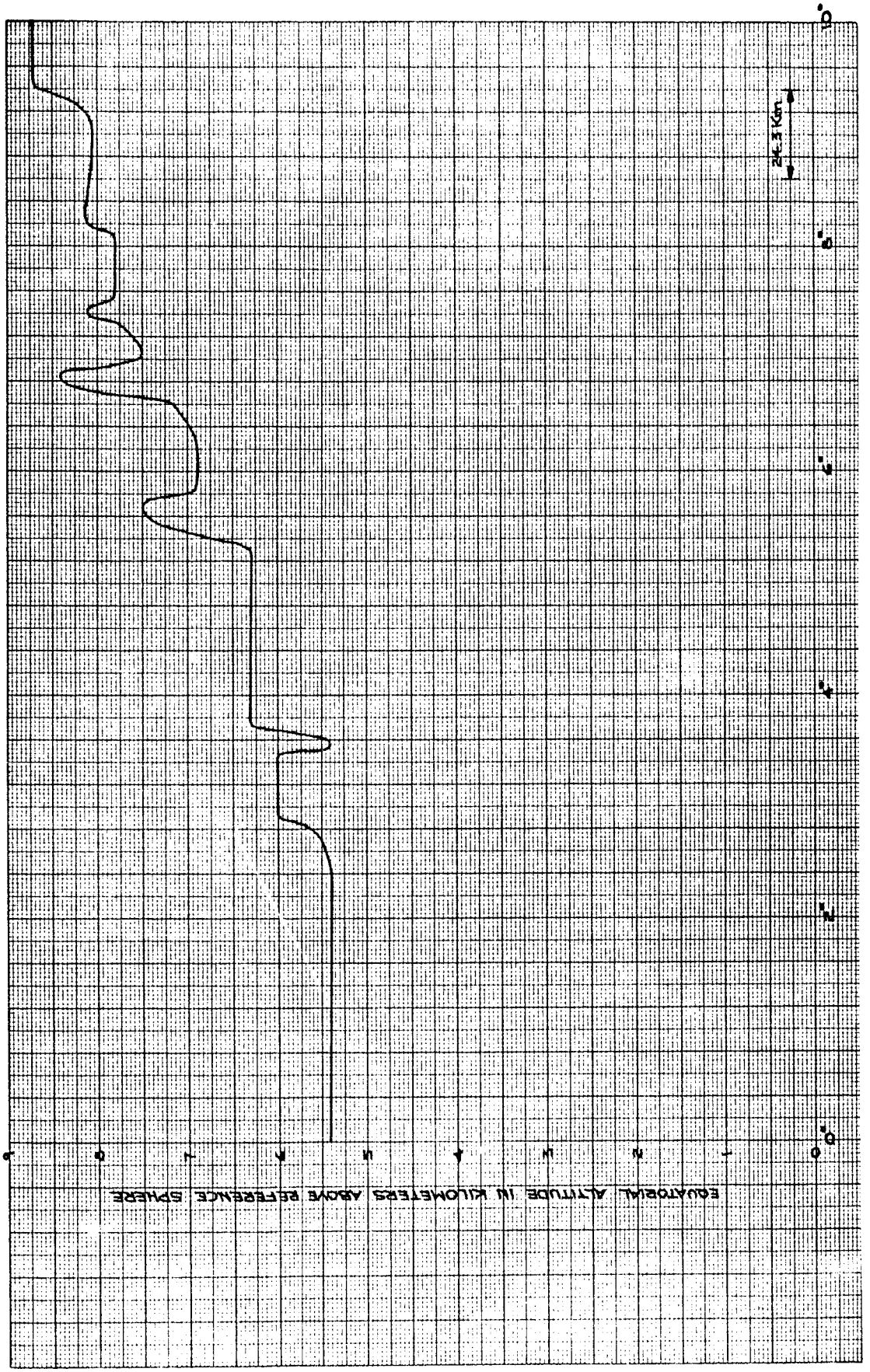

Figure B-10. Lunar Equatorial Altitude Versus East Longitude (View 1)

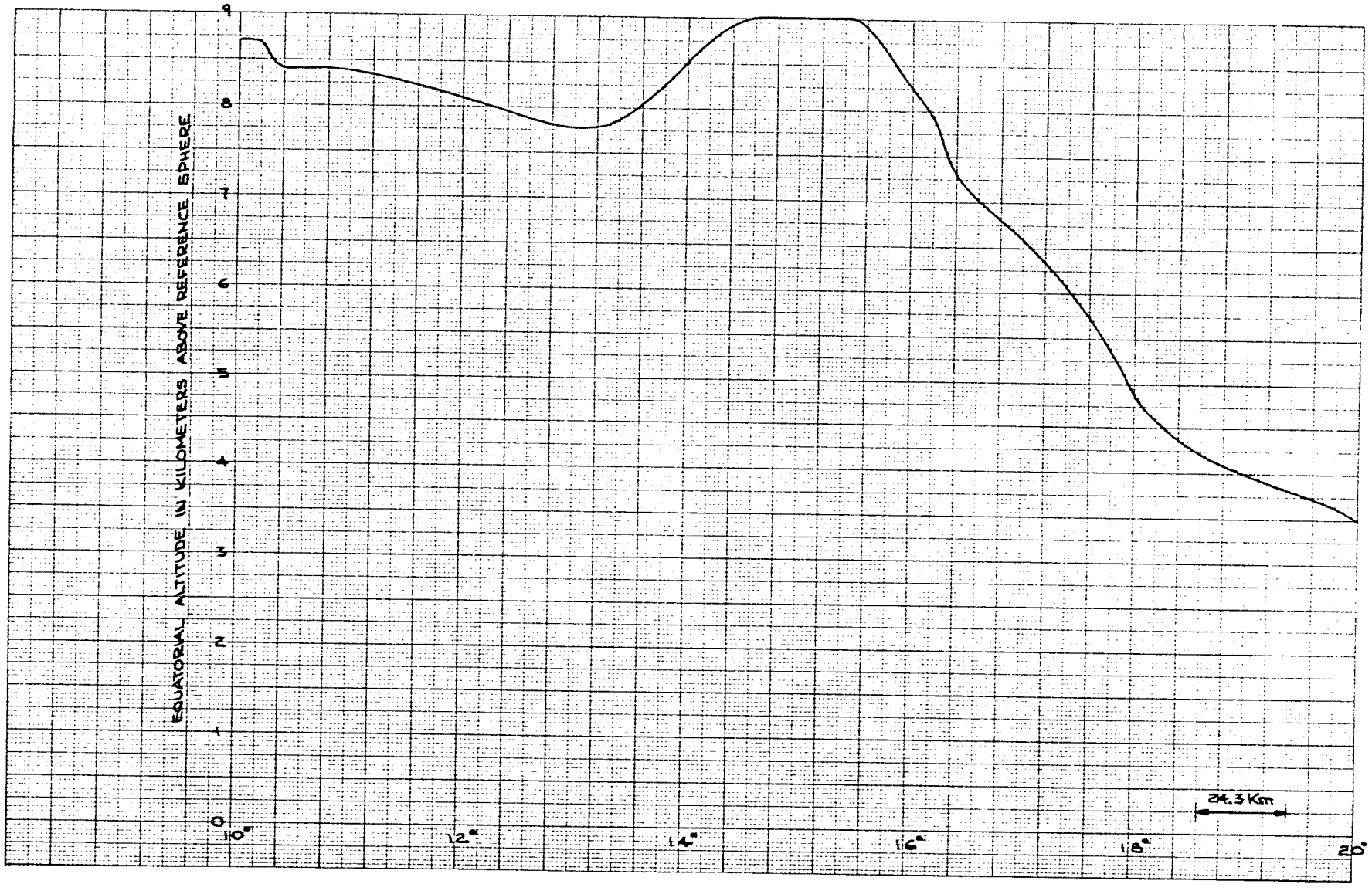

Figure B-11. Lunar Equatorial Altitude Versus East Longitude (View 2)

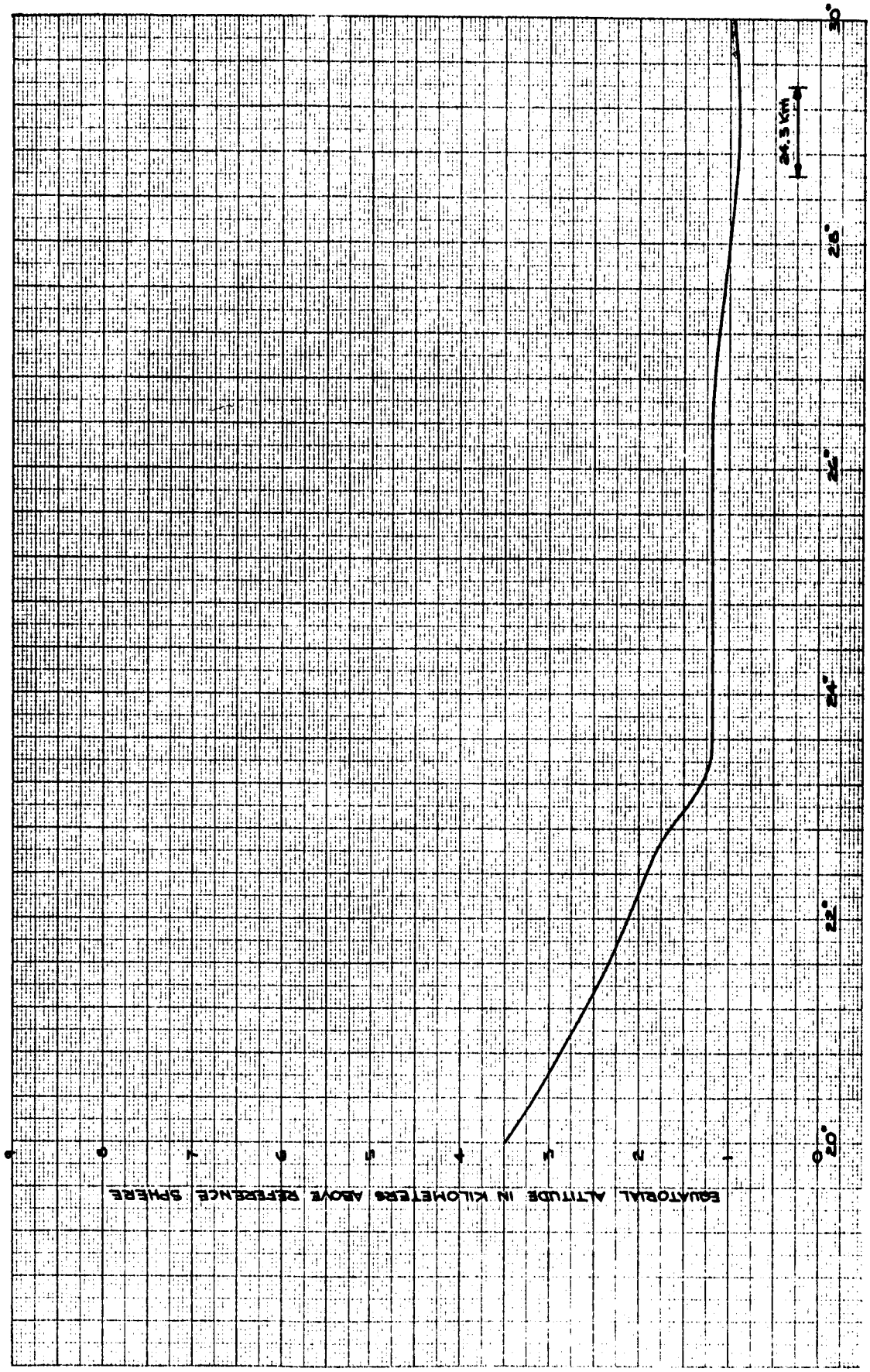

Figure B-12. Lunar Equatorial Altitude Versus East Longitude (View 3)

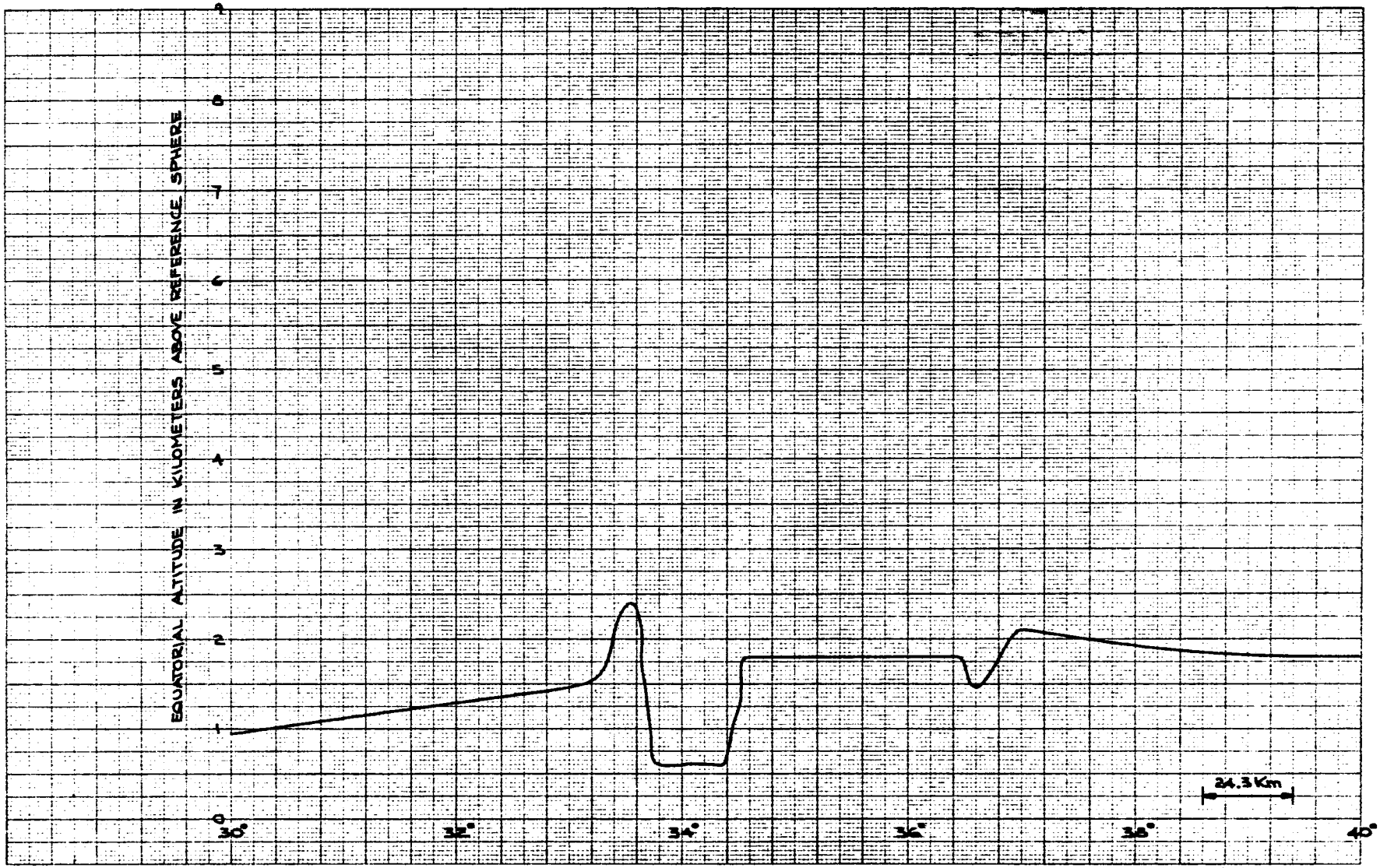

Figure B-13. Lunar Equatorial Altitude Versus East Longitude (View 4)

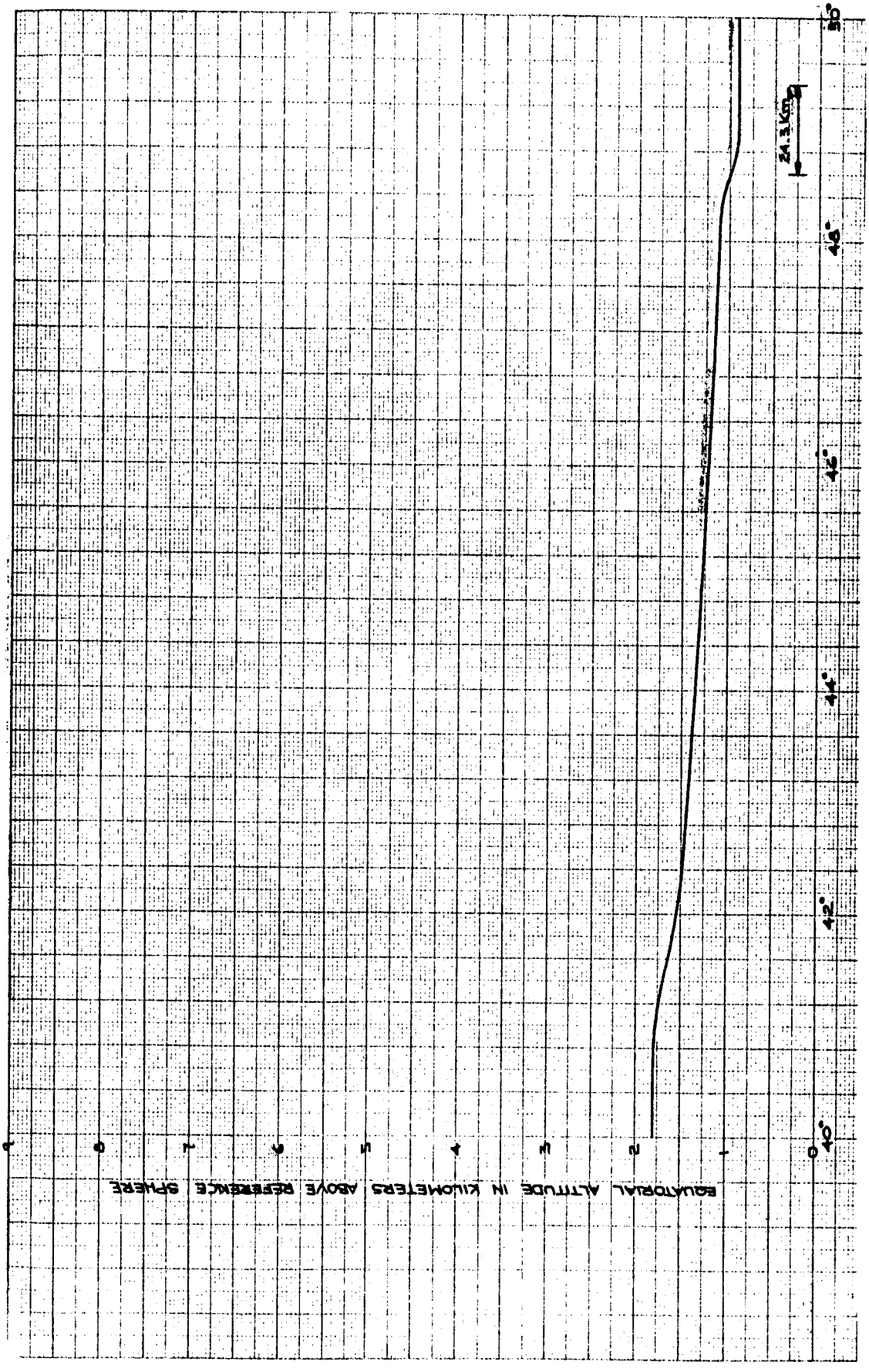

Figure B-14. Lunar Equatorial Altitude Versus East Longitude (View 5)

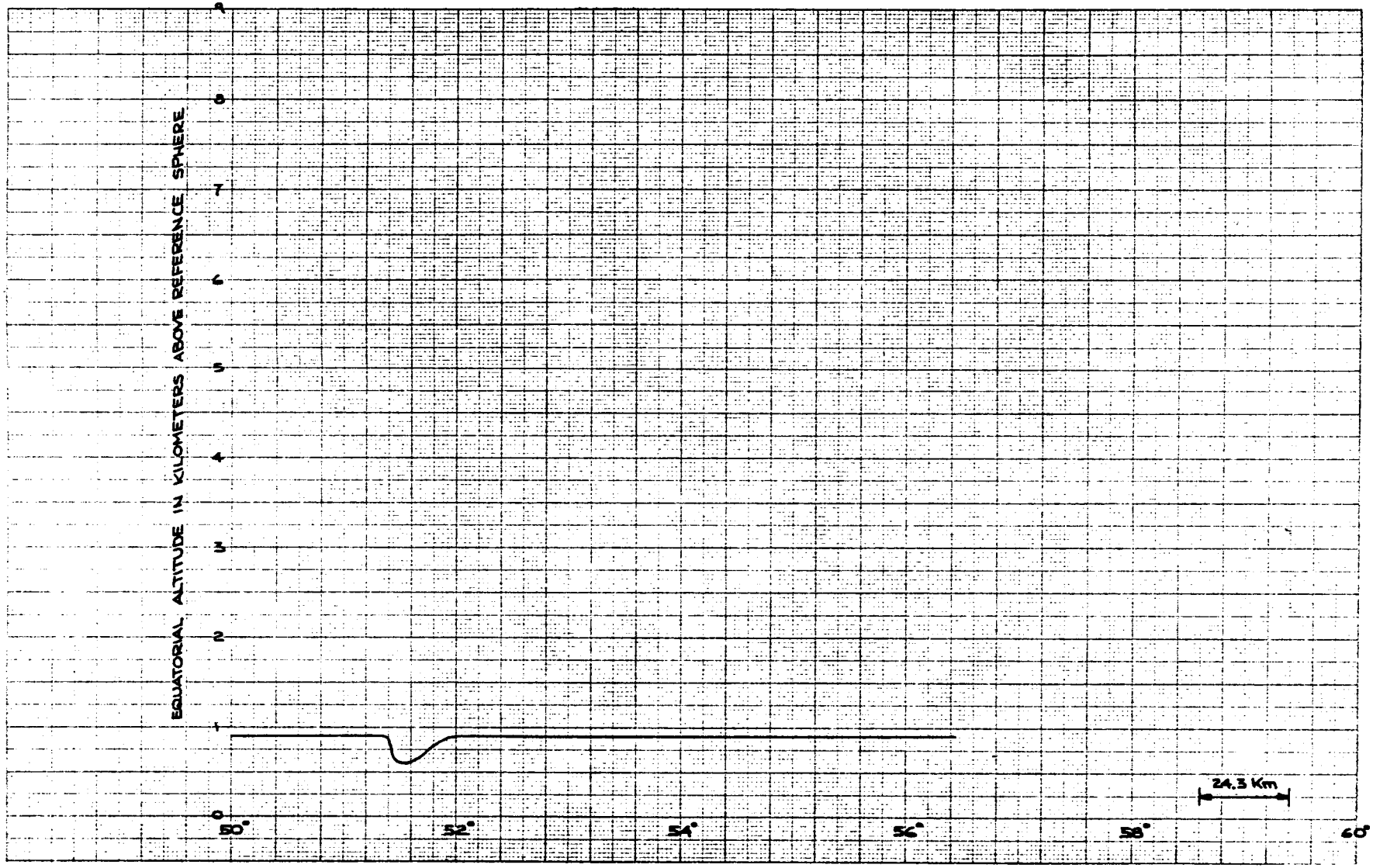

Figure B-15. Lunar Equatorial Altitude Versus East Longitude (View 6)

or

$$r_m = \frac{r_a r_b}{\sqrt{r_a^2 - \left(r_a^2 - r_b^2\right)\cos^2\theta}} \tag{B.2}$$

Let

$$e = \frac{1}{2}\,\frac{r_a^2 - r_b^2}{r_a^2} \tag{B.3}$$

Then

$$r_m = \frac{r_b}{\sqrt{1 - 2e\cos^2\theta}} \tag{B.4}$$

where

$$e = \frac{1}{2}\,\frac{r_a - r_b}{r_a}\,\frac{r_a + r_b}{r_a} \approx \frac{1}{2}\,\frac{r_a - r_b}{r_a}\,\frac{2r_a}{r_a} = \frac{r_a - r_b}{r_a}$$

and $\frac{r_a - r_b}{r_a}$ is sometimes called the ellipticity of the equator.

The lunar contour maps supplied estimates of rm, designated by r_m^* for 1,204 values of θ. A least squares fit to this data was then made in order to determine the parameters r_b and e of the reference ellipse. In order to make a least squares fit, Equation (B.4) was linearized to give

$$\Delta r_m = \frac{\partial r_m}{\partial r_b}\,\Delta r_b + \frac{\partial r_m}{\partial e}\,\Delta e \tag{B.5}$$

where

$$\Delta r_m = r_m - r_m\Big|_{\text{nominal}}$$

$$\Delta r_b = r_b - r_b\Big|_{\text{nominal}}$$

$$\Delta e = e - e\Big|_{\text{nominal}}$$

and

$$\frac{\partial r_m}{\partial r_b} = \frac{1}{\sqrt{1-2e\cos^2\theta}} \tag{B.7}$$

$$\frac{\partial r_m}{\partial_e} = r_m \frac{\cos^2\theta}{1-2e\cos^2\theta} \tag{B.8}$$

The partials are evaluated with nominal values of r_m, r_b, and e.

The state vector will be

$$\Delta x = \begin{bmatrix} \Delta r_b \\ \Delta e \end{bmatrix} \tag{B.9}$$

The measurement vector will be

$$\Delta y^* = \begin{bmatrix} r^*_{m,1} - r_{m,1} \\ r^*_{m,2} - r_{m,2} \\ \vdots \\ r^*_{m,1204} - r_{m,1204} \end{bmatrix} \tag{B.10}$$

where $r_m = r_m \Big|_{\text{nominal}}$

The measurement matrix is

$$M = \begin{bmatrix} \left.\frac{\partial r_m}{\partial r_b}\right|_{\theta_1} & \left.\frac{\partial r_m}{\partial e}\right|_{\theta_1} \\ \left.\frac{\partial r_m}{\partial r_b}\right|_{\theta_2} & \left.\frac{\partial r_m}{\partial e}\right|_{\theta_2} \\ \vdots & \vdots \\ \left.\frac{\partial r_m}{\partial r_b}\right|_{\theta_{1204}} & \left.\frac{\partial r_m}{\partial e}\right|_{\theta_{1204}} \end{bmatrix} \qquad \text{(B.11)}$$

where the partials in M are evaluated with the nominal values of r_b and e.

The least squares solution for Δx is

$$\Delta x = (M^T M)^{-1} M^T \Delta y^* \qquad \text{(B.12)}$$

and the improved estimate of r_b and e is

$$\begin{bmatrix} \hat{r}_b \\ \hat{e} \end{bmatrix} = \begin{bmatrix} r_b \\ e \end{bmatrix}_{\text{nominal}} + (M^T M)^{-1} M^T \Delta y^* \qquad \text{(B.13)}$$

This new estimate of r_b and e is then used as a new nominal value for another least squares estimate, the process continuing until there is no further change in the estimate of r_b and e. The starting nominal values of r_b = 1736 km and e = 0.4×10^{-2} were used. After five passes through the least squares equations, no further improvement (or change) was noted and the resulting final values of

$$r_b = 1735.0 \text{ km} \qquad e = 0.3186 \times 10^{-2}$$

were obtained.

The footnotes on the previously referenced maps indicated a probable error of 1,000 meters in the reference sphere to which the altitudes were referenced. A probable error of 1,000 meters corresponds to a standard

deviation of 1.483 km. Since the footnotes indicated that this error would soon be reduced as more data was examined, an alternate standard deviation of 1.483/3 km was also used for the study. Thus, r_b was taken as

$$r_b = 1735.0 \pm 1.48 \text{ km}$$
$$\pm 0.495 \text{ km, alternately.}$$

It was assumed that the figure of the moon was an ellipsoid given by

$$\frac{x^2}{r_a^2} + \frac{y^2}{r_b^2} + \frac{z^2}{r_c^2} = 1 \qquad \text{(B.14)}$$

where the positive z axis is the north polar axis of the moon. Let

$$x = r_m \cos\phi \cos\theta \qquad y = r_m \cos\phi \sin\theta \qquad z = r_m \sin\phi \qquad \text{(B.15)}$$

where θ is east longitude, ϕ is north latitude, and r_m is the radial distance from the center of the moon to the surface of the ellipsoid. Then

$$r_m^2 \left[\frac{\cos^2\theta \cos^2\phi}{r_a^2} + \frac{\sin^2\theta \cos^2\phi}{r_b^2} + \frac{\sin^2\phi}{r_c^2} \right] = 1$$

or

$$r_m = \frac{r_c}{\sqrt{1 - \frac{r_b^2 - r_c^2}{r_b^2}\cos^2\phi - \frac{r_c^2}{r_b^2}\frac{r_a^2 - r_b^2}{r_a^2}\cos^2\theta \cos^2\phi}} \qquad \text{(B.16)}$$

Since this study only dealt with equatorial orbits and since a complete set of lunar contour maps is not yet available in the polar direction, it was assumed that $r_c = r_b$. Thus, Equation (B.16) becomes

$$r_m = \frac{r_b}{\sqrt{1 - 2e\cos^2\theta \cos^2\phi}} \qquad \text{(B.17)}$$

which was taken as the figure of the moon in the vicinity of the equator.

B. CORRELATED TERRAIN NOISE

The previously mentioned least squares program also calculated the altitude of the lunar equatorial surface with respect to the ellipsoidal figure of the moon. Altitude referenced to the ellipsoid is shown in the bottom graph of Figure B-2. Since, in this study, the altimeter is used to obtain estimates of the distance to the center of the moon, the surface altitudes above the figure of the moon are equivalent to a noise input to the system. That is distance from the center of the moon to the spacecraft is

$$r = r_m + \varepsilon_c + h \tag{B.18}$$

where h is the altitude above the lunar surface, and ε_c is the distance from the figure of the moon to the lunar surface. The quantity ε_c is that function shown in the lower graph of Figure B-2.

The autocorrelation function of ε_c was computed using the 1204 residuals calculated by the least squares program. This autocorrelation function was then plotted as the solid line shown in Figure B-16. This autocorrelation function was then approximated by

$$\phi_{(\theta)} = \phi_o e^{-a\theta} \cos b\theta \tag{B.19}$$

where

$$\phi_o = 2.59 \text{ km}^2$$

$$a = 1.73 \text{ } (\theta \text{ in radians})$$

$$= 0.0302 \text{ } (\theta \text{ in degrees})$$

$$b = 6.57$$

Equation (B.19) is shown as the dashed curve in Figure B-16.

The difference equation which generates noise with an autocorrelation function as shown in Equation (B.19) is

$$\varepsilon_{c,n} = b_1 \varepsilon_{c,n-1} - b_2 \varepsilon_{c,n-2} + a_1 \varepsilon_{w,n-1} + a_2 \varepsilon_{w,n-2} \tag{B.20}$$

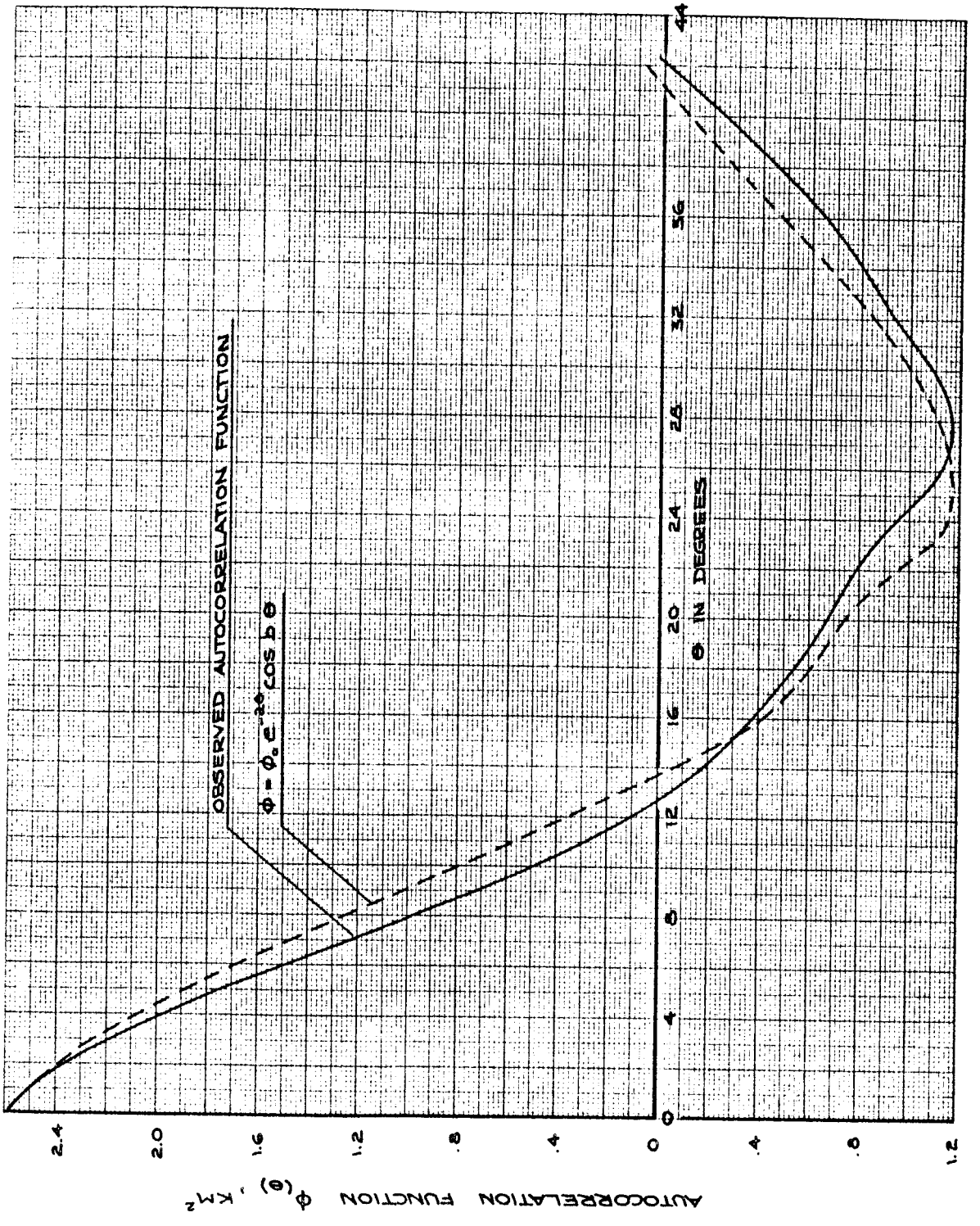

Figure B-16. Autocorrelation Function of Terrain Noise

where

$$E\left[\varepsilon_{w,n}\right] = 0$$

$$E\left[\varepsilon_{w,n}\varepsilon_{w,n-i}\right] = 0 \qquad i \neq 0$$

$$= 1 \qquad i = 0$$

$$b_1 = 2e^{-a\Delta\theta}\cos b\Delta\theta$$

$$b_2 = e^{-2a\Delta\theta}$$

$$a_1 = \frac{1}{2}\sqrt{(1-b_2)\phi_o}\left[\sqrt{1 + b_2 - b_1} - \sqrt{1 + b_2 + b_1}\right]$$

$$a_2 = \frac{1}{2}\sqrt{(1-b_2)\phi_o}\left[\sqrt{1 + b_2 - b_1} + \sqrt{1 + b_2 + b_1}\right]$$

and where $\Delta\theta$ = change in central orbit angle in one computing cycle. It is not too difficult to show that

$$E\left[\varepsilon_{c,n}\varepsilon_{c,n-i}\right] = \phi_o e^{-ai\Delta\theta}\cos bi\Delta\theta$$

The Kalman filter requires that the present value of the state vector depends only on the values of the state variables exising in the previous cycle (see Appendix A). In order to get Equation (B.20) into this form, a dummy state variable

$$\varepsilon_{d,n} = \varepsilon_{c,n-1} - \frac{a_2}{b_2}\varepsilon_{w,n-1} \tag{B.23}$$

was introduced. Then Equation (B.20) becomes

$$\varepsilon_{c,n} = b_1\varepsilon_{c,n-1} - b_2\varepsilon_{d,n-1} + a_1\varepsilon_{w,n-1} \tag{B.24}$$

which are the forms necessary for use in the Kalman filter.

APPENDIX C

MODEL OF THE ALTIMETER USED IN THE KALMAN FILTER SIMULATION

The mathematical model used for the altimeter was (Reference 1)

$$\left[\left(\pi - \omega_{r(t)}\tau(t)\right)K_o K_D\right] * g_{c(t)} + \omega'_r = \omega_{r(t)} \qquad \text{(C.1)}$$

where

$\omega_r = \frac{\pi c}{2h_o}$

c = speed of light

h_o = altitude output from altimeter

$\tau = 2\frac{h_i}{c}$

h_i = altitude input to altimeter

K_o = constant = $1.256.10^5 \frac{\text{rad/sec}}{\text{volt}}$ for this study

K_D = an adjustable gain = $\frac{222}{\text{altitude in km}} K'_D$

K'_D = 1.7 volts/rad for this study

$*$ = convolution in the time domain

ω'_r = VCO rest frequency.

and

$$g_{c(t)} = L^{-1}\left\{K_c \frac{T_2 s+1}{(T_3 s+1)(K_c T_1 s+1)}\right\} \qquad \text{(C.2)}$$

where

L^{-1} = inverse Laplace transform

K_c = constant = 1000 for this study

T_2 = adjustable time constant = $\sqrt{\frac{\text{alt in km}}{222}} T'_2$

T'_2 = 2.51 sec for this study

T_3 = fixed time constant = 78.6 sec

T_1 = adjustable time constant = $\sqrt{\frac{\text{alt in km}}{222}}$ T'_1

T'_1 = 8.68 sec for this study.

Substituting the definition of the ω_r and τ into Equation (C.1) gives

$$K_o K_D \left(1 - \frac{h_i}{h_o}\right) * g_{c(t)} + \frac{\omega'_r}{\pi} = \frac{c}{2h_o} \qquad \text{(C.3)}$$

In order to obtain the elements in the updating matrix for the Kalman filter (see Appendix A), the variational equation for Equation (C.3) will be obtained. Let

$$h_i = h'_i + \Delta h_i \qquad h_o = h'_o + \Delta h_o \qquad \text{(C.4)}$$

where h'_i and h'_o are nominal values, and Δh_i and Δh_o are the deviations from nominal. Then Equation (C.3) becomes, assuming small deviations,

$$K_o K_D \left(1 - \frac{h'_i}{h'_o}\right) * g_{c(t)} - K_o K_D \frac{1}{h'_o}\left(\Delta h_i - \frac{h'_i}{h'_o}\Delta h_o\right) * g_{c(t)} + \frac{\omega'_r}{\pi}$$

$$= \frac{c}{2h'_o} - \frac{c}{2h'^2_o}\Delta h_o \qquad \text{(C.5)}$$

But the nominal value of h'_o will be obtained by solving Equation (C.3) when h'_i is used as the input. Thus

$$K_o K_D \left(1 - \frac{h'_i}{h'_o}\right) * g_{c(t)} + \frac{\omega'_r}{\pi} = \frac{c}{2h'_o}$$

and so Equation (C.4) becomes the variational equation

$$K_o K_D \left(\Delta h_i - \frac{h'_i}{h'_o}\Delta h_o\right) * g_{c(t)} = \frac{c}{2h'_o}\Delta h_o$$

Assuming that $h'_i \approx h'_o = h$, then

$$K_o K_D (\Delta h_i - \Delta h_o) * g_{c(t)} = \frac{c}{2h} \Delta h_o \tag{C.6}$$

Taking the Laplace transform of both sides of this equation, and assuming h is approximately constant over each computing interval, then

$$L\left\{\Delta h_o\right\} = \frac{\frac{2h}{c} K_o K_D G_{c(s)}}{1 + \frac{2h}{c} K_o K_D G_{c(s)}} L\left\{\Delta h_i\right\} \tag{C.7}$$

where

$$G_{c(s)} = K_c \frac{T_2 s + 1}{(T_3 s + 1)(K_c T_1 s + 1)} \tag{C.8}$$

At high altitudes, h = 185 km, Equation (C.7) gave a time to peak of about 2.2 sec with an overshoot of 20 percent. At low altitudes, h = 18.5 km, the time to peak was about 1.6 sec with an overshoot of 70 percent.

The technique of expanding into a Taylor series (Appendix A) could now be used to obtain that part of the updating matrix corresponding to the altimeter dynamics. However, a Taylor series expansion would have limited the integration interval to be much less than the time constants in Equation (C.7). Another very serious objection to the Taylor series expansion was that it involved repeated differentiations of $\Delta h_i = \Delta r - \Delta r_m$ which would have been very complicated. Thus it was decided to obtain the updating difference equations from

$$\Delta h_o^* = (1 - e^{-\Delta T s})\left(\frac{1}{s} G_{(s)}\right)^* \Delta h_i^* \tag{C.9}$$

where

$$G_{(s)} = \frac{\frac{2h}{c} K_o K_D G_{c(s)}}{1 + \frac{2h}{c} K_o K_D G_{c(s)}} \tag{C.10}$$

and where * represents the z transform (Reference 2)*. Taking the z transform of $\frac{1}{s} G_{(s)}$ in Equation (C. 9) gave the difference equation

$$\Delta h_{o,n} = b_3 \Delta h_{o,n-1} - b_4 \Delta h_{o,n-2} + a_3 \Delta h_{i,n-1} + a_4 \Delta h_{i,n-2} \qquad (C.11)$$

where

$$b_3 = 2e^{-\zeta\omega\Delta T} \cos \omega\sqrt{1-\zeta^2}\,\Delta T$$

$$b_4 = e^{-2\zeta\omega\Delta T}$$

$$a_3 = \left[1 - \frac{1}{2} b_3 + \frac{A\omega/B - \zeta}{\sqrt{1-\zeta^2}} e^{-\zeta\omega\Delta T} \sin \omega\sqrt{1-\zeta^2}\,\Delta T\right] B$$

$$a_4 = \left[b_4 - \frac{1}{2} b_3 - \frac{A\omega/B - \zeta}{\sqrt{1-\zeta^2}} e^{-\zeta\omega\Delta T} \sin w\sqrt{1-\zeta^2}\,\Delta T\right] B$$

and where

$$B = \frac{\frac{444}{c} K_o K'_D K_c}{1 + \frac{444}{c} K_o K'_D K_c} \qquad A = B\sqrt{\frac{h}{222}}\, T'_2$$

$$\omega = \sqrt{\frac{1 + \frac{444}{c} K_o K'_D K_c}{K_c T'_1 T_3 \sqrt{\frac{h}{222}}}}$$

$$\zeta = \frac{1}{2} \frac{T_3 + \left(K_c T'_1 + \frac{444}{c} K_o K'_D K_c T'_2\right)\sqrt{\frac{h}{222}}}{\sqrt{\sqrt{\frac{h}{222}}\, K_c T'_1 T_3 \left[1 + \frac{444}{c} K_o K'_D K_c\right]}}$$

* $\left(\frac{1}{s} G_{(s)}\right)^*$ listed in Appendix 1 of Reference 2 for the $G_{(s)}$ above is incorrect.

This difference equation, Equation (C. 11), is not as sensitive to the computing or integration interval as a Taylor series expansion would have been. In fact, Equation (C. 11) is exact when the input is "stair-stepwise" continuous. Hence if Δh_i is slowly varying, with respect to the computing interval, then Equation (C. 11) is a good approximation to the exact solution of Equation (C. 7).

In order to use the difference equation in the Kalman filter, current values must be expressed in terms of only the preceeding cycle. In order to get Equation (C. 11) into this form, an intermediate state variable

$$\Delta h_{d,n} = \Delta h_{o,n-1} - \frac{a_4}{b_4} \Delta h_{i,n-1} \qquad \text{(C. 12)}$$

will be introduced. Thus Equation(C. 11) becomes

$$\Delta h_{o,n} = b_3 \Delta h_{o,n-1} - b_4 \Delta h_{d,n-1} + a_3 \Delta h_{i,n-1} \qquad \text{(C. 13)}$$

which is the desired form.

REFERENCES

1. "Study of Lunar Landing Sensor Performance," Interim Report No. 1, NASA Report No. NAS8-5205, 21 June 1963.

2. Tou, Julius, "Digital and Sampled-Data Control Systems," McGraw-Hill Book Co., 1959.

APPENDIX D

DERIVATION OF ISOLATION REQUIREMENTS AND MEASUREMENT TECHNIQUES

A. DERIVATION OF ISOLATION REQUIREMENTS

Two categories of power entering a radar receiver will be considered. The first is called leakage and is the portion of the transmitter output power that enters the receiver without having traversed the space between radar and target. The second is the signal and is the power that has traversed the radar-target interspace. The term isolation for any radar component will be defined here as the relative attenuation of the average leakage and signal powers when passing through that component. Figure D-1 illustrates this concept. By this definition it is clear that such components as wide-band amplifiers and attenuators in the transmit-receive path contribute no isolation factors. System isolation is simply the product of the isolation factors contributed by the individual components.

$$A_S = \frac{\overline{P_{Si}}}{\overline{P_{So}}} > 1$$

$$A_L = \frac{\overline{P_{Li}}}{\overline{P_{Lo}}} > 1$$

$$I = \frac{A_L}{A_S} > 1$$

where

$\overline{P_{Si}}$ and $\overline{P_{So}}$ are the average input and output signal powers, respectively,

$\overline{P_{Li}}$ and $\overline{P_{Lo}}$ are the average input and output leakage powers, respectively,

I is the isolation factor contributed by the component.

Figure D-1. Definition of Isolation

It is the primary intent of this appendix to determine the system isolation required of a particular, yet representative, type of radar device which has been designed to provide lunar landing altimetry up to altitudes of about 220 km. A second objective will be to show that the isolation contributed by a radar component may be determined experimentally without the necessity of actually processing a return signal.

From the system shown in Figure D-2, it is clear that the transmit-receive losses undergone exclusively by the signal (i.e., not undergone by the leakage) are those associated with transmission and free-space propagation. When ranging against an extended target as is the case in altimetry, the total of these losses L_s at the maximum altitude may be determined as follows:

$$L_s = \frac{\sigma_o A_R \varepsilon L^2}{4\pi h^2} \qquad \text{(D. 1)}$$

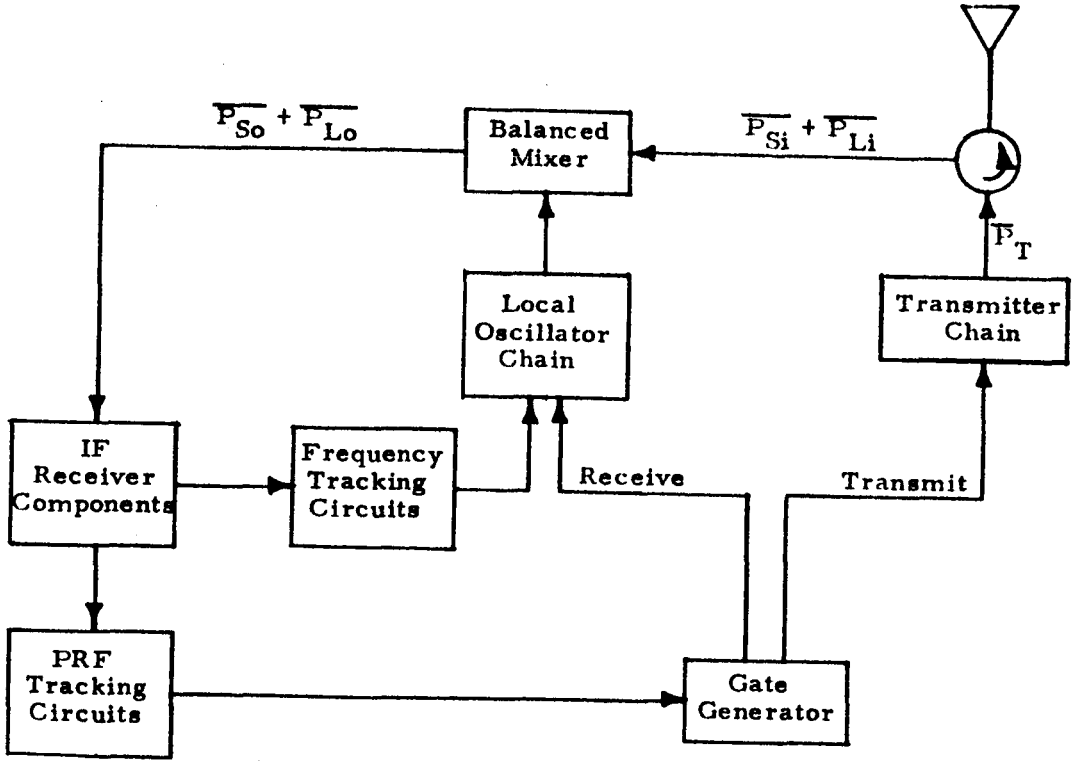

Figure D-2. System Considered for Derivation of Isolation Requirements

where

σ_o = average surface reflection coefficient

A_R = aperture area of the antenna

ϵ = effective antenna efficiency

L = effective circulator-to-space microwave losses

h = altitude above the lunar surface.

Performing the computation in terms of power ratios

$\sigma_o = 0.1$	-10 db
$A_R = \pi \left(\frac{D}{2}\right)^2 = \pi \left(\frac{0.6m}{2}\right)^2 = 0.283\ m^2$	-5.5
$\epsilon = 0.6$	-2.2
$L^2 = 2(-0.25\ db) = -0.5\ db$	-0.5
$4\pi = 12.6$	-11.0
$h^2 = (220\ km)^2 = 4.84 \times 10^{10}\ m^2$	-106.9
Total	-136.1 db

Thus the total signal loss factor at the maximum altitude of 220 km is 2.46×10^{-14}. This factor varies as the square of the altitude, giving the following expression for signal loss as a function of altitude:

$$L_s = 2.46 \left(\frac{220\ km}{h\ km}\right)^2 10^{-14} \qquad (D.2)$$

Therefore, the loss factor at the minimum design altitude of 1.8 km is about 3.66×10^{-10} or -94.4 db.

The next step is to determine the signal-to-leakage ratio required in the receiver bandpass circuits. The effect that a leakage carrier has on altitude tracking is entirely dependent upon its position and movement in the predetection bandpass relative to the signal carrier.* These relative

* The signal carrier is centered in the predetection bandpass by action of the frequency-tracking circuits. It will be assumed as somewhat of a worst case condition here that the leakage carrier also falls in this bandpass. Note that this implies near-zero doppler shift which in turn implies near-zero altitude rates typical of circular orbits. This condition, which negates the possibility of deriving an isolation component by means of frequency discrimination, will be assumed throughout the derivation contained in this appendix.

conditions are in turn dependent upon altitude rate and acceleration, in addition to inherent frequency jitter in the transmitter and frequency track circuits. These factors and the finite spectral width of the leakage carrier create a "smearing" effect across the bandpass. For the purpose of analysis, it will therefore be assumed that the leakage carrier power may be characterized as an average or uniform power density function across the predetection bandpass. The effective leakage density P_L is thus

$$P_L = \frac{P_{LC}}{B_{PD}} \tag{D.3}$$

where P_{LC} is the power contained in the leakage carrier, and B_{PD} is the predetection bandwidth (about 200 cps).

Because of the coherent nature of the leakage, it is desired to keep its effective power density about 10 db below the thermal noise density at maximum altitude. This criterion assures that system noise, rather than the leakage, poses the ultimate limitation on altitude capability. Thus let

$$P_L \leq \frac{N_o}{10} \tag{D.4}$$

where N_o is the thermal noise density in the predetection bandpass. To maintain efficient signal detection, it is necessary to keep the total noise power at least 5 db (factor of about 3.16) below the signal carrier power in the predetection bandwidth. Now, it has been determined in other analyses that a signal carrier frequency spread of about 4 kc/s can occur under orbital conditions (velocity vector approximately horizontal) because of the existence of doppler velocity components across the finite antenna beamwidth. It can be shown that if the return carrier spectrum is assumed to be cosine-shaped across the total 4 kc/s, then the fraction of power passing through the 200 cps bandwidth is about 8.25 percent or -10.8 db. Thus, the maximum total noise power P_N in the predetection bandwidth may be expressed as

$$P_N = N_o B_{PD} \leq \frac{P_{SC}(0.0825)}{3.16} = 2.61 \times 10^{-2} P_{SC} \tag{D.5}$$

where P_{SC} is the total power in the unfiltered signal carrier.

Combining the information from Equations (D. 4) and (D. 5), we get

$$P_{LC} = P_L B_{PD} \leq 2.61 \times 10^{-3} P_{SC} \qquad (D.6)$$

where P_{LC} is the total power in the leakage carrier. (It has been assumed that all the leakage power is in the carrier. Actually, some of the power is contained in sidebands which have been rejected by bandpass action.)

For a 50 percent duty-factor system the average signal power is 3 db above its carrier power. Therefore, the required ratio of average signal to average leakage power S/L at the input to the receiver circuits (i.e., at the output of the first mixer) is

$$S/L = \frac{\overline{P}_s}{\overline{P}_L} = \frac{2P_{SC}}{P_{LC}} = \frac{2}{2.61 \times 10^{-3}} = 7.67 \times 10^2 = 28.8 \text{ db} \qquad (D.7a)$$

where

$\overline{P}_s$ = average carrier power

$\overline{P}_L$ = average leakage power.

The above derivation of the S/L requirement (Equation D. 7a) was based upon signal and noise conditions at maximum altitude. As altitude decreases, the receiver noise level remains constant at the receiver input, while the signal strength increases as $1/h^2$. Thus, if the leakage level is required to remain less than the noise level, the S/L requirement must also vary as $1/h^2$. In this case, system performance would improve rapidly with decreasing altitude. If, on the other hand, only the initial relationship between signal and leakage is required to be maintained, the S/L must obviously be constant and equal to 28. 8 db. In this case, isolation requirements decrease rapidly with decreasing altitude. Therefore, a variation of required S/L inversely proportional to altitude h will be specified as a reasonable compromise between increased system performance and relaxed isolation requirements. Thus let

$$S/L = 767 \frac{220 \text{ km}}{h \text{ km}} \qquad \text{(D. 7b)}$$

Substitution of Equation (D. 9) into Equation(D. 8) yields the required system isolation as a function of PRF:

$$I_{req} = \frac{1.07 \times 10^{19}}{Fr} \qquad \text{(D. 10)}$$

It is assumed here that only two means of achieving the required isolation are available. These are the inherent directional properties of the circulator and the virtues of varactor bias gating. Isolation by means of frequency discrimination is not considered here because near-zero altitude-rate can occur under orbital conditions. Assuming a circulator isolation contribution of about 24 db (factor of about 250) the component of isolation required of varactor bias gating becomes:

$$I_{req} = \frac{4.28 \times 10^{16}}{Fr} \qquad \text{(D. 11)}$$

It is important to note that this requirement is somewhat of a worst case condition because during the descent as well as in other applications (e. g., direct descent) frequency discrimination may in fact be feasible. In addition, other means of achieving contributions to isolation such as the inclusion of RF switches, bias modulation of mixer diodes and gating of IF components may also be feasible. Equation (D. 11) has been plotted and is shown in Figure D-3. This graph has been included to provide a tangible means of evaluation of experimental results. It should not be considered as representing an absolute requirement.

B. DERIVATION OF MEASUREMENT TECHNIQUES

The approach used in this portion of the analysis is two fold. An expression will first be derived which describes the isolation factor (per the original definition of isolation) achieved by means of gating in an actual system such as the one shown in Figure D-2. It will then be shown that this factor can be measured experimentally without having to process an actual received signal.

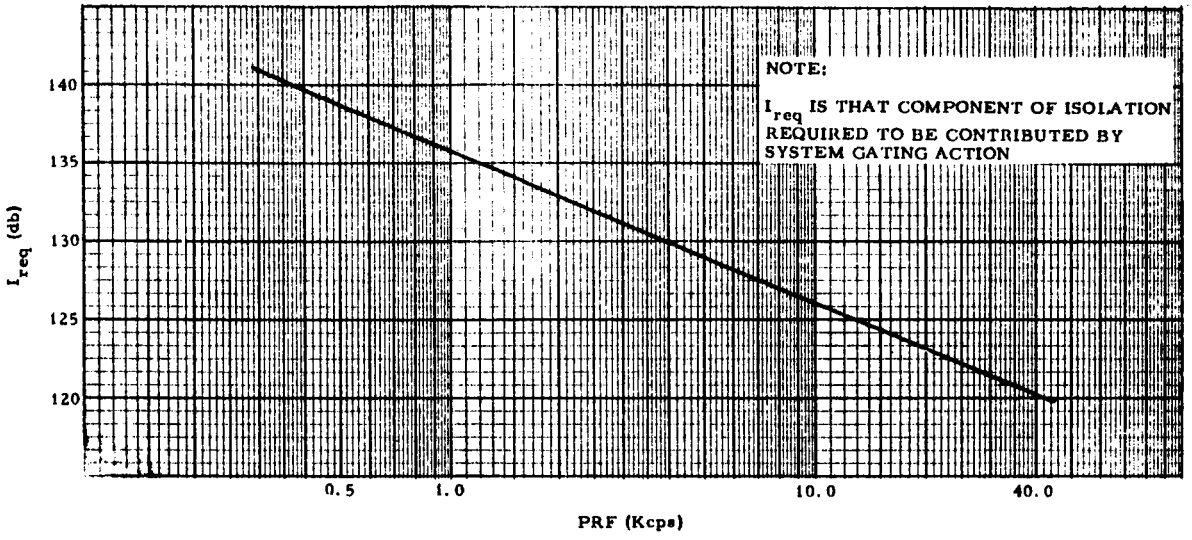

Figure D-3. Isolation Requirements as a Function of System PRF

It is convenient to associate the isolation contributed by means of varactor bias gating with the balanced mixer shown in Figures D-2 and D-4. The pertinent quantities and waveforms are also shown in Figure D-4. By the previous definition, the isolation contributed by the gating-mixing action is simply the relative attenuation of the average signal and leakage power levels as they pass through the mixer. The attenuation of any given input* when passing through a mixer is, however, dependent upon the level of local oscillator (LO) power as well as the power level of the input itself. As the waveforms shown in Figure D-4 indicate, both these quantities vary as functions of time. Before beginning the analysis, it is therefore necessary to define four attenuation factors corresponding to the various combinations of concern. These are:

* At any instant of time, the effective input may be primarily signal, leakage, neither, or both.

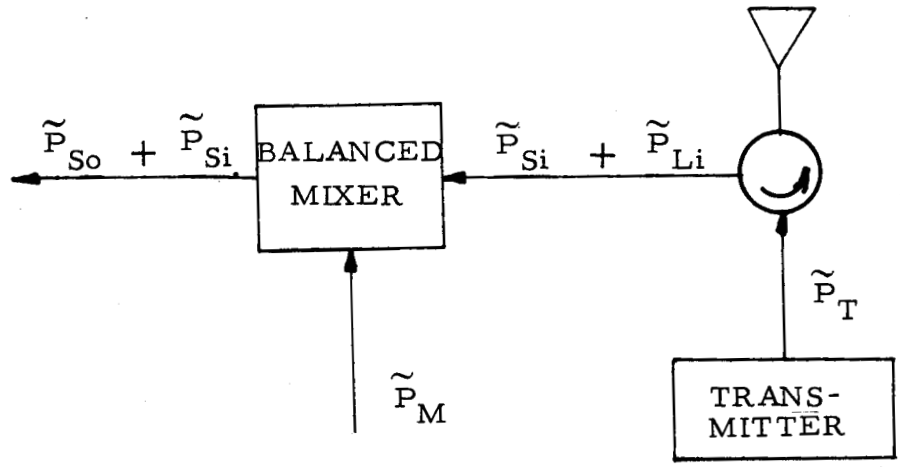

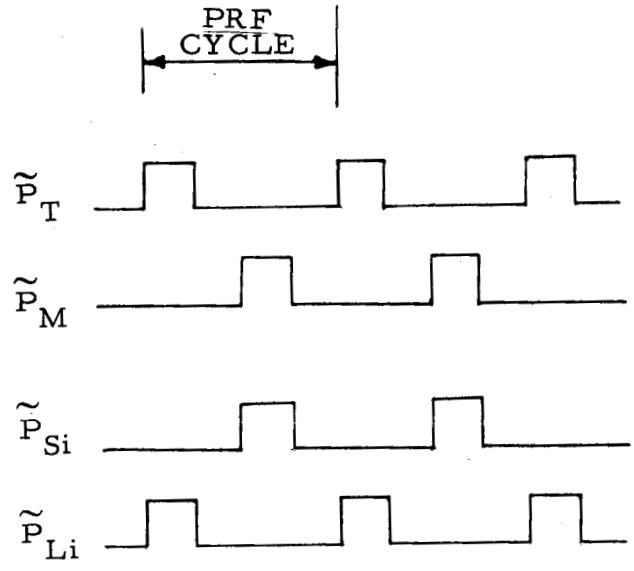

where

$\tilde{P}_T$ is the transmitter output power,

$\tilde{P}_M$ is the local oscillator power input to the mixer and therefore devotes the mixer-gating action,

$\tilde{P}_{Si}$ is the received signal power input to the mixer,

$\tilde{P}_{Li}$ is the leakage power input to the mixer,

$\tilde{P}_{So}$ is the signal power output from the mixer,

$\tilde{P}_{Lo}$ is the leakage power output from the mixer.

Figure D-4. Configuration for Determination of Isolation Contributed by Gating

A_{m1} : LO "on", large (>-20 dbm) input
A_{m2} : LO "on", small (<-20 dbm) input
A_{m3} : LO "off", large input
A_{m4} : LO "off", small input

The quantity A_{m2} is essentially the usual conversion loss associated with normal CW mixer operation and is considerably smaller than any of the other three attenuation factors. All four attenuations quantities are greater than unity. Using these definitions and the waveforms of Figure D-4, it becomes possible to write expressions*, term by term, for the average power of interest for system operation at any duty factor F_d:

$$\overline{P}_T = P_T F_d + \frac{P_T(1-F_d)}{A_T} \cong P_T F_d \qquad (D.12)$$

$$\overline{P}_{Si} = \frac{P_{Si}(1-F_d)}{A_T} + P_{Si} F_d \cong P_{Si} F_d \qquad (D.13)$$

$$\overline{P}_{Li} = P_{Li} F_d + \frac{P_{Li}(1-F_d)}{A_T} \cong P_{Li} F_d \qquad (D.14)$$

$$\overline{P}_{So} + \overline{P}_{Lo} = \frac{F_d(P_{Si}/A_T + P_{Li})}{A_{m3}} + \frac{1-2F_d}{2} \frac{P_{Si}/A_T + P_{Li}/A_T}{A_{m4}}$$

$$+ \frac{F_d(P_{Si} + P_{Li}/A_T}{A_{m2}} + \frac{1-2F_d}{2} \frac{P_{Si}/A_T + P_{Li}/A_T}{A_{m4}} \qquad (D.15)$$

where

$\overline{P}_T$, $\overline{P}_{Si}$, and $\overline{P}_{Li}$ denote the average values of the transmitter output, signal input, and leakage input powers, respectively

* For the altimeter under prime consideration, the leakage power incident upon the mixer is about -5 dbm during the peak portion of the cycle and therefore must be considered as a "large" input. The peak signal power is always less than about -80 dbm and may, therefore, be considered a "small" input.

P_T, P_{Si}, and P_{Li}	denote the peak power of transmitter output, signal input, and leakage input, respectively.
$A_T >> 1$	represents the effective attenuation internal to the transmitter during the "off" portion of the transmitter cycle
$\overline{P}_{So}$ and $\overline{P}_{Lo}$	denote the average values of the signal and leakage, respectively, at the output of the mixer.

The signal and leakage components in Equation (D. 15) may now be reseparated. Their individual attenuations will be solved for in the following equations.

$$P_{So} = \frac{P_{Si}F_d}{A_T A_{m3}} + \frac{P_{Si}(1-2F_d)}{A_T A_{m4}} + \frac{P_{Si}F_d}{A_{m2}} \qquad \text{(D. 16)}$$

but

$A_{m2} << A_T$

$A_{m2} < A_{m3}$ and A_{m4}

$0.1 < F_d < 0.5$ for considerations here

$\overline{P}_{Si} \cong P_{Si}F_d$

Thus

$$P_{So} \cong \frac{P_{Si}F_d}{A_{m2}} \qquad \text{(D. 17)}$$

and

$$A_S = \frac{\overline{P}_{Si}}{\overline{P}_{So}} = A_{m2} \qquad \text{(D. 18)}$$

where A_S is the effective attenuation of the signal in passing through the mixer. (Note that even in the gated configuration, the signal is attenuated in passing through the mixer only by the usual mixer conversion loss.)

$$\overline{P}_{Lo} = \frac{P_{Li}F_d}{A_{m3}} + \frac{P_{Li}(1-2F_d)}{A_T A_{m4}} + \frac{P_{Li}F_d}{A_T A_{m2}} \qquad (D.19)$$

but

$$A_{m4} >> A_{m2}$$

$$P_{Li} \cong P_{Li}F_d$$

Thus

$$\overline{P}_{Lo} \cong P_{Li}F_d \frac{A_T A_{m2} + A_{m3}}{A_T A_{m2} A_{m3}} \qquad (D.20)$$

and

$$A_L = \frac{\overline{P}_{Li}}{\overline{P}_{Lo}} = \frac{A_T A_{m2} A_{m3}}{A_T A_{m2} + A_{m3}} \qquad (D.21)$$

where A_L is the effective attenuation of the leakage in passing through the mixer. Thus, the isolation factor I_G contributed by on-off gating the transmitter and local oscillator may be expressed as:

$$I_G = \frac{A_L}{A_s} = \frac{A_T A_{m3}}{A_T A_{m2} + A_{m3}} \qquad (D.22)$$

Even with the convenient Equation (D. 22), the isolation contributed by gating cannot be calculated. This is because the factors A_T and A_{m3} are, in general, unknown and are direct functions of such system factors as pulse widths, rise and decay characteristics, spurious components, and intermodulation products. Such factors may well be functions of PRF and duty factor and are therefore not predictable even when static test data are available.

The question at hand is how to measure the isolation factor I_G experimentally without actually processing a received signal. Various methods for achieving this goal are possible. However, because of the nonlinear

nature of the mixing and gating processes, it is difficult to ascertain if any particular method actually gives I_G as given by Equation (D. 22) (recall the four different mixer processing factors which were required in the previous analysis). One such method suggests that I_G is equal to the ratio of the average power outputs of the mixer when the transmitter and local oscillator are gated in time-phase* (coincidence condition) and out of phase (anti-coincidence condition), respectively. In this procedure, the antenna shown in Figure D-4 is replaced by a matched load. The remaining analysis is dedicated to deriving the relationship between the result thus obtained and the desired isolation factor I_G as given by Equation (D. 22).

Proceeding analytically, the average leakage power out of the mixer may be determined for operation in the anti-coincidence condition when no return signal is present. Since the signal was small to begin with, however, the elimination of the signal does not change the mixer attenuation parameters of Equation (D. 15). The result then is again given by Equation (D. 20) which is rewritten here for easy reference:

$$\overline{P}_{Lo} \cong P_{Li} F_d \frac{A_T A_{m2} + A_{m3}}{A_T A_{m2} A_{m3}} \qquad \text{(D. 20)}$$

The average mixer power output $\overline{P}_{Lo}'$ for operation in the coincidence condition when no signal is present may be determined as follows:

$$\overline{P}_{Lo}' = \frac{F_d P_{Li}}{A_{m1}} + \frac{(1-F_d) P_{Li}/A_T}{A_{m4}} \cong \frac{P_{Li} F_d}{A_{m1}} \qquad \text{(D. 23)}$$

* We are interested only in transmit and receive pulses of approximately equal duration since such a condition is necessitated by the nature of the PRF scheme considered.

The ratio R_L of the two measurements $\overline{P}_{Lo}$ and $\overline{P}_{Lo}'$ is thus

$$R_L = \frac{\overline{P}_{Lo}'}{\overline{P}_{Lo}} = \frac{A_T A_{m2} A_{m3}}{A_{m1}(A_T A_{m2} + A_{m3})} = \left(\frac{A_{m2}}{A_{m1}}\right) \frac{A_T A_{m3}}{A_T A_{m2} + A_{m3}} \qquad (D.24)$$

which differs from the desired isolation parameter I_G, as given by Equation (D.22) by the factor A_{m2}/A_{m1}. Thus this test as such would not have given the correct result. Fortunately, the deficiency can easily be remedied. If, in the coincidence measurement indicated in Equation (D.23), a sufficient amount of attenuation (say, >20 db) is placed in series ahead of the mixer, the large leakage input becomes small, and the mixer attenuation factor A_{m1} in Equation (D.23) is replaced by the factor A_{m2}. Therefore, the new power level in the coincidence condition becomes:

$$\overline{P}_{Lo}' = \frac{F_d P_{Li}}{A A_{m2}} + \frac{(1-F_d) P_{Li}}{A A_T A_{m4}} \cong \frac{P_{Li} F_d}{A A_{m2}} \qquad (D.25)$$

where $A > 20$ db is the amount of attenuation introduced ahead of the mixer. Thus, the new power ratio R_L becomes:

$$R_L = \frac{A_T A_{m3}}{A(A_T A_{m2} + A_{m3})} = \frac{I_G}{A} \qquad (D.26)$$

Thus

$$I_G = A R_L \qquad (D.27)$$

where A is the amount of attenuation introduced ahead of the mixer during the coincidence measurement, R_L is the ratio of average power at the output of the mixer when operating in the coincidence and anti-coincidence conditions, respectively. This factor may be determined experimentally by any reasonable technique.